



Elementary spin excitations in ultrathin itinerant magnets



Khalil Zakeri

Max-Planck-Institut für Mikrostrukturphysik, Weinberg 2, D-06120 Halle, Germany

ARTICLE INFO

Article history:

Accepted 6 August 2014

Available online 20 August 2014

editor: G. E. W. Bauer

Keywords:

Spin excitations

Spin waves

Magnons

Magnetic nanostructures

Magnetic monolayers

Low-dimensional ferromagnets

Spin-polarized spectroscopy

Spin-polarized electron energy loss

spectroscopy

Spin dynamics

ABSTRACT

Elementary spin excitations (magnons) play a fundamental role in condensed matter physics, since many phenomena e.g. magnetic ordering, electrical (as well as heat) transport properties, ultrafast magnetization processes, and most importantly electron/spin dynamics can only be understood when these quasi-particles are taken into consideration. In addition to their fundamental importance, magnons may also be used for information processing in modern spintronics.

Here the concept of spin excitations in ultrathin itinerant magnets is discussed and reviewed. Starting with a historical introduction, different classes of magnons are introduced. Different theoretical treatments of spin excitations in solids are outlined. Interaction of spin-polarized electrons with a magnetic surface is discussed. It is shown that, based on the quantum mechanical conservation rules, a magnon can only be excited when a minority electron is injected into the system. While the magnon creation process is forbidden by majority electrons, the magnon annihilation process is allowed instead. These fundamental quantum mechanical selection rules, together with the strong interaction of electrons with matter, make the spin-polarized electron spectroscopies as appropriate tools to excite and probe the elementary spin excitations in low-dimensional magnets e.g. ultrathin films and nanostructures. The focus is put on the experimental results obtained by spin-polarized electron energy loss spectroscopy and spin-polarized inelastic tunneling spectroscopy. The magnon dispersion relation, lifetime, group and phase velocity measured using these approaches in various ultrathin magnets are discussed in detail. The differences and similarities with respect to the bulk excitations are addressed. The role of the temperature, atomic structure, number of atomic layers, lattice strain, electronic complexes and hybridization at the interfaces are outlined. A possibility of simultaneous probing of magnons and phonons in complex low-dimensional ferromagnetic oxide nanostructures is discussed. The influence of the relativistic spin-orbit coupling on high-energy magnons is addressed. It is shown how the spin-orbit coupling breaks the energy degeneracy of the magnons excited in an ultrathin ferromagnet, and how it influences their lifetime, amplitude, group and phase velocity. A potential application of these new effects in modern spintronics is outlined. It is illustrated how one can take advantage of collective nature of magnons and use these quasi-particles for probing the magnetic exchange interaction at buried interfaces.

© 2014 Elsevier B.V. All rights reserved.

Contents

| | |
|--|----|
| 1. Introduction..... | 48 |
| 2. Basic concepts | 50 |
| 2.1. Spin excitations in an exchange coupled spin system | 50 |

E-mail address: zakeri@mpi-halle.de.

URL: <http://www.mpi-halle.de>.

<http://dx.doi.org/10.1016/j.physrep.2014.08.001>

0370-1573/© 2014 Elsevier B.V. All rights reserved.

| | | |
|--------|--|----|
| 2.2. | Spin Hamiltonian | 50 |
| 2.2.1. | Coupling of spin to an external magnetic field | 50 |
| 2.2.2. | Spins in the presence of magnetic anisotropy | 51 |
| 2.2.3. | Symmetric exchange interaction | 51 |
| 2.2.4. | Antisymmetric exchange interaction | 51 |
| 2.2.5. | Long-range dipolar interaction | 52 |
| 2.3. | The magnon dispersion relation | 52 |
| 3. | Spin excitations in itinerant-electron ferromagnets | 53 |
| 3.1. | Collective excitations | 53 |
| 3.2. | Single particle Stoner excitations | 53 |
| 3.3. | Single particle versus collective excitations | 54 |
| 3.4. | Lifetime of spin excitations | 54 |
| 4. | Experimental techniques | 55 |
| 4.1. | Low-energy excitations | 55 |
| 4.1.1. | Ferromagnetic resonance | 55 |
| 4.1.2. | Brillouin light scattering | 55 |
| 4.1.3. | Time-resolved spectroscopies | 56 |
| 4.2. | High-energy excitations | 56 |
| 4.2.1. | Neutron scattering | 56 |
| 4.2.2. | Resonant inelastic X-ray scattering | 56 |
| 4.2.3. | Spin-polarized electron energy loss spectroscopy | 57 |
| 4.2.4. | Spin-polarized inelastic tunneling spectroscopy | 58 |
| 5. | Theoretical approaches | 59 |
| 5.1. | Adiabatic approach | 59 |
| 5.2. | Dynamical susceptibility approach | 61 |
| 6. | Probing magnons by spin-polarized electrons | 63 |
| 7. | Simultaneous probing of magnons and phonons | 65 |
| 8. | Magnons in a ferromagnetic monolayer | 67 |
| 9. | Atomic structure and magnon dispersion relation | 68 |
| 9.1. | Coordination number | 68 |
| 9.2. | Lattice relaxation | 69 |
| 9.3. | Lattice modification | 69 |
| 10. | The magnon lifetime | 71 |
| 11. | Real space representation of magnons | 73 |
| 12. | The effect of spin-orbit coupling on magnons | 74 |
| 12.1. | The magnon Rashba effect | 74 |
| 12.2. | The effect of spin-orbit coupling on the magnon lifetime | 76 |
| 13. | Probing exchange interaction at the interface | 78 |
| 14. | Magnons in thin films with perpendicular easy axis | 81 |
| 15. | Magnetic excitations in antiferromagnetic films | 84 |
| 15.1. | The magnon dispersion relation | 84 |
| 15.2. | The magnon lifetime | 85 |
| 16. | Magnetic excitations in atoms and clusters | 85 |
| 17. | Conclusions and outlook | 86 |
| | Acknowledgments | 87 |
| | References | 87 |

1. Introduction

One of the most profound and fundamental ideas in the quantum theory of condensed matter physics is the idea of “quasi-particles”. Usually, the behavior of a complex many-body system is understood in terms of simple models of interacting or noninteracting quasi-particles. For instance, in a piece of metal, where a large number of electrons is placed in a small volume, the electrons become dressed by the presence of the other electrons in the system and form quasi-particles. The Coulomb interactions among the electrons can become unimportant. Although these quasi-particles still obey the Fermi statistics (because they are still fermions), their interaction is weak and can be neglected to the first order. On the other hand the collective excitations of these strongly interacting electrons can be regarded as bosonic quasi-particles called plasmons. Most of the properties of a given system can be understood by investigating the behavior of the fermionic and bosonic quasi-particles of the system.

Magnetism, as another fascinating phenomenon in nature, is also a many-body effect. Although the first scientific discussion on magnetism goes back to 600 BC, it is noticeable that still the research on magnetism is one of the pillars of condensed matter physics. In the quantum formalism, the collective modes of spin excitations in a magnetic solid are referred to as spin waves and their representative quasi-particles are called magnons. The word magnon is chosen in analogy to the quantized lattice vibrations, named phonons. Similar to phonons, plasmons, excitons, magnons are also bosons. Magnons are essential to understand many observed phenomena e.g. magnetic ordering, ultrafast magnetization processes, electrical and heat

conductivity, current induced magnetization reversal and electron/spin dynamics. Recently, it has been demonstrated that the coupling between electrons and high-energy magnons is a possible mechanism, which leads to superconductivity in high-temperature superconductors [1–3]. Besides these core fundamental aspects, magnons are of great importance for modern spintronics, since they are generated in tunneling magneto resistance (TMR) and spin transfer torque (STT) devices [4–6] and also in the read and write head of magnetic recording elements [7].

Magnons have entered the picture very early in the history of modern magnetism [8,9], shortly after the time when Heisenberg explained the origin of the magnetic coupling on the quantum mechanical basis [10,11]. The temperature dependence of spontaneous magnetization of a ferromagnet has been explained by introducing new type of elementary excitations (magnons). This concept is known as Bloch's law and could only explain the temperature dependence of magnetization at low temperatures, far below the transition temperature of ferromagnetic to paramagnetic state [8,9].

In the case of magnetic materials with localized moments, it is rather straightforward to imagine the magnons. One may imagine a ferromagnetic solid composed of magnetic atoms which are ferromagnetically coupled. In the ground state, all the moments are aligned parallel and give rise to a spontaneous magnetization. In the excited state, the precessional motion of each individual atomic moment results in a propagating wave in the ferromagnetic solid. Magnons in antiferromagnets can also be imagined in analogy to the ones in ferromagnets. Since in 3d ferromagnets like Fe, Co and Ni the magnetism is governed by conduction electrons, this description cannot provide a similarly straightforward picture for magnons in these materials. A major controversy developed soon after introducing this new type of quasi-particles. The question of debate was: "Are there magnons in itinerant ferromagnets?"

The answer of Stoner and Wohlfarth to this question was negative. In fact Stoner and Wohlfarth looked at the problem from a band-model view, in which the properties of a ferromagnetic metal can be described by the single particle excitations (known as Stoner excitations) [12–14]. Within this picture, the exchange interaction in metals does not allow low energy magnons to exist. Experimentally, however, the ferromagnetic resonance was already observed [15] and explained by a phenomenological approach [16,17]. Van Kranendonk and Van Vleck had a different opinion. They pointed out that magnons may exist in metals [18,19]. Based on a quantum theory, Herring and Kittel showed that magnons do exist in itinerant ferromagnets [20]. Magnons in antiferromagnets could be explained by a similar formalism [21]. The dispersion relation, which connects the magnons energy E (or eigenfrequency, ω) to their wave vector q , is found to be $\varepsilon = \hbar\omega \propto q^2$ for ferromagnets and $\varepsilon = \hbar\omega \propto q$ for antiferromagnets in the small wave vector regime. Dyson further used this formalism for a complete description of the thermodynamic properties of ferromagnets based on magnons and their interactions [22]. In addition to the description of the low temperature magnetic order (Bloch's law), the scattering cross section of magnons was also addressed. He estimated a spin–spin mean free path being proportional to $T^{-7/2}$.

The direct experimental evidence of the existence of magnons in ferromagnetic metals was first appeared when the neutron scattering techniques were established. In fact the theory of Herring and Kittel was proven by the experiments performed on bulk crystals [23–32].

However, still it was not quite clear how the classical magnons, explained by classical dynamics e.g. by phenomenology [16,33–36], can be understood from a microscopic point of view i.e. by looking at the electronic band structure. As it was pointed out by Stoner at the beginning of the development of the quantum theory of magnetism, the thermodynamic properties of a ferromagnetic metal, like magnetic phase transition and paramagnetic state above the Curie temperature, can be attributed to the single spin-flip particle interband transitions.

On this basis, many authors tried to shed light on the relation between the so-called spin wave theory by Herring and Kittel [20] and the so-called collective electron theory by Stoner [12,13] and Wohlfarth [14]. By starting from a single band ferromagnetic metal, Edwards [37,38], Callaway [39,40] and Sokoloff [41–43] proposed a way of calculating the magnons energy in ferromagnetic metals. This theory was further developed for more realistic multi-band systems and could explain the magnon dispersion relation in itinerant electron ferromagnets [44–53]. In this description the magnons are treated similar to the excitons (electron–hole pairs) in which the electron and hole have opposite spins. The wavefunction of such an electron–hole pair is a linear superposition of electron and hole states (spin triplet particle–hole excitations). This theory is now developed for low-dimensional magnets [54–61].

Since low-dimensional magnets show novel properties, the concept of spin excitations in this class of materials is of fundamental interest. For instance, according to the Mermin–Wagner theorem, an ideal two-dimensional spin system with an isotropic and short-range interaction cannot exhibit any long-range magnetic order at a finite temperature [62]. This theorem is even generalized for a lattice of spins which are coupled to itinerant interacting electrons in one- and two-dimension [63]. However, in real two-dimensional spin systems, like ferromagnetic monolayers, small magnetic anisotropies or dipolar interactions are sufficient to stabilize a long-range magnetic order [64–66]. It would be of great fundamental interest to probe the magnon dispersion relation in a real two-dimensional ferromagnetic system, e.g. one atomic layer of a ferromagnet grown on a surface, and to see how it changes with changing the system's parameter such as temperature, number of atomic layers involved, chemical environment, etc. All these key experiments lie in the central understanding of the system's behavior. When the wavelength of magnons approaches the nanometer scale, their excitation energy is governed by the quantum mechanical exchange interaction. In this case, the excitations are strongly confined in both time and space. Hence, they cannot be treated similar to the long wavelength magnons by the classical dynamics. This implies that a quantum mechanical description of the system is needed. Moreover, since the translation symmetry in a ferromagnetic monolayer grown on a surface is broken, one would expect very interesting dimensionality effects, which are reflected in the properties of magnons. Hence, the experimental study of such excitations would provide an insightful microscopic view of the system.

Recently, the dream of measuring elementary spin excitations in low-dimensional spin systems from magnetic monolayers down to clusters, chains and adatoms has become a reality. This is due to the development of spin-polarized spectroscopy methods such as high resolution spin-polarized electron energy loss spectroscopy and spin-polarized spin excitation spectroscopy.

In this work, the recent studies of elementary spin excitations in ultrathin itinerant magnets are reviewed. The paper is organized as follows: the concept of spin excitations is discussed in Section 2. The experimental and theoretical approaches used to investigate the magnons are introduced in Section 4 and Section 5, respectively. The important mechanisms which lead to magnon excitations are outlined in Section 4.2.3, where an introduction to the spin-polarized electron energy-loss spectroscopy and tunneling spectroscopy techniques, is provided. The important properties of magnons such as their excitation energy, dispersion relation and lifetime probed in different systems are discussed in detail in Sections 8–15, where various examples are provided and discussed. The fundamental mechanisms involved in the excitation mechanism are presented in Section 6. The possibility of probing magnons and phonons simultaneously is discussed in Section 7. The results of spin excitations in an ideal model system, a ferromagnetic monolayer are presented in Section 8. The impact of atomic structure on the magnon dispersion relation is discussed in Section 9. The results of magnon lifetime and their real space representation are presented in Sections 10 and 11, respectively. The consequences of the relativistic spin–orbit coupling on the spin excitations are explained in Section 12. The possibility of using magnons for spectroscopy of buried interfaces is discussed in Section 13. In Section 14 the first experimental attempts to measure the magnons in ultrathin films with out-of-plane easy axis are discussed. The magnetic excitations probed by inelastic tunneling spectroscopy in antiferromagnetic γ -Mn films are discussed in Section 15 and are compared to the magnetic excitations in ultrathin Fe and Co films. Section 16 provides a bridge to the excitations of adatoms and clusters on surfaces. This topic is not fully covered in the present review. Section 17 provides a summary and a perspective for future works.

2. Basic concepts

2.1. Spin excitations in an exchange coupled spin system

We start with the localized moment picture to describe a magnetic solid. In this description the local magnetic moment on each atomic site is regarded as a rigid entity (it is referred to as atomic spin). The next step is to introduce a mathematical way of treating such a system. Mathematically, the spin maybe considered as a vectorial object. This oversimplified picture might be useful for an intuitive thinking. However, it does not reflect its quantum mechanical origin. Therefore, in the course of this review we consider the spin as a quantum mechanical observable. Since it is an extra degree of freedom, it can be treated by the quantum mechanics algebra.

Similar to all quantum mechanical degrees of freedom, spin has a discrete set of basis states, which are labeled by quantum numbers. The components of a spin should change sign under time reversal. In the mathematical treatment of the spin Hamiltonian we use here, the term “spin” is general and can be the representative of any given system e.g. a localized single electron’s (or hole’s) spin in a semiconductor, the overall spin of several d -electrons in transition metals or the atomic spin. As far as the spin Hamiltonian of these systems has the same form, all these systems shall behave similarly.

2.2. Spin Hamiltonian

In a very general case the Hamiltonian of a spin system including all the possible contributions can be written as:

$$\mathcal{H} = \mathcal{H}_B + \mathcal{H}_{An} + \mathcal{H}_{Ex} + \mathcal{H}_{DM} + \mathcal{H}_{Dip}. \quad (1)$$

\mathcal{H}_B describes the coupling of the spins to an external magnetic field. \mathcal{H}_{An} describes the system in the presence of anisotropy. The last three contributions describe the spin–spin interactions in the system and do not exist for the case of a single spin. \mathcal{H}_{Ex} is the so-called symmetric exchange term, \mathcal{H}_{DM} is the antisymmetric exchange term and \mathcal{H}_{Dip} describes the long range dipolar interaction among spins.

2.2.1. Coupling of spin to an external magnetic field

An external magnetic field can couple to a spin in free space. The spin Hamiltonian describing this coupling can be written as: $\mathcal{H}_B = -g\mu_B\mathbf{S}\cdot\mathbf{B}$, where g is the g -factor, μ_B is the Bohr magneton, \mathbf{S} represents the spin and \mathbf{B} denotes the magnetic field. This term is commonly referred to as Zeeman term. For an array of noninteracting spins the Hamiltonian maybe written as:

$$\mathcal{H}_B = -\mathbf{B}\cdot\sum_i g_i\mu_B\mathbf{S}_i. \quad (2)$$

The effect of this term is classically equivalent to a torque that puts a classical spin, e.g. the magnetic moment of an atom or the magnetization of a ferromagnetic object, into precession, if it is not parallel to the direction of the magnetic field. In a more general case where the microscopic spin–orbit coupling is also important, the scalar constant g has to be replaced by the g -tensor. Discussion of this topic is out of the scope of the present review. Further information may be found elsewhere [67].

One can show that the dynamics of a single spin in an external magnetic field can be written in the following form:

$$\frac{d\mathbf{S}}{dt} = -\gamma (\mathbf{S} \times \mathbf{B}), \quad (3)$$

where, $\gamma = g\mu_B/\hbar$ is the so-called gyromagnetic ratio.

In fact, if the term introduced in Eq. (2) is the only term in the total Hamiltonian of the system, it brings the spin to a uniform precession around the magnetic field with the eigenfrequency $\omega = \gamma B$. Eq. (3) is the basis of the classical descriptions of spin dynamics in the presence of a magnetic field. For instance, if a ferromagnetic object with a spontaneous magnetization is placed in an external magnetic field, one can use Eq. (3) to describe the dynamics. For that \mathbf{S} should be simply replaced by the macro-spin i.e. the total magnetization. In addition to this, a damping term should also be added for a more realistic description. Such a treatment has been first introduced by Landau and Lifshitz and the corresponding equation is known as Landau–Lifshitz equation of motion [68]. In Section 4.1.1 we will demonstrate the practical use of this equation in the case of uniform spin motion that is usually referred to as ferromagnetic resonance (FMR).

2.2.2. Spins in the presence of magnetic anisotropy

To imagine the effect of the anisotropy on the spin one may think of the coupling of the spin to the “anisotropy field”. In fact, presence of the anisotropy in the spin system is in analogy to a field which breaks the symmetry of the system. The coupling is very similar to what we discussed for the case of coupling of spins to an external magnetic field. If the magnetic anisotropy is of uniaxial character, the Hamiltonian of the system can be written as:

$$\mathcal{H}_{\text{An}} = -\frac{1}{2}K (\mathbf{S} \cdot \hat{\mathbf{e}}_i)^2. \quad (4)$$

This Hamiltonian is basically the same as the one introduced by Ising [69] to explain the ferromagnetism of an atomic chain. Here K is the magnetic anisotropy constant and $\hat{\mathbf{e}}$ denotes the spin easy axis (anisotropy axis). One may also consider the higher-order anisotropy terms. However, they become less important in terms of energy and can be neglected. For instance, if the system has a biaxial anisotropy the spin Hamiltonian will include terms with S^4 .

2.2.3. Symmetric exchange interaction

The simplest form of the spin Hamiltonian for interacting spins can be written as:

$$\mathcal{H}_{\text{Ex}} = -\sum_{i \neq j} J_{ij} \mathbf{S}_i \cdot \mathbf{S}_j, \quad (5)$$

where the parameters J_{ij} represent the exchange coupling constants between spins \mathbf{S}_i and \mathbf{S}_j . For the case of a ferromagnetic (antiferromagnetic) coupling the exchange parameter is positive (negative). The exchange interaction is not restricted to the neighboring spins and can be extended beyond the nearest neighbors [9,20,22]. It is apparent that the Hamiltonian, given above, guarantees rotational symmetry.

In the spin model introduced above, the origin of the exchange interaction does not appear explicitly. In the case of electrons' spin it originates from the overlap of the electronic wavefunctions. In fact the exchange interaction is a consequence of the Coulomb interaction between electrons and Pauli exclusion principle and can be derived from the quantum mechanics, considering two interacting electrons with the spin of 1/2 [10,11].

2.2.4. Antisymmetric exchange interaction

In the discussion above, we considered only the bilinear term of two interacting spins. However, in a more general case the scalar product given in Eq. (5) can be written in the form of $\sum_{\sigma, \delta} C_{\sigma, \delta} S_{i, \sigma} S_{j, \delta}$, where σ and δ label the Cartesian components of the coupling matrix $C_{\sigma, \delta}$, describing more complex couplings. Any matrix can, in principle, be decomposed into (i) a multiple of the unit matrix, (ii) a traceless symmetric matrix and (iii) an antisymmetric matrix. The first term gives rise to the symmetric exchange interaction, presented in Eq. (5). The second term leads to any kind of anisotropic exchange term. The antisymmetric term (the third term) can be written in the form of a vector product of spins. We define the spin Hamiltonian of the antisymmetric exchange interaction, known as Dzyaloshinskii–Moriya (DM) interaction, as:

$$\mathcal{H}_{\text{DM}} = -\sum_{i \neq j} \mathbf{D}_{ij} \cdot \mathbf{S}_i \times \mathbf{S}_j. \quad (6)$$

Here \mathbf{D}_{ij} is the so-called Dzyaloshinskii–Moriya vector. Note that there is also a possibility to have anisotropic exchange terms. This means that the coupling of spins along different axes are different ($J_{ij, x} \neq J_{ij, y}$). Such situations usually happen when a cubic crystal is tetragonally distorted. For the case of ultrathin films grown on a substrate these situations are rather common due to the film epitaxy. Based on the symmetry arguments, we classify such kind of interactions as symmetric exchange interaction.

The symmetric Heisenberg exchange interaction favors a parallel (or antiparallel) alignment of spins while DM interaction favors a non-collinear ground state. For a system of interacting electrons one can show that the antisymmetric DM

interaction is a consequence of the spin–orbit coupling and absence of the inversion symmetry in the system. The DM interaction vanishes for the systems with inversion symmetry. In the case of layered magnetic structures the presence of the surfaces or interfaces often breaks the inversion symmetry (in addition to the fact that it breaks the translation symmetry) and therefore leads to the existence of the DM interaction. The spin Hamiltonian discussed in Eq. (6) has first been proposed in 1957 by Dzyaloshinskii based on symmetry arguments [70]. It has been shown at the same time by Moriya that, in principle, this interaction can be analytically derived by considering the relativistic spin–orbit correction in the Hamiltonian of the electronic system [71]. In the systems with large spin–orbit coupling and in the presence of broken inversion symmetry DM interaction can lead to very exotic ground states [72–76]. Recently, a correlated band theory of spin and orbital contributions to DM interaction has been reported [77]. This theory allows one to calculate the components of the DM vector from first principles via the construction of a reliable tight-binding parametrization of the electronic Hamiltonian with the spin–orbit interaction included.

One can show that this term leads to a linear term in the magnon dispersion relation in the limit of small wave vectors (see Section 2.3).

2.2.5. Long-range dipolar interaction

A spin can also be coupled to the magnetic stray field created by the other spins located in longer distances. The term describing this long-range interaction is similar to the term introduced in Eq. (2) in which \mathbf{B} is replaced by the magnetic field induced by the other spins. The dipolar interaction has the form:

$$\mathcal{H}_{\text{Dip}} = - \sum_{ij} \frac{(g\mu_B)^2}{r_{ij}^3} [\mathbf{S}_i \cdot \mathbf{S}_j - 3(\hat{\mathbf{r}}_{ij} \cdot \mathbf{S}_i)(\hat{\mathbf{r}}_{ij} \cdot \mathbf{S}_j)], \quad (7)$$

where \mathbf{r}_{ij} represents the displacement vector of spins \mathbf{S}_i and \mathbf{S}_j , located at \mathbf{r}_i and \mathbf{r}_j , respectively. This term is responsible for the demagnetizing field and ferromagnetic domains in ferromagnets.

2.3. The magnon dispersion relation

The magnon dispersion relation, which connects the energy (or eigenfrequency) to the wave vector, can be obtained by finding the eigenvalues of the spin Hamiltonian of the system. One may start with the classical dynamics introduced in Ref. [21]. Another approach is introduced in Refs. [9,22,19]. We do not aim to discuss, in detail, how the equations are derived. Details may be found in textbooks or in Sec. 7.2.3 of [78] and in Sec. 2 of [79]. For the case of a simple lattice with only one magnetic atom in the primitive cell and considering only the symmetric exchange interaction and only the nearest neighbors, the resulting magnon dispersion relation can be written as:

$$\varepsilon = \hbar\omega = 2nJS \left[1 - \frac{1}{n} \sum_{\mathbf{R}} \cos(\mathbf{q} \cdot \mathbf{R}) \right], \quad (8)$$

where n is the number of nearest neighbors, S is the magnitude of spin, J is the exchange coupling constant between the neighbors and \mathbf{R} represents the position vector of the respective neighbor.

It is relatively straightforward to imagine that the dimensionality aspects have a large impact on the magnon dispersion relation. For instance, if the system consists of a few monolayers of a ferromagnetic material, different magnon modes are expected and each mode may have a different contribution to the dispersion relation. The lowest in energy magnon mode is usually referred to as the “acoustic mode”. In the absence of the relativistic effects, when the spin Hamiltonian of the system includes only the symmetric exchange interaction (Eq. (5)), this magnon mode shall satisfy the Goldstone theorem. This means that the energy of this mode shall be zero for $q = 0$. The higher energy magnon modes of the system are usually referred to as “optical modes”. These modes have a finite energy at $q = 0$ even in the absence of the relativistic effects.

Since the dispersion relation is one of the main subjects of the present review we will discuss it in various places. No prediction concerning the magnon lifetime can be made by the Heisenberg spin Hamiltonian given in Eq. (1). Within this description, magnons shall live forever, which is not certainly true for the case of itinerant electron magnets.

One can show that in the limit of $q \rightarrow 0$ Eq. (8) can be simplified to:

$$\varepsilon = \hbar\omega = Dq^2 + \mathcal{O}(q^4), \quad (9)$$

where $D = JS\delta$ is the so-called spin-wave stiffness constant.

Now let us consider only the DM term, introduced in Eq. (6). In this case one can show that the dispersion relation of this term considering only the nearest neighbors interactions can be written as [80,81]:

$$\varepsilon_{DM} = c \sin^2 \theta \sum_{\mathbf{R}} (\mathbf{D}_1 \cdot \hat{\mathbf{e}}) \sin(\mathbf{q} \cdot \mathbf{R}). \quad (10)$$

Here c is the chirality rotation index (being $+1$ for right rotating sense and -1 for the left rotating one), θ denotes the relative angle between the neighboring spins, \mathbf{D}_1 is the DM vector of the nearest neighbors, $\hat{\mathbf{e}}$ denotes the direction of the

easy axis and \mathbf{R} represent the position vector of nearest neighbors. Equation (10) implies that only the components of the DM vector parallel to the easy axis contribute to the magnon energies. It is apparent that for the limit of $q \rightarrow 0$ this term can be approximated by a term which is linear with respect to q .

For a ferromagnetic system in the presence of a large spin–orbit coupling and in the absence of the inversion symmetry both the symmetric exchange interaction and the antisymmetric DM interaction are active. In this case the resulting magnon dispersion relation will include the term introduced in Eq. (8) and also the one introduced in Eq. (10). As a result the dispersion relation will be asymmetric with respect to q , meaning that $\varepsilon(q) \neq \varepsilon(-q)$. We will come to this point in Section 12.

3. Spin excitations in itinerant-electron ferromagnets

In literature, the quantized spin excitations are referred to as magnons. In many occasions the terms “magnons” and “spin waves” are interchanged. In our opinion, this is rather misleading, since the nature of spin excitations in itinerant ferromagnets is somewhat different from those in the ferromagnetic insulators. In itinerant electron ferromagnets the elementary spin excitations may be divided into collective and single particle excitations, which we will discuss them in Sections 3.1 and 3.2, respectively.

In low-dimensional itinerant ferromagnets such as thin films grown on a nonmagnetic substrate the situation is even more complicated. First, the translation symmetry is broken and as a consequence, the momentum of the electronic states along the direction perpendicular to the surface of the film is not conserved anymore. Second, the electronic states of the ultrathin ferromagnetic film and the substrate may hybridize. Hence, the spectrum of single particle excitations in momentum–energy space may be very much different from that of the bulk ferromagnets. This would imply that the magnon lifetime in ultrathin ferromagnets may also be substantially different from that in the bulk.

We use the term magnon as an elementary quasi-particle which describes the elementary collective spin excitations in an itinerant electron ferromagnet.

3.1. Collective excitations

As discussed above, in a magnetic solid with any ground state magnetic ordering (ferromagnets, antiferromagnets, ferrimagnets, etc.) one may consider the quasi-particles of spin ordering in analogy to the ones of crystal ordering (phonons). Although in itinerant ferromagnets magnetism is caused by the itinerant electrons [82], one may consider that the electrons are partially localized on atomic sites. This allows one to associate a magnetic moment to each atomic site. The wave-like excitations of these magnetic moments that propagate through the lattice are of collective nature. Similar to other quasi-particles, the energy of spin waves’ representative quasi-particles is also quantized in units of $\hbar\omega$, where ω represents the eigenfrequency of the magnon with a given wave vector q . One may describe the magnons by a Heisenberg type of Hamiltonian as discussed in Section 2.2. In such a description, the interaction of spins is treated in the form of an effective interatomic exchange parameter which couples the moments. The dispersion relation may be derived by starting with a simple spin Hamiltonian in which the coupling constant is the effective interatomic exchange coupling. Although this picture is not complete, it provides a simple description of the system. Such kinds of approaches are usually referred to as adiabatic methods.

3.2. Single particle Stoner excitations

According to the band theory of magnetism, in a ferromagnetic solid the degeneracy of the electronic bands is lifted [83]. This degeneracy breaking originates from the electron–electron interaction in ferromagnets, which leads to a separation of the electronic bands for majority and minority electrons. The effect may be described as perturbations of a degenerate paramagnetic band from which the energy degeneracy is lifted by the “exchange energy”. Generally, the exchange splitting depends on the energy and the wave vector of the electrons. In the case that the Fermi-level lies between the bands derived from a single degenerate paramagnetic band, the lower energy (majority) states are occupied, while the higher energy (minority) states are unoccupied. This fact leads to a net spin polarization of the conduction electrons and can explain the magnetic state of the system. Now it is relatively easy to imagine that the spin-split bands across the Fermi-level can lead to the possibility of a unique single-particle excitation in the system. For instance an electron can jump from an occupied majority band and occupy a state in the minority band after undergoing a spin reversal. In such a case a hole of majority spin character will remain in the majority band. The resulting electron–hole pair which is usually referred to as “Stoner pair” carries a total angular momentum of $1\hbar$. Since it is created within the momentum–energy space, there is a wave vector and energy associated with that. The momentum (energy) of such a pair is the momentum (energy) difference of the electron and hole in the minority and majority bands, respectively (see Fig. 1(a)). Stoner excitations are spread over a large area of the Brillouin zone, see Fig. 1(b). These excitations have first been introduced by Stoner within the collective electron theory [12,13] and later by Slater [84]. Van Kranendonk [19] has tried to connect this type of excitations to the collective modes of the itinerant ferromagnets.

The direct measurement of Stoner excitations has been reported much later when the spin-polarized electron spectroscopy techniques were developed [85–88]. The substantial development of the theory of spin-polarized electron scattering which happened at the same time could help for a better understanding of the experiments [89–91]. One of the

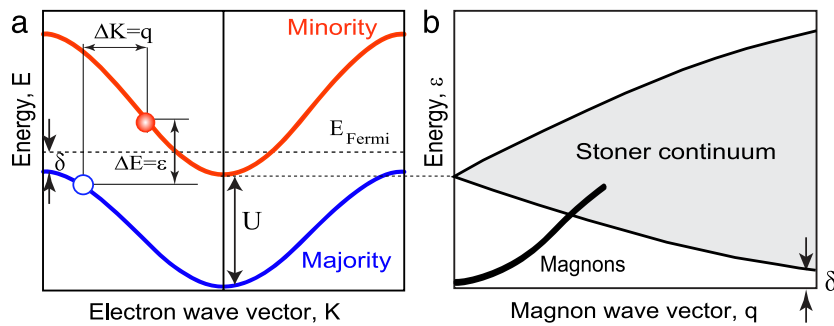


Fig. 1. (a) A schematic representation of Stoner excitations in an itinerant ferromagnet. A majority electron jumps from an occupied state below the Fermi-level to an unoccupied state above the Fermi-level, leaving a hole with majority spin behind. (b) Stoner density of states for a bulk metallic ferromagnet with a non-zero Stoner gap, δ .

key experiments has been performed by Kirschner who has used a spin-polarized beam and a spin-polarized detector to measure all the possible spin dependent features from a ferromagnetic surface [85]. The reader is referred to Ref. [92] for a review.

3.3. Single particle versus collective excitations

From a band view of magnetism the magnons may be considered as a coherent superposition of electron–hole pairs in which the electron and hole have opposite spins. The wavefunction of a magnon is a linear superposition of the wavefunctions of electron and hole states in the system. Consequently, the coupling of magnons to Stoner excitations (single particle electron–hole pair excitations) is a possible mechanism which can lead to strong damping of magnons. Indeed, it is the main damping mechanism in itinerant electron ferromagnets and is usually referred to as Landau damping. Note that in ultrathin ferromagnets the location and the shape of the Stoner continuum depends also on the degree and the type of electronic hybridizations between the film and substrate. Hence, the situation can be rather complicated [93,94].

3.4. Lifetime of spin excitations

There are different mechanisms which determine the magnons' lifetime. Here we only briefly discuss the mechanism which is responsible for the lifetime of high wave vector magnons in itinerant ferromagnets. For high wave vector magnons, the lifetime is determined by the decay of the collective excitations into the single particle Stoner excitations and hence it depends strongly on the available Stoner states in the system. As discussed above in low-dimensional systems, such as magnetic monolayers, the Stoner continuum may be very much different from that of the bulk ferromagnets and hence the lifetime of magnons in these systems is different. If the hybridization of the electronic states of the magnetic film with the ones of the substrate is such that a large number of Stoner states are created near the Fermi level, the lifetime of magnons will be very short. This means that the presence of the nonmagnetic substrate provides an addition decay channel of collective magnon modes into single particle Stoner excitations. In other words, the energy and the angular momentum of the spin system is transferred by the conduction electrons of the underlying substrate. This concept has been discussed in detail in Refs. [93,94] and is attributed to the formation of the interfacial electronic complexes at the interface between the film and substrate. For example if the substrate features prominent surface states, these states can hybridize very efficiently with the states of the ferromagnetic film grown on top and form the interfacial electronic complexes. Due to the formation of the electronic complexes a large number of Stoner states can appear near the Fermi-level. In such systems the magnons excited in the ferromagnetic film will decay rather quickly. We will come back to this point again when we discuss the magnon lifetime in ultrathin Co and Fe films (see Section 10). However, there are cases in which the formation of the electronic complexes is not favored. For these cases it is expected that the magnons in the ferromagnetic film live for a longer time. It is important to point out that there are other sources for the damping of magnetic excitations. Even in the localized moment ferromagnets the high wave vector excitations are damped. This damping may be imagined as the dephasing of a certain magnon mode with a given q to all the other possible magnons with different wave vectors [95,96].

Finally, it is important to mention that the damping of magnons does not only involve the transfer of energy but also the transfer of angular momentum. The angular momentum stored in the spin system shall flow to other subsystems e.g. to the lattice. When the magnons decay to Stoner excitations, the angular momentum remains still in the spin system. The flow of both the energy and the angular momentum from the spin system ultimately ends up in the lattice. Consequently, the lattice experiences a torque. The transfer of the angular momentum from the spin system to the lattice requires a coupling mechanism which couples the spin to the lattice i.e. the spin–orbit coupling.

For $q = 0$ the magnon lifetime is governed by the spin–orbit coupling. In this case the phenomenological damping parameter (known as Gilbert damping) shall explain the damping of the magnons in the system. In some cases, processes like two-magnon scattering may also be very important. Since here we mainly deal with the high wave vector magnons, we

do not discuss those kinds of damping mechanisms further. A detailed explanation of those mechanisms and how to treat the damping of magnons with $q = 0$ may be found in Ref. [97] and references therein.

4. Experimental techniques

In this section we shall briefly discuss the fundamental mechanisms which lead to magnon excitations in low-dimensional magnets. We will start with a brief outline of the schemes used for probing spin excitations. The methods are traditionally divided into two classes. Some are appropriate for probing low-energy excitations and some for high-energy ones.

4.1. Low-energy excitations

4.1.1. Ferromagnetic resonance

If a ferromagnetic object is placed in an external static magnetic field, all the atomic spins will precess about the direction of the static magnetic field. This uniform precession of all moments is usually referred to as ferromagnetic resonance (FMR). The frequency of the uniform precession (the magnon with $q = 0$) is on the order of a few tens of gigahertz (energies on the order of micro-electron-volt). The dynamics of such processes is usually discussed using Eq. (3) including a phenomenological damping term [97].

In an FMR experiment the sample is placed in the microwaves field, and one observes resonant absorption of the microwaves as soon as the microwaves frequency matches the eigenfrequency of the uniform precession (the magnon mode with $q = 0$). The magnetic field component of the microwaves is orthogonal to the applied static magnetic field. In metallic ferromagnets, the penetration of the microwaves field into the sample is not uniform. There is a so-called skin depth in which the microwaves field can penetrate. Generally, the skin depth depends on the microwaves frequency. At the resonance condition, the effective skin depth is only a few tens of nanometers. This leads to the fact that if the thickness of the sample is much larger than the skin depth, a nonuniform excitation will take place. The resulting FMR spectrum will contain not only the uniform precession (the magnon with $q = 0$) but also the magnons with finite wave vectors (between 0 and 10^{-2} \AA^{-1}). Since in the experiment one keeps the microwaves frequency constant, scans the static magnetic field and measures microwaves absorption, one observes more than a single absorption peak in the measured spectra.

In films of finite thickness, due to confinement effects the perpendicular component of the wave vector is quantized ($q_z = n\pi/t$, where t is the thickness of the film, and n denotes an integer number). Kittel showed that in such a situation one should see the so-called spin-wave resonance modes with odd numbers [98]. Due to the boundary conditions, the modes with even numbers are not allowed to be excited (because the spins are assumed to be pinned down at the boundaries of the sample due to the presence of the surface anisotropy). The mode with $n = 0$ is the well-known uniform FMR mode ($q = 0$), wherein all spins precess in phase. The higher order modes are the so-called spin wave resonance modes. Starting with the equation of motion introduced in Eq. (3) and replacing \mathbf{S} with the macro-spin i.e. the magnetization of the sample \mathbf{M} , one can show that in such a situation the dispersion relation of the modes for a ferromagnetic sample in the form of a disk and neglecting the in-plane magnetic anisotropy terms will be as follows:

$$\omega = E/\hbar = \gamma (B_{\text{res}} + \mu_0 M_{\text{eff}} + Dq_z^2), \quad (11)$$

where B_{res} is the resonance field, $M_{\text{eff}} = 2K_{\perp}/M - \mu_0 M$ denotes the effective out-of-plane anisotropy field (K_{\perp} is the out-of-plane uniaxial anisotropy and M is the saturation magnetization of the sample) and D is the spin wave stiffness constant. Eq. (11) is valid when the applied magnetic field \mathbf{B} is applied perpendicular to the film surface, along the z -direction (see the measurement geometry in the inset of Fig. 2). For a detailed discussion on the ways that the resonance equations are derived by a classical dynamics the reader is referred to Refs. [98,34–36,67]. For the resonances $q_z = n\pi/t$ (t is the film thickness and n is the mode number). Evidence of such spin wave resonance modes has first been observed by Seavey and Tannenwald in a 560 nm thick permalloy film [99]. Fig. 2 shows the spin wave resonance modes of the sample measured by Seavey and Tannenwald. The odd spin wave resonances are clearly visible. A plot of the resonance field versus n^2 would lead to a direct determination of the spin wave stiffness constant D .

The sensitivity of the technique is such that one can detect the signal of a nominal one atomic layer of a ferromagnet. It can also be integrated into ultrahigh vacuum in order to measure the objects in the absence of any protecting layer [67,100]. Recently, the technique is developed for the detection of a single magnetic nano-particle resonance [101]. In addition, FMR is a powerful tool to investigate the damping mechanism of the uniform mode. The discussion of the damping mechanism is out of the scope of the present review and hence we will not discuss it further. We refer the reader to Ref. [97].

4.1.2. Brillouin light scattering

Magnons may be excited within inelastic scattering of light from the matter. This phenomenon is the basis of the Brillouin light scattering (BLS) spectroscopy. The first observation of light scattering by magnons was observed by Fleury and co-workers [102] on FeF₂ samples. In the conventional BLS experiments, a constant magnetic field is applied and the frequency shift of the light is measured after the scattering process [103].

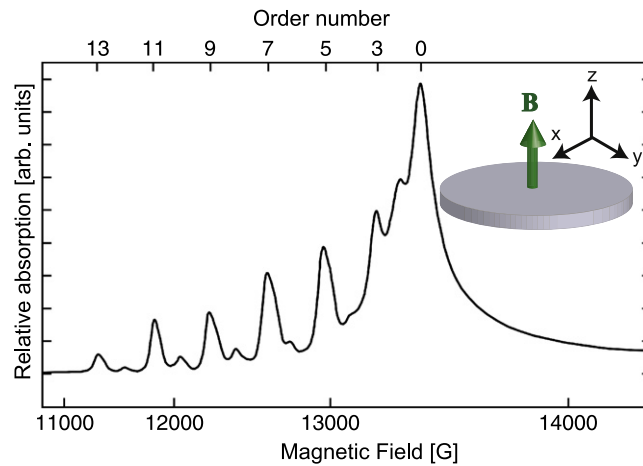


Fig. 2. Spin wave resonance modes of a 560 nm thick permalloy film measured by Seavey and Tannenwald [99]. In this experiment the static magnetic field was applied along the film normal as shown in the inset. Due to the boundary conditions only the odd resonance modes are expected to be excited [98]. Source: Adopted from [99].

© 1958, by the American Physical Society.

The interaction mechanism is based on the modulation of the dielectric constant of the medium through the magneto-optical constants. When a photon with a certain energy and momentum is scattered from a magnetic medium a magnon can be excited by energy and momentum transfer from the photon. The scattering process of the light which leads to the excitation of magnons can be understood as follows. Due to the magneto-optical effects a phase grating is created in the magnetic medium by a magnon. This phase grating propagates through the medium with the phase velocity of the magnon. As a result when the light is scattered from the phase grating, its frequency is Doppler-shifted by the frequency of the magnon [104]. The main restriction of the technique is that it only allows the measurement of low-energy (and low-wave-vector, $q < 10^{-3} \text{ \AA}^{-1}$) magnons. The technique allows the investigation of magnons in low-dimensional magnetic structures [104].

4.1.3. Time-resolved spectroscopies

Methods discussed above allow probing the spin excitations in the frequency domain. In addition to those conventional methods there are also methods which allow one to probe the excitations in the time domain. In most of these experiments, the system is first excited and the evolution of the spins is then followed as a function of the time. Depending on the excitation scheme, one may investigate a desired type of magnons. The excitation may be done by magnetic field pulses, microwaves or photons. A full description of those method is out of the scope of the present review. We do not aim to discuss them here, useful information may be found in [105].

4.2. High-energy excitations

4.2.1. Neutron scattering

Inelastic neutron scattering (INS) relies on the interaction of spin 1/2 of an incoming neutron interacting with an electron's spin in the solid, via the magnetic dipole interaction, which allows for a simultaneous spin-flip of neutron and electron. The scattered neutron then carries the information on the energy and momentum of elementary excitations left behind in the solid. The magnetic interaction between a neutron and an electron's spin that generates the spin-flip is local, but the excitation created in the scattering process can of course be delocalized being characterized by the wave vector \mathbf{q} and the energy ε transferred from the neutron to the magnetic quasi-particles in the system.

Since the interaction of neutrons with matter is relatively weak, this technique does not allow probing magnons in low-dimensional magnets.

4.2.2. Resonant inelastic X-ray scattering

Similar to INS, one may imagine a magnetic scattering using X-ray photons. Since a photon carries an angular momentum of $1\hbar$, which can in principle be transferred to the spin-system, it can create elementary spin excitations. However, the direct interaction between the photon and the spin via the magnetic part of the electromagnetic field is extremely small. This fact prevents a simple experimental implementation of this idea. However, one may take advantage of resonant process of photon absorption. In resonant inelastic X-ray scattering (RIXS) one scatters X-ray photons inelastically from the sample and measures the energy, momentum, and polarization change of the scattered photon. The changes in energy, momentum, and polarization of the photon are transferred to intrinsic excitations of the material under study. RIXS takes the advantage of resonant process in which the energy of the incident photon is chosen such that it coincides with, and hence resonates with,

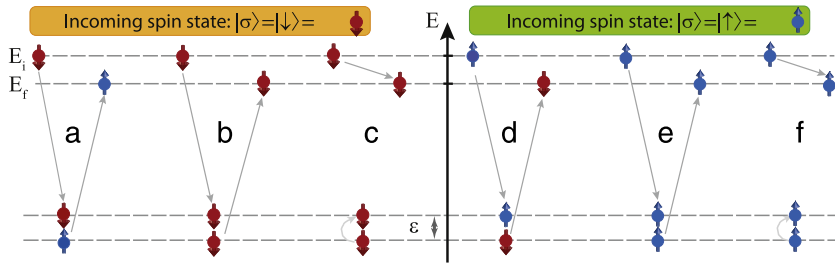


Fig. 3. A schematic representation of the possible processes taking place in the scattering of spin-polarized electrons from a magnetic surface. An electron with a given spin state $|\sigma\rangle = |\downarrow\rangle$ (left) or $|\sigma\rangle = |\uparrow\rangle$ (right) is incident to the sample. The spin state of the scattered electron can be either $|\sigma\rangle = |\downarrow\rangle$ or $|\uparrow\rangle$. Processes marked as (a) and (d) are referred to as “flip” processes, since the spin state of the scattered electron is opposite to the one of the primary electron. Processes in which the spin of the scattered electron is the same as the one of the incoming electron are referred to as “non-flip” processes ((b), (c), (e) and (f)). Processes (c) and (f) are usually called as direct processes whereas the other processes are called as exchange processes.

one of the atomic X-ray transitions of the system. The resonance can largely enhance the inelastic scattering cross section, sometimes by orders of magnitude, and offers a unique way to probe magnetic excitations on a selective atomic site in a crystal [106]. Since in RIXS process the core electrons are involved, one takes the advantage of large spin-orbit coupling of core electrons. In the so-called indirect RIXS process, an electron from a core level is promoted to a valance state by absorption of the X-ray photon. In the intermediate state the core-hole with a spin of $1/2$ experiences a very strong spin-orbit coupling and if the core-hole orbital is of p character and thus has an angular momentum of $1\hbar$, the core-hole can exchange part of its angular momentum with its spin momentum, thereby flipping the spin of the core-hole. The promoted electron cannot anymore decay into this core-hole since it does not have the right spin. The core hole can only be annihilated by an electron of opposite spin to the promoted electron. This fact leads to the creation of a magnon with a total angular momentum of $1\hbar$.

It has been proven that this technique can be applied to complex bulk samples, mainly magnetic oxides [106]. However, at the time of this review we are unaware of any investigation of low-dimensional systems. Only very recently the magnons in superlattices of La_2CuO_4 have been reported [107].

4.2.3. Spin-polarized electron energy loss spectroscopy

Spin-polarized high resolution electron energy loss spectroscopy (SPHREELS or simply SPEELS) is based on the scattering of spin-polarized electrons from a magnetic surface, in which the elementary excitations are excited. It is often assumed that the basic concepts of SPEELS are similar to the ones of INS. In fact the fundamental basis of these two techniques are different. In SPEELS experiments the exchange mechanism plays an important role while in INS experiments the type of the interaction that is important is the dipolar interaction between the neutron’s magnetic moment with the magnetic moment of the unit cell.

In the following we will discuss how does the exchange mechanism during the scattering process lead to magnon excitations within the SPEELS experiments.

A. Spin-dependent electron scattering

Before we discuss the contributions to the inelastic scattering of the spin-polarized electrons, let us define the spin direction of the incoming and outgoing electron beam. It is defined with respect to the majority and minority spins of the sample (or with respect to the quantization axis, which is usually defined as the direction of the sample magnetization). When the spin of the electron is parallel to the spin of the majority electrons of the sample, it is called spin-up electron and when it is parallel to the spin of the minority electrons, it is called spin-down electron. The inelastic scattering of spin-polarized electrons is a rather complicated topic. A complete description of the mechanisms involved in such processes is out of the scope of the present review. An extended discussion can be found in Refs. [108,92]. If an electron with a given spin is incident onto a ferromagnetic surface at a certain geometry, the outgoing electron has either the spin orientation parallel or antiparallel to the one of the incoming electron. Although in the former case an exchange of the electrons with the same spin is possible, in the latter case one can clearly talk about the exchange process. This means that the incident electron occupies an unoccupied state above the Fermi-level and another electron from an occupied state below the Fermi-level is scattered out. The possible processes involved in the scattering of the spin-polarized electrons from a magnetic surface are schematically illustrated in Fig. 3 for incidence of spin-down ($|\sigma\rangle = |\downarrow\rangle$, left) and spin-up ($|\sigma\rangle = |\uparrow\rangle$, right) electrons. The processes in which the incident and scattered electrons have the same spin character are usually referred to as “non-flip” processes and the ones in which the spin of the scattered electron is opposite to the one of the incident electron are called “flip” processes. It is essential to notice that no direct spin reversal is involved in the processes mentioned above. The underlying mechanism is the exchange process. The flip process describes the process in which an incident electron with a given spin direction is exchanged with an electron from the sample with opposite spin orientation (for an extended discussion see for example [78]).

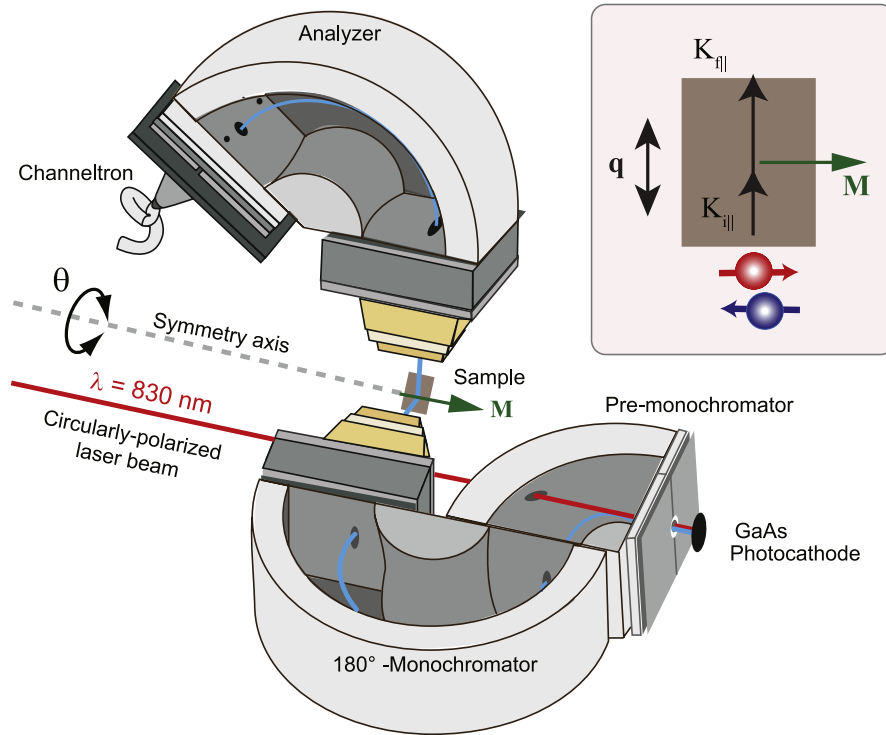


Fig. 4. A schematic representation of the SPEELS spectrometer used for studying spin excitations. A spin-polarized electron beam is generated by photoemission from the GaAs spin source using a circularly polarized laser beam with the wavelength of $\lambda = 830$ nm. The spin-polarized electron beam is focused on the sample surface after passing through a pre- and a 180° -monochromator. The scattered electrons are collected by a channeltron after energy analysis. Inset shows the propagation direction of magnons with respect to the parallel momentum of the incoming (K_{\parallel}) and outgoing (K'_{\parallel}) electron beam and the sample magnetization \mathbf{M} .

B. Experimental details

As mentioned above, SPEELS is based on the scattering of spin-polarized electrons from a magnetic surface [109,85,110–114]. Spin-polarized electrons are created by using spin-polarized photoemission from a GaAs photocathode. A circularly polarized laser beam is incident into the photocathode. According to the selection rules, the spin of the photo-emitted electrons is either parallel or antiparallel to the incident direction of the laser beam, depending on the helicity of the incoming photon. Since a normal GaAs provides only a total polarization of 50% (based on the spin dependent photoemission selection rules), usually a so-called strained semiconductor heterostructure is used for this purpose. Taking the advantage of heteroepitaxy one can grow a semiconductor heterostructure with a large lattice strain. The large strain modifies the band structure so that a large spin polarization (as large as 90%) can be achieved [115]. The spin-polarized electrons are monochromatized and are focused onto the sample surface. The spin of the incoming electrons is either parallel or antiparallel to the spin of the majority electrons of the sample. The former types of electrons are usually called spin-down and the latter ones are called spin-up electrons. The scattered electrons are collected by a channeltron at a given scattering geometry and their energy is analyzed [113]. Note that no spin-resolved detection is involved in this experiment (see Fig. 4). The experiment is usually performed for both spin polarizations of the incoming electron beam.

In Fig. 5, the scattering geometry is schematically sketched. If one assumes that the energy and momentum in initial and final states before and after scattering are E_i , K_i and E_f , K_f , respectively, the energy $\varepsilon = \hbar\omega$ and the wave vector q of the excitations can be given by the following expressions:

$$\varepsilon = \hbar\omega = E_f - E_i; \quad q = -\Delta K_{\parallel} = K_i \sin \theta - K_f \sin(\theta_0 - \theta). \quad (12)$$

In addition to the conservation of energy and momentum, the total angular momentum has to also be conserved. Hence, magnon excitations are allowed only when spin-down electrons are incident. As a result the magnon peak appears only in the spin-down SPEELS spectra. Magnon excitations are forbidden when spin-up electrons are incident onto the sample surface.

4.2.4. Spin-polarized inelastic tunneling spectroscopy

Magnons can also be excited within the tunneling process in scanning tunneling spectroscopy experiments [116–119]. Basically, the mechanism is similar to the one in SPEELS experiments. The tunneling electrons interact with the ones of the sample, and when they have enough kinetic energy to create an excitation, the tunneling current is enhanced. The excitation process leads to a step in the differential conductivity that is dI/dU and consequently a peak in d^2I/dU^2 . The main difference here is that the excitation may happen in the forward and backward tunneling directions. This means that the peaks

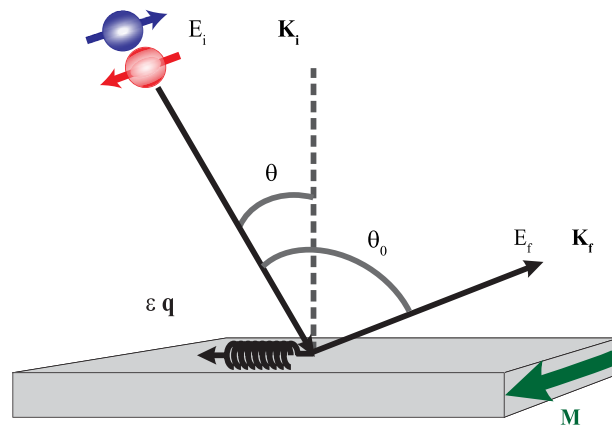


Fig. 5. A schematic representation of the scattering geometry used in SPEELS experiments. A monochromatic beam with a well-defined energy and momentum is scattered from the sample surface at a given geometry and the energy distribution of the scattered beam is measured for both spin orientations of the incoming beam.

associated with the excitations shall be observed in both positive and negative bias voltages (the bias voltage is the voltage applied between the scanning tunneling microscope (STM) tip and the sample). The process which leads to the creation of a magnon in the forward tunneling process is schematically sketched in Fig. 6. If the tunneling electron is of minority character and during this process is exchanged with an electron of majority character, a magnon is created. In the backward tunneling (tunneling of electrons from the sample to the tip) if a majority electron of the sample is injected into the tip states a magnon is created.

Generally, the excitations seen in the tunneling spectra can be of magnetic or nonmagnetic nature. By using a magnetic tip and changing the magnetization direction of the tip, one may confirm that the excitations are of magnetic origin. Another way would be to apply an external magnetic field and investigate the evolution of the excitation energy as a function of the magnetic field (the shift of the energy due to the Zeeman term). The main disadvantage of this technique is that the control of the tip magnetization is usually difficult. The tunneling current is almost perpendicular to the sample surface and the tunneling process takes place on a very small area (atomic length scales). This fact leads to the creation of local excitations, which can be described as a superposition of the magnons with many different wave vectors. Unlike SPEELS, the technique cannot be used to excite magnons in a wave vector selective manner. However, when the magnons of different wave vectors are confined in a film or nanostructure, standing waves are formed due to the confinement effects. Only then one would be able to assign different peaks observed in the tunneling spectra to those confined magnons and their wave vector to the corresponding quantized wave vector of the standing waves [116–119]. For the investigation of magnons in ultrathin films, usually the tunneling spectra are recorded on films (or terraces) of different thicknesses. The observed peaks in the spectra are associated with the standing waves confined in the z -direction (perpendicular to the surface). In this case the wave vector is given by $q_z = n\pi/t$, where $n = 0, 1, \dots$ is an integer number and t is the film thickness. The capability of measuring the magnetic excitations of adatoms and clusters on a surface is a unique possibility of this method [120,119,121–123].

5. Theoretical approaches

5.1. Adiabatic approach

The most common theoretical approach of treating the magnons is the so-called adiabatic approach [124–127,50,128–137,80,138–142]. In this approach, first the atomic magnetic moments are regarded as rigid entities which are coupled by

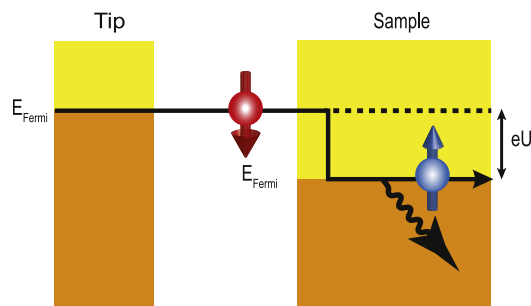


Fig. 6. The spin dependent tunneling process which leads to the excitation of a magnon in forward tunneling. The tunneling electron of minority character tunnels to the Fermi sea. If during this process it is exchanged with an electron of majority character, a magnon will be created.

an effective Heisenberg type of exchange coupling. The Hamiltonian of such a system is given by an effective Heisenberg Hamiltonian. This approach is based on the assumption that the precession of the magnetization is much slower than the characteristic times of electronic motions (the site-to-site hopping rate and the precession of an electron under the exchange field). This assumption is fairly valid when the magnon energy is small (the limit of small energy and momentum).

Frozen magnon approximation

In the so-called *frozen magnon approximation*, one computes the energy $E(\mathbf{q})$ of a spin-spiral configuration, which simulates a magnon with a certain momentum \mathbf{q} [128,129]. Such a calculation can be done by using the Bloch theorem for the spin-spiral [143]. In this formalism one assumes that the ground state is collinear with the magnetization pointing along a certain direction. The excited state of the system is a spin-spiral in which the direction of a given atomic moment i is determined by two angles. The polar angle θ_i is the angle between the moment and the direction of the ground state and can be associated with the amplitude of the magnon. The azimuthal angle ϕ_i determines the phase of the moment in its precessional motion and is determined by \mathbf{q} , $\phi_i = \mathbf{q} \cdot \mathbf{d}_i$, where \mathbf{d}_i stands for the position of the i th atomic site. One estimates the magnon energy $\varepsilon(\mathbf{q})$ as the difference between the energy of the configuration of moments forming a magnon, $E(\{\theta_i\}, \mathbf{q})$, and the ground state energy E_0 as:

$$\varepsilon(\mathbf{q}) = \frac{2}{\Delta M} [E(\{\theta_i\}, \mathbf{q}) - E_0], \quad (13)$$

where $\Delta M = \sum_i (1 - \cos \theta_i) \mu_i$, μ_i being the magnetic moment of the atom at site i . The normalization ensures that each magnon changes the system magnetization by $2\mu_B$. $E(\{\theta_i\}, \mathbf{q})$ can be calculated using the spin-spiral technique [143].

Magnetic force theorem

Another alternative is using the so-called *magnetic force theorem* [137]. One calculates the energy change of the system associated with the constrain rotation of the moment of different atoms. Generally, this leads to a difficult task of calculating the electronic structure of a non-collinear system. For the small rotation angles between the moments one can show that the change in the energy is proportional to the second order of the change in the moment direction:

$$\varepsilon_{\text{Tot.}}(\delta \mathbf{u}_{\mathbf{R}}) = \sum_{\mathbf{R}, \mathbf{R}'} A_{\mathbf{R}, \mathbf{R}'} \delta \mathbf{u}_{\mathbf{R}} \cdot \delta \mathbf{u}_{\mathbf{R}'}, \quad (14)$$

where $\delta \mathbf{u}_{\mathbf{R}}$ represents the change in the direction of the moment from the ground state. The above equation can be written in terms of an effective Heisenberg Hamiltonian:

$$H_{\text{eff}} = - \sum_{\mathbf{R}, \mathbf{R}'} J_{\mathbf{R}, \mathbf{R}'} \hat{\mathbf{e}}_{\mathbf{R}} \cdot \hat{\mathbf{e}}_{\mathbf{R}'}. \quad (15)$$

The exchange parameters can be calculated by expressing Eq. (14) in terms of changes in single-particle eigenvalues due to non-selfconsistent changes of the effective one-electron potential accompanying the infinitesimal rotations of the quantization axis. The resulting exchange parameters will be given by:

$$J_{\mathbf{R}, \mathbf{R}'} = \frac{1}{\pi} \Im \int_{-\infty}^{E_f} \int_{\Omega_{\mathbf{R}}} \int_{\Omega_{\mathbf{R}'}} B_{xc}(\mathbf{r}) G_{\uparrow}(\mathbf{r}, \mathbf{r}'; E + i0) B_{xc}(\mathbf{r}') G_{\downarrow}(\mathbf{r}, \mathbf{r}'; E + i0) dE d\mathbf{r} d\mathbf{r}'. \quad (16)$$

In the above equation E_f stands for the Fermi energy, $\Omega_{\mathbf{R}}$ ($\Omega_{\mathbf{R}'}$) represents the Wigner–Seitz cell around the atom on site \mathbf{R} (\mathbf{R}'), B_{xc} is the so-called exchange–correlation field and is defined as:

$$B_{xc}(\mathbf{r}) = \frac{1}{2} [V_{\downarrow}(\mathbf{r}) - V_{\uparrow}(\mathbf{r})], \quad (17)$$

where $V_{\downarrow}(\mathbf{r})$ and $V_{\uparrow}(\mathbf{r})$ are the local spin density approximation potentials and $G_{\downarrow}(\mathbf{r}, \mathbf{r}'; E + i0)$ and $G_{\uparrow}(\mathbf{r}, \mathbf{r}'; E + i0)$ are the single-electron retarded Green functions of the same potentials. The exchange parameters calculated by Eq. (16) do not contain contributions due to constraining magnetic fields needed to keep a frozen non-collinear spin structure a stationary state of the Kohn–Sham equation. These contributions can be neglected in systems with large local magnetic moments. Once the exchange parameters are calculated, Eq. (15) can be easily employed to calculate the magnon energy [124]. For ferromagnetic crystals with one atom in the primitive cell, the magnon energy $\varepsilon(\mathbf{q})$ is related to the lattice Fourier transform $J(\mathbf{q})$ of the exchange parameters:

$$\varepsilon(\mathbf{q}) = \frac{4}{M} \sum_{\mathbf{R}} J_{0, \mathbf{R}} [1 - \exp(i\mathbf{q} \cdot \mathbf{R})]. \quad (18)$$

Atomistic spin dynamics simulations

Once the exchange parameters are known one can calculate all the desired dynamical properties. In the computational scheme called *atomistic spin dynamics simulations* one uses the first-principles exchange parameters to compute the

dynamical structure factor. This quantity, which is usually probed in INS experiments, is calculated by a Fourier transform of the space- and time-displaced correlation function. The magnon dispersion relation can be constructed by finding the peak position of the dynamical structure factor computed for different \mathbf{q} [140–142].

Static transverse susceptibility technique

In the so-called *static transverse susceptibility technique*, one applies a spiral external field in the form of $B_{\mathbf{R}'+\mathbf{T}}^x + iB_{\mathbf{R}'+\mathbf{T}}^y = |\mathbf{B}_{\mathbf{R}'}| \exp(i\mathbf{q} \cdot \mathbf{T})$ to one moment, instead of prescribing a frozen-magnon configuration for the moments [136]. Here \mathbf{T} is the translation vector. The field is constant on a given moment and forms a spin-spiral in the whole system. The static susceptibility $\chi_{\mathbf{R},\mathbf{R}'}$ can then be evaluated as:

$$M_{\mathbf{R}}^x + iM_{\mathbf{R}}^y = \chi_{\mathbf{R},\mathbf{R}'}^\perp |\mathbf{B}_{\mathbf{R}'}|. \quad (19)$$

Since the induced magnetic moments caused by the field are calculated selfconsistently, this method also applies to materials with small exchange fields. The magnon dispersion relation is obtained by finding the peak position of the static susceptibility calculated for different \mathbf{q} .

In the adiabatic approach the Stoner excitations are neglected, therefore, no prediction regarding the magnons lifetime can be made. However, the method provides a reasonable account of the magnons energy.

5.2. Dynamical susceptibility approach

As the adiabatic calculations, based on DFT, do not involve adjustable parameters, in this respect, they are useful for description of the magnons energy in the limit of small energy and momentum and provide reasonably good results. Note that for the calculations based on Eq. (18) one has to restrict the sum over a finite number of neighbors. Since in metals the exchange integrals oscillate as a function of distance and decay as power laws, in the first approximation, the series that determines the magnon energy or magnon stiffness constant D is very slowly convergent. Thus, even in the limit of small energy and momentum, where the adiabatic approximation is supposed to be exact, another approximation has to be made. The adiabatic calculations do not provide information regarding the magnon lifetime, since the Stoner excitations are not taken into account. In addition to that, in the limit of high energy high momentum the presence of the Stoner continuum can also cause a renormalization of the magnons energy.

Using a single band ferromagnetic metal, one may calculate the magnons energy. This approach has been first proposed by Edwards [37,38], Callaway [39,40] and Sokoloff [41–43] and later on it has been further developed for more realistic multi-band systems [44–53]. In this description the magnons are treated similar to the excitons. The wavefunction of such an electron-hole pair is a linear superposition of electron and hole states.

The proper way of calculating both energy and the lifetime of excitations is to calculate the wave vector and energy dependent transverse dynamical magnetic susceptibility $\chi(\omega, \mathbf{q})$. In this approach since both the collective magnons and Stoner excitations are taken into account, both energy and lifetime of excitations can be calculated. The poles of the dynamical susceptibility are associated with the magnon in the energy space. The real part of the pole position gives the energy of the magnon with a given \mathbf{q} and the inverse of the imaginary part can be regarded as the magnon lifetime:

$$\chi(\omega, \mathbf{q}) = \frac{A(\mathbf{q})}{\omega - \varepsilon(\mathbf{q})/\hbar + i\Delta(\mathbf{q})}, \quad (20)$$

where $A(\mathbf{q})$ is directly related to the amplitude of the magnon wavefunction, $\varepsilon(\mathbf{q})$ is the magnon energy and $\Delta(\mathbf{q})$ represents the inverse of the lifetime. The imaginary part of such a function has the form of Lorentzian lineshape in which the peak position describes the magnon energy and the linewidth is the inverse of the lifetime:

$$\Im\chi(\omega, \mathbf{q}) = \frac{A(\mathbf{q})\Delta(\mathbf{q})}{[\omega - \varepsilon(\mathbf{q})/\hbar]^2 + \Delta^2(\mathbf{q})}. \quad (21)$$

Generally, for calculating $\chi(\omega, \mathbf{q})$ one requires to solve a Dyson equation. The solution of this master equation in a general form can be written as:

$$\chi(\omega, \mathbf{q}) = \frac{\chi_0(\omega, \mathbf{q})}{\mathbf{1} - Z\chi_0(\omega, \mathbf{q})}. \quad (22)$$

The terms $\chi_0(\omega, \mathbf{q})$ and Z in Eq. (22) are defined differently depending on the technical scheme used for calculating $\chi(\omega, \mathbf{q})$. $\chi_0(\omega, \mathbf{q})$ represent the single-electron (or noninteracting) susceptibility and Z describes the electron correlations in the system. Obviously, for $Z = 0$ (no correlation) one immediately realizes that the poles of $\chi(\omega, \mathbf{q})$ are the poles of $\chi_0(\omega, \mathbf{q})$. These solutions shall describe the single-particle Stoner excitations of the system. It is apparent that Eq. (22) has singularities when the denominator is zero. These solutions describe the collective excitations of the system and can be regarded as spin waves.

Practically, there are three major technical schemes to compute $\chi(\omega, \mathbf{q})$: (i) Empirical tight-binding theory (ETBT), (ii) Many-body perturbation theory (MBPT) and (iii) Linear response time-dependent density functional theory (LRTDFT). In the following we shall provide a short description of these schemes.

Empirical tight-binding theory (ETBT)

In the ETBT scheme one starts with a general tight-binding Hamiltonian including all the necessary orbitals [29,46,144, 91,49,54,56,55,145,57,58]. $\chi(\omega, \mathbf{q})$ can be defined in terms of the time Fourier transform of the two-particle retarded Green function $G(\omega, \mathbf{q})$:

$$\chi(l'; \omega, \mathbf{q}) = \sum_{\mu\nu} \sum_{\mu'\nu'} F_{\mu\nu}(\mathbf{q}) G_{\mu\nu, \mu'\nu'}(l'; \omega, \mathbf{q}) F_{\mu'\nu'}(-\mathbf{q}), \quad (23)$$

where $F_{\mu\nu}(\mathbf{q})$ is a magnetic form factor and is given by $\langle i\mu | \exp(-i\mathbf{q} \cdot \mathbf{r}) | i\nu \rangle$ and l represents the index of the atomic plane. $G(\omega, \mathbf{q})$ may be written in terms of noninteracting retarded Green function $G_0(\omega, \mathbf{q})$ via the Dyson equation:

$$G(\omega, \mathbf{q}) = \frac{G_0(\omega, \mathbf{q})}{\mathbf{1} - U G_0(\omega, \mathbf{q})}, \quad (24)$$

where U describes the effective electron–electron interactions. $G_0(\omega, \mathbf{q})$ is directly related to the one-electron retarded g and advanced g^- Green functions:

$$G_{0, \mu\nu, \mu'\nu'}(l'; \omega, \mathbf{q}) = \frac{1}{N} \sum_{\mathbf{k}} \int d\omega' f(\omega') [\Im g_{l\nu', l\mu}^{\uparrow}(\mathbf{q}, \omega') g_{l\nu', \mu'}^{\downarrow}(\mathbf{q} + \mathbf{k}, \omega' + \omega) + \Im g_{l\nu', \mu'}^{\downarrow}(\mathbf{q} + \mathbf{k}, \omega') g_{l\nu', l\mu}^{-\downarrow}(\mathbf{k}, \omega' - \omega)]. \quad (25)$$

Here N is the number of sites in layer l , \mathbf{k} is the electron momentum (small letter means that it is a continuous variable) and $f(\omega)$ is the Fermi distribution function. For calculating $\chi(\omega, \mathbf{q})$ one first needs to calculate g and g^- . It is apparent from a comparison of Eqs. (22) and (24) that $G_0(\omega, \mathbf{q})$ can be used to calculate $\chi_0(\omega, \mathbf{q})$, which in this scheme is commonly called as noninteracting susceptibility. For detailed information on technical implementation of this technique the reader is referred to Refs. [49,54]. This approach is applicable to low-dimensional magnets and has been used to describe the magnons in ultrathin films [91,49,54,56,55,145,57,146,147,58,148,149]. The main disadvantage of this scheme is that one has to start with reliable tight-binding parameters in order to have a direct comparison to the experiment. In many cases such parameters are not easily available and one has to perform electronic structure calculations.

Many-body perturbation theory (MBPT)

In the MBPT scheme, one calculates the dynamical susceptibility in a perturbative manner [150,151]. The dynamical susceptibility is given by:

$$\chi^{ij}(1, 2) = -i \langle \mathcal{T} [\hat{\psi}^i(\mathbf{r}_1, t_1), \hat{\psi}^j(\mathbf{r}_2, t_2)] \rangle, \quad (26)$$

where \mathcal{T} represents the time-ordering operator and $\hat{\psi}^i(\mathbf{r}_1, t_1)$ are the spin density operators with $i \in \{x, y, z, -, +\}$ ($-$ and $+$ represent the spin annihilation and creation operators, respectively).

The expectation value of $\hat{\psi}^i(\mathbf{r}_1, t_1)$ with respect to the many-body ground state $|0\rangle$ can be given in terms of single particle Green's function G and Pauli spin matrices σ as:

$$\langle \hat{\psi}^i(\mathbf{r}_1, t_1) \rangle = -i \sum_{\alpha, \beta} \sigma_{\beta, \alpha}^i G_{\alpha, \beta}(\mathbf{r}_1, t_1; \mathbf{r}_1, t_1^+). \quad (27)$$

The superscript $+$ indicates that the time variable is increased by an infinitesimal value ensuring a proper time ordering. The dynamical susceptibility can be calculated by the functional derivative with respect to the magnetic field:

$$\chi^{ij} = \frac{\delta \hat{\psi}^i(\mathbf{r}_1, t_1)}{\delta B_j(\mathbf{r}_2, t_2)}. \quad (28)$$

Green's function represented in Eq. (27) can be written in terms of a Dyson equation similar to the one in Eq. (24). This leads to the fact that the dynamical susceptibility can be written in terms of a noninteracting part and also a part which includes the electron–electron interactions in solid. In the scattering experiments e.g. INS and SPEELS the imaginary part of the susceptibility in energy (frequency) and momentum space $\Im \chi(\omega, \mathbf{q})$ is probed. For a direct comparison to the experiment, one should calculate the Fourier transformation of χ^{ij} . Şaşıoğlu et al. proposed a computational scheme based on the T -matrix approximation [53,152]. For decreasing the numerical costs they proposed a Wannier function approach. The numerical results for bulk ferromagnetic transition metals are in good agreement with the experimental data reported by neutron scattering experiments. This scheme is very suitable for the systems in which the electron correlations are strong. However, due to complexities of this scheme, its implementation to low-dimensional magnets is not done so far.

Linear response time-dependent density functional theory (LRTDFT)

In the LRTDFT scheme one takes advantage of the parameter-free description of the system when it is subjected to a dynamic magnetic field [153–157,126,50,158,159]. For that one needs to compute the susceptibility $\chi^{ij}(\mathbf{x}, \mathbf{x}', \omega)$ in two steps.

In the first step the so-called Kohn–Sham susceptibility $\chi_0^{ij}(\mathbf{x}, \mathbf{x}', \omega)$ is calculated by using:

$$\chi_0^{ij}(\mathbf{x}, \mathbf{x}', \omega) = \sum_{k,m} \sigma_{\alpha\beta}^i \sigma_{\gamma\delta}^j (f_k - f_m) \frac{\psi_k(\mathbf{x}\alpha)^* \psi_m(\mathbf{x}\beta) \psi_m(\mathbf{x}'\gamma)^* \psi_k(\mathbf{x}'\delta)}{\omega + (\epsilon_k - \epsilon_m) + i0^+}, \quad (29)$$

where $\mathbf{x}\alpha$ indicate the spacial and spin degree of freedom, $\psi_j(\mathbf{x})$ and ϵ_j denote the Kohn–Sham eigenstates and eigenvalues, respectively. $\sigma_{\alpha\beta}^0$ is the density operator and σ^i represent the Pauli spin matrices. $f_j(\epsilon_j)$ is the Fermi–Dirac distribution function. The 0^+ ensures that one deals with retarded quantities.

In the second step one computes the susceptibility, selfconsistently:

$$\chi^{ij}(\mathbf{x}, \mathbf{x}', \omega) = \chi_0^{ij}(\mathbf{x}, \mathbf{x}', \omega) + \sum_{k,l=0}^3 \int \int d\mathbf{x}_1 d\mathbf{x}_2 \chi_0^{ik}(\mathbf{x}, \mathbf{x}_1, \omega) \left(K_{xc}^{kl}(\mathbf{x}_1, \mathbf{x}_2, \omega) + \frac{2\delta_{k0}\delta_{l0}}{|\mathbf{x}_1 - \mathbf{x}_2|} \right) \chi^{jl}(\mathbf{x}_2, \mathbf{x}', \omega), \quad (30)$$

where $\delta_{ij} \equiv \sigma_{\alpha\beta}^0$ corresponds to the density operator and K_{xc}^{ij} is the so-called exchange–correlation kernel and is defined as the functional derivative of exchange–correlation potential with respect to the density. As in many cases of many-body problems the exact exchange–correlation potential is not known and one has to start with an approximation. For instance in adiabatic local density approximation it is approximated by the frequency independent part of the local spin density approximation exchange–correlation potential. One can show that in the case of a collinear ground state the induced transverse magnetization due to a transverse magnetic field results in an additional effective transverse exchange–correlation field. This means that magnons and non-spin-flip excitations are decoupled and hence one can separate the Dyson equation of the transverse magnetic susceptibility from the longitudinal one and also the charge response. Practically, it is sufficient to consider only the transverse components (xx and xy) of the magnetic susceptibility to calculate the magnons in collinear systems. For a direct comparison to the experimental results obtained by scattering techniques e.g. INS, ITS and SPEELS, one should calculate the Fourier transformation of $\chi^{ij}(\mathbf{x}, \mathbf{x}', \omega)$. The computational implementation of this scheme for calculating the magnon properties in ultrathin ferromagnetic films grown on nonmagnetic substrates is recently done by Buczek et al. [160,59,161,162,93,94].

As it is mentioned above, within the ETBT scheme the term describing the correlations in the system (the term Z in Eq. (22)) is not easily accessible. Lounis et al. suggested a way of solving this problem by using TDFT for calculating this term [60,61]. The scheme is similar to ETBT but is based on TDFT and thereby on the *ab initio* selfconsistent electronic structure calculation of the system. One can show that Z can be calculated based only on the Kohn–Sham susceptibility and the ground state magnetization [61]. This approach takes the advantage of Korringa–Kohn–Rostoker (KKR) Green functions. Although some simplifications are done with respect to the standard KKR methods, such as considering only d -states and neglecting the energy dependence of the wavefunctions, the agreement of the results with the experiment is rather good. The main advantage of this scheme is that it can be used to calculate the dynamical response of adatoms and clusters on surfaces as probed by ITS experiments [60,61,122].

6. Probing magnons by spin-polarized electrons

For the study of spin excitations in low-dimensional ferromagnets, initially an atomically clean sample has to be obtained. Such surfaces can be prepared by means of conventional thin film growth techniques under ultrahigh vacuum conditions. Usually, prior to the SPEELS measurements the films are magnetically saturated along the easy magnetization axis by applying a static magnetic field. The measurements are performed in the remanent state. As mentioned in Section 4.2.3, magnons carry a total angular momentum of $1\hbar$, therefore, they are created by minority electrons (see Fig. 7). Due to thermal fluctuations, a spin system possesses a large variety of magnons at a finite temperature. These are usually referred to as thermally excited magnons and are spread over a large momentum and energy space, depending on the temperature. The population of this class of magnons is given by Bose–Einstein statistics, which determines the statistical distribution of identical indistinguishable bosonic quasi-particles over the energy states in thermal equilibrium. In principle, the thermally excited magnons can be annihilated by majority electrons. A majority electron can be scattered into a minority one via the exchange scattering mechanism and hereby a magnon is annihilated (see Fig. 7). In this process, the energy of the electron in the final state is larger than the one in the initial state, and hence such a process can be observed in the energy gain region. The intensity of the peak associated with the magnon annihilation process depends on the population of the thermally excited magnons at the measurement temperature. The ratio between the gain and loss peak is given by a Boltzmann factor, which is about 0.17 for the magnons with an excitation energy of 46 meV at $T = 300$ K. It is nearly zero for $T = 10$ K. This means that at low temperatures the magnon annihilation process is expected to be suppressed and at high temperatures it is pronounced. Note that such a behavior is also expected for phonons that are also classified as bosons.

It is important to mention that in principle an electron beam with any polarization vector (or even an unpolarized beam) can be used to excite and probe magnons. However, the interpretation of data would not be as straightforward as in the case where the beam polarization is parallel and antiparallel to the sample magnetization (the quantization axis). We will discuss in Section 14 how a transversally spin-polarized beam can be used to excite and probe magnons in an ultrathin film with out-of-plane easy axis.

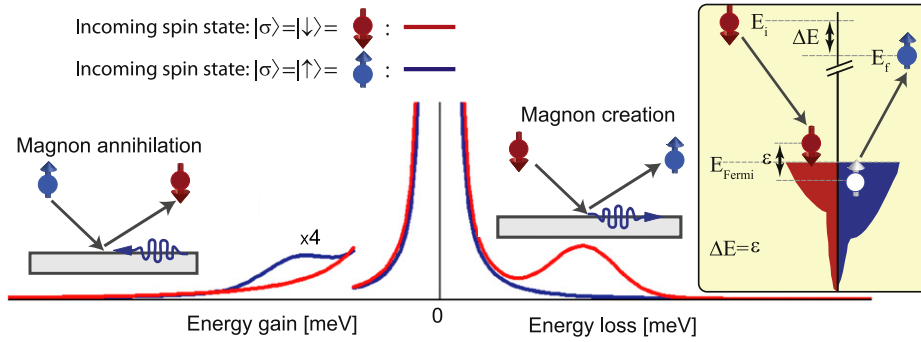


Fig. 7. A schematic representation of SPEELS spectra. The magnon excitation (creation) process takes place in the energy loss region when an incoming electron of minority spin state is scattered into an electron of majority spin state. The magnon annihilation process taking place in the energy gain region is accomplished with incident electrons of majority spin state. Inset provides detailed information on the magnon excitation process. An electron of minority spin state occupies an empty state above the Fermi level and an electron of majority spin character leaves the sample from a state below the Fermi level.

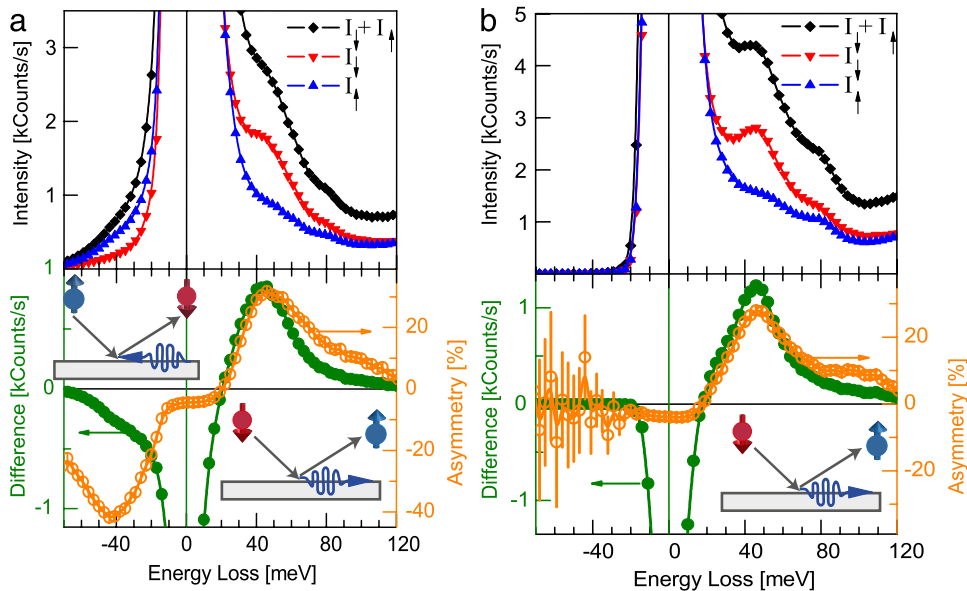


Fig. 8. SPEELS spectra measured at $\Delta K_{||} = 0.5 \text{ \AA}^{-1}$ on an ultrathin Fe(110)/W(110) film with a thickness of 2 ML at (a) 300 K and (b) 10 K. The upper panels show the spin up (I_{\uparrow}), spin down (I_{\downarrow}) and the sum ($I_{\uparrow} + I_{\downarrow}$) spectra. The lower panels show the difference ($I_{\downarrow} - I_{\uparrow}$) and asymmetry ($(I_{\downarrow} - I_{\uparrow}) / (I_{\downarrow} + I_{\uparrow})$) spectra. The magnon creation and annihilation processes are schematically sketched in the insets.

Source: Reprinted figure with permission from Zakeri and Kirschner [78].
© 2013, by Springer.

An example of the experimental data is provided in Fig. 8 where the SPEELS spectra measured at different temperatures are presented. The spectra are recorded on a 2 monolayer (ML) thick Fe(110) film grown on W(110) at a wave vector of 0.5 \AA^{-1} . The magnon propagation direction in this particular experiment is along the [001]-direction of the Fe(110) surface ($\vec{\Gamma}-\vec{H}$ direction of the surface Brillouin zone). For each case the spectra for spin-up (I_{\uparrow}) and spin-down (I_{\downarrow}) electrons are measured. In addition, the sum ($I_{\downarrow} + I_{\uparrow}$), difference ($I_{\downarrow} - I_{\uparrow}$), and asymmetry $[(I_{\downarrow} - I_{\uparrow}) / (I_{\downarrow} + I_{\uparrow})]$ spectra are also presented. Let us first start with Fig. 8(a). It is apparent that the spectra are dominated by the presence of the quasi-elastic peak at $E = 0 \text{ meV}$. The magnon creation and annihilation peaks are located beside the quasi-elastic peak in the energy loss and gain region, respectively. These two processes are sketched schematically in the insets of Fig. 8(a). The asymmetry curve shows a change in the sign from negative to positive, when going from gain to loss region. The maxima (in the loss region) and the minima (in the gain region) are the places where the excitation and annihilation processes take place. If one neglects the spin-orbit coupling effects in the system the maxima and minima should be located at the same energies (one negative and the other positive). As it was mentioned earlier, at low temperature where the population of the thermally excited magnons is very low, the magnon annihilation peak is supposed to be strongly suppressed. This fact can be clearly seen in Fig. 8(b), where the measurements at 10 K, performed on the same sample, are presented. No trace of magnon annihilation could be detected neither in the difference nor in the asymmetry spectrum. In order to obtain the magnon dispersion relation, usually the spectra are recorded for different wave vectors [163–168,78]. The desired wave vector is achieved by changing the scattering geometry.

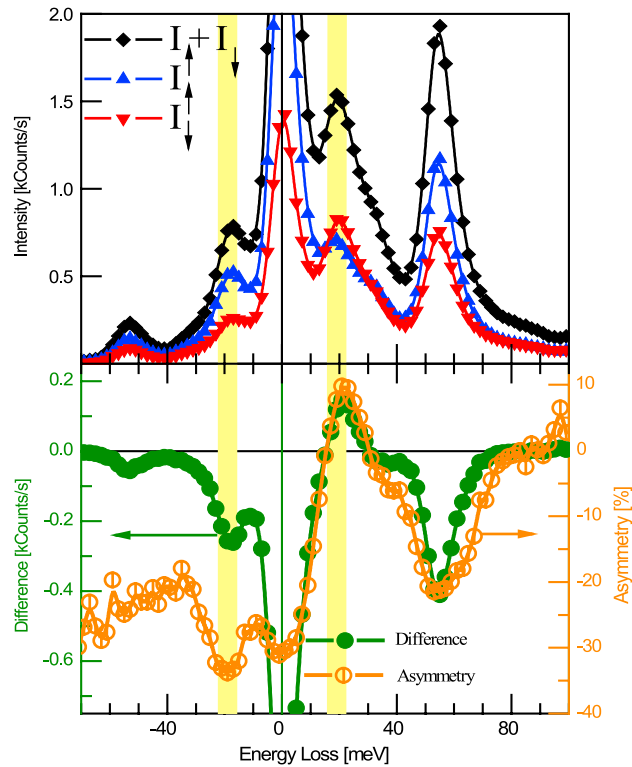


Fig. 9. SPEELS spectra measured on the Fe(001)–O(1 × 1) surface at $T = 300$ K and $\Delta K_{\parallel} = 0.3 \text{ \AA}^{-1}$. The upper panel shows the spin up (I_{\uparrow}), spin down (I_{\downarrow}) and the sum ($I_{\uparrow} + I_{\downarrow}$) spectra. The lower panel shows the difference ($I_{\downarrow} - I_{\uparrow}$) and asymmetry ($(I_{\downarrow} - I_{\uparrow}) / (I_{\downarrow} + I_{\uparrow})$) spectra. The vertical yellow lines mark the position of the peaks resulting from the magnon excitation (energy loss) and annihilation (energy gain) processes.

Source: Reprinted figure with permission from Zhang et al. [169].

© 2011, by the American Physical Society.

7. Simultaneous probing of magnons and phonons

In principle, both magnons and phonons can be excited by electrons. Since both kinds of excitations may take place in the same energy window, it is rather difficult to distinguish between them experimentally. However, it has been shown that using the spin degree of freedom of spin-polarized electrons opens a possibility to separate magnons from phonons [169]. As magnons carry a total angular momentum of $1\hbar$, they can only be excited by the incidence of minority electrons. The time reversal process happens for the incidence of majority electrons, which leads to the magnon annihilation. This fact would lead to a sign change in the asymmetry curve in gain and loss regions (see the lower panel of Fig. 8(a)).

In the case of phonons, the situation is different. Since phonons are spin-independent quasi-particles, they can be created and annihilated by the incidence of electrons with any spin direction. Note that the process which leads to phonon creation can also be mediated by the exchange process (the exchange of the electrons with the same spin, see the discussion in Section 4.2.3). The particular dependence of magnon creation and annihilation on the spin of the incident electrons, as it is different from phonon excitations, is a fundamental feature, which can be used to distinguish between magnons and phonons in spin-polarized electron scattering experiments. The best way to identify the nature of an excited quasi-particle (magnon or phonon), is to compare the sign of the asymmetry curve in loss and gain regions. An example is provided in Fig. 9, where the spectra of an oxygen passivated Fe(001) film, measured at $T = 300$ K and $\Delta K_{\parallel} = 0.3 \text{ \AA}^{-1}$, are presented. The magnon and phonon excitations coincide within the same energy window. Interestingly, the intensity of all excitations depends on the spin orientation of the incoming beam. As it is discussed above, the identification of phonons and magnons can be done by looking at their different spin nature. The asymmetry of loss and gain regions of the peaks marked by the vertical yellow lines in Fig. 9 (at energies of ± 19 meV) changes the sign, and hence the peaks are associated with magnon excitations. The asymmetry of the other excitations has the same sign and almost identical magnitudes; therefore, they are caused by phonon excitations. It is interesting to mention that in the case of the O/Fe(001)–p(1 × 1) surface the asymmetry of the phonon induced peaks is always negative. A complementary experiment showed that the asymmetry of the phonon peaks follows the one of the quasi-elastic peak [169].

In order to clarify the origin of the observed spin asymmetry of the phonons, the spin-resolved intensities for elastically and inelastically scattered electrons have been measured as a function of the incident electron energy. The results of those measurements are summarized in Fig. 10. The intensity of the scattered beam is measured for the electrons with the

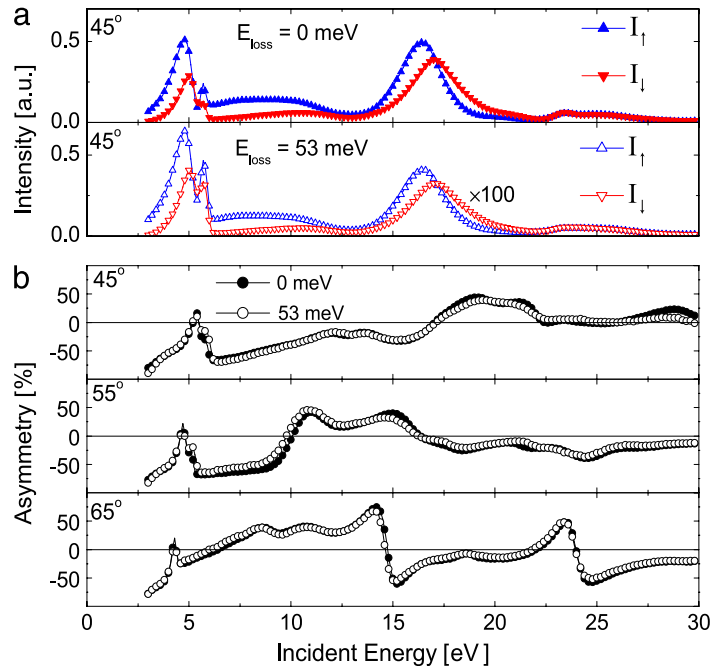


Fig. 10. (a) Intensity of scattered electrons as a function of the energy of the primary beam measured in the specular geometry and for elastically ($E_{\text{loss}} = 0$, upper panel) and inelastically ($E_{\text{loss}} = 53$ meV, lower panel) scattered electrons. The angle of incidence was 45° and the data are recorded for incoming electrons of spin-up (I_\uparrow) and spin-down (I_\downarrow) character. (b) The asymmetry curves $[(I_\downarrow - I_\uparrow)/(I_\downarrow + I_\uparrow)]$ for the elastically and inelastically scattered electrons measured at the specular geometry and for different angles: 45° , 55° and 65° .

Source: Reprinted figure with permission from Zhang et al. [169].
© 2011, by the American Physical Society.

energy loss of zero ($E_{\text{loss}} = 0$ meV i.e. the elastically scattered electrons) and also for the electrons with an energy loss of $E_{\text{loss}} = 53$ meV, equal to a phonon energy (the inelastically scattered electrons). The intensity profiles are presented in Fig. 10(a). It has been observed that the intensities of elastic and inelastic electrons are very similar, except for the fact that the intensity of the inelastically scattered electrons is smaller by two orders of magnitude. Hence, the resulting spin asymmetry for both elastically and inelastically scattered electrons is exactly the same (see the upper panel of Fig. 10(b)). The asymmetry depends strongly on the energy of the incident electrons. It may even change the sign while changing the electrons energy. The intensity profiles of both elastically and inelastically scattered electrons depend on the scattering geometry i.e. scattering angle. Therefore, one would expect that the asymmetry curve should also depend on the scattering angle. This has been verified by performing the same experiment at different scattering angles. As it is apparent from the two lower panels of Fig. 10, the shape of the asymmetry curve is different for different scattering angles. However, the asymmetry curve of the inelastic beam follows exactly the one of the elastic beam. This experiment as a solid experimental evidence demonstrates that the origin of the observed asymmetry for both elastically and inelastically scattered electrons is the same.

It is well-known that the spin asymmetry of the elastically scattered electrons is caused by the exchange scattering, as the dipolar scattering does not involve the electron's spin. In this case the exchange scattering only involves the electrons with the same spin orientation (incoming and outgoing electrons have the same spin character, see the discussion in Section 4.2.3). Otherwise, it would lead to a change of the energy of the electron (as the incident electron must occupy an unoccupied state above the Fermi level, the one with the opposite spin shall leave the system from a state below the Fermi level, and this leads to an energy difference between the initial and final states). Since the asymmetry curve of the inelastic excitation at 53 meV is almost identical to the one of the elastically scattered electrons, independent of the scattering geometry, therefore, the physical origin of the observed large spin asymmetry for both the elastic and inelastic intensities is very likely the same. The origin of the asymmetry is mainly the exchange scattering of electrons of the same spin character. In other words, the similarity of the spin asymmetry for the elastic and inelastic scattering strongly suggests that the inelastic peak at 53 meV is also of the non-spin-flip nature and the observed large asymmetry of this peak is due to the exchange of the electrons with the same spin.

The dispersion relation of magnons and phonons could be measured simultaneously by repeating the experiment for different wave vectors and the dispersion branches could be separated based on their different spin nature. A careful fitting of the spectra using a superposition of Gaussian profiles revealed five excitation branches in both energy loss and energy gain regions. Here, the choice of Gaussian is done for simplicity. It provides a rather good estimation of the excitation energies. Note that in order to properly estimate the linewidth broadening, associated with the finite lifetime effects, one should fit the spectra with a convolution of Lorentzian and Gaussian profiles in which the Lorentzian represents the intrinsic excitation peak and the Gaussian represents the instrumental broadening (see Section 10 for an extended discussion). Fig. 11 shows

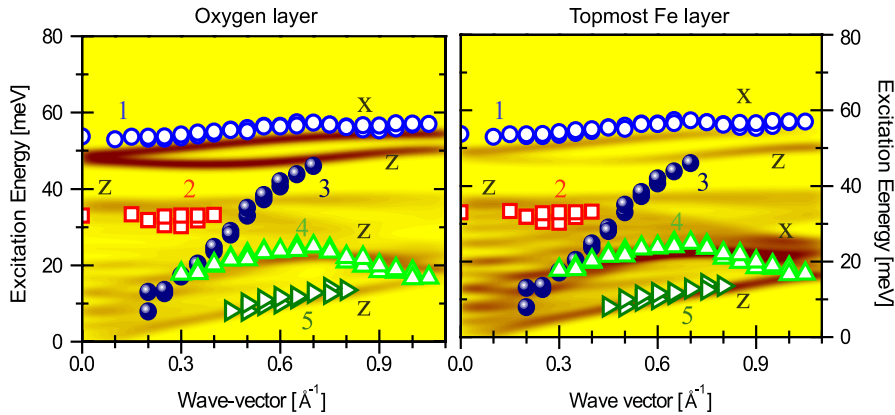


Fig. 11. Dispersion relation of all elementary excitations probed on the Fe(001)–O(1 × 1) surface. The color map represents the theoretically calculated phonon spectral density projected on the oxygen layer (left) and the topmost Fe layer (right). Open symbols denote the phonon branches numbered by 1, 2, 4 and 5; filled symbol denotes the magnon branch and is numbered by 3. Letters “x” and “z” near each phonon band denote displacement directions of the corresponding phonon modes.

Source: Reprinted figure with permission from Zhang et al. [169].

© 2011, by the American Physical Society.

the dispersion relation of magnons and all different kinds of phonons measured on the O/Fe(001)–p(1 × 1) surface. One clearly observes four different phonon modes and one magnon mode. Phonon branches are represented by open symbols, while the magnon branch is shown by filled symbols. The magnon branch disperses from 16 to about 40 meV as the wave vector increases from 0.2 to 0.7 Å^{−1}. Magnon excitation peaks become very broad at high wave vectors. This broadening can be explained by the strong decay of magnons in itinerant electron systems. We will discuss this point in Section 10.

ab initio calculations in the framework of the direct calculations of the force matrix [170] can account for a more precise description of the observed phonon modes in the system. The results of the calculations are shown in Fig. 11. Based on the theoretical calculations, the mode numerated as “5” with the lowest energy originates from the acoustical z-polarized transversal oscillations of atoms located at the topmost Fe and O layers. It is the so-called Rayleigh mode of the surface, which has been also observed in the He-atom scattering experiments [171]. The next phonon mode “4” shown in Fig. 11 with upward-oriented triangles is also localized in the two topmost layers. In the Fe layer mode “4” is a longitudinal acoustic phonon with x polarization, while in the oxygen layer it is transversal with z polarization. Phonon mode “2”, plotted with open squares in Fig. 11, is a z-polarized surface resonance of the phonons of the Fe slab. Finally, the two high-energy branches at 50 meV are associated with the optical z-transversal and x-longitudinal phonons localized mostly on the oxygen sites. In the experiment, however, only one branch is observed (branch “1”). The anharmonicity of oxygen vibrations, which couples the x- and z-polarized modes might be a reason for such discrepancy between the theory and experiment. The mode shown by filled symbols is a magnon mode.

8. Magnons in a ferromagnetic monolayer

One of the most fundamental aspects in the field of spin excitations in low-dimensional magnets is the magnon spectrum in a real two-dimensional spin system e.g. a ferromagnetic monolayer grown on a nonmagnetic substrate. Here, the fundamental questions are: if the magnons in real two-dimensional ferromagnets do exist, is it possible to see their signature of excitations in SPEELS spectra? How does the magnon dispersion relation look like in a ferromagnetic monolayer grown on a nonmagnetic substrate?

In order to address these questions SPEELS experiments have been performed on a prototype ferromagnetic monolayer; one atomic layer Fe(110) grown on W(110) [172]. Since the Curie temperature of the Fe monolayer on W(110) is below room temperature ($T_c \simeq 223$ K [173]), the spectra have been recorded at low temperatures. It has been observed that in the Fe monolayer the magnon excitations occur at very low energies. In addition to that the spectra are very broad. The measured magnon dispersion relation is presented in Fig. 12. For a better comparison the results of the surface mode of a thicker Fe film (with a thickness of 24 atomic layers) grown on the same substrate are also presented. Fig. 12 which provides a direct comparison between the results of the monolayer Fe and the surface mode of Fe(110), reveals that the magnon energies in the Fe monolayer are very small. Experimental results on magnon dispersion relation measured at 10 K showed that the magnon energies are slightly higher (about 10 meV) with respect to the ones measured at 120 K. This observation indicates the effect of the temperature on magnon energies.

As it is mentioned in Section 2.2 the nature of spin excitations in itinerant ferromagnets is rather complicated and the Heisenberg description of magnons would not lead to an appropriate description of the system. However, one may put the interaction in a form of an effective exchange coupling, in order to estimate the strength of the coupling in the system. Taking this simple approach, one can then derive an equation for the magnon dispersion relation as discussed in Section 2.3. Fitting the experimental results with the calculated magnon dispersion relation within this model, results in a very small

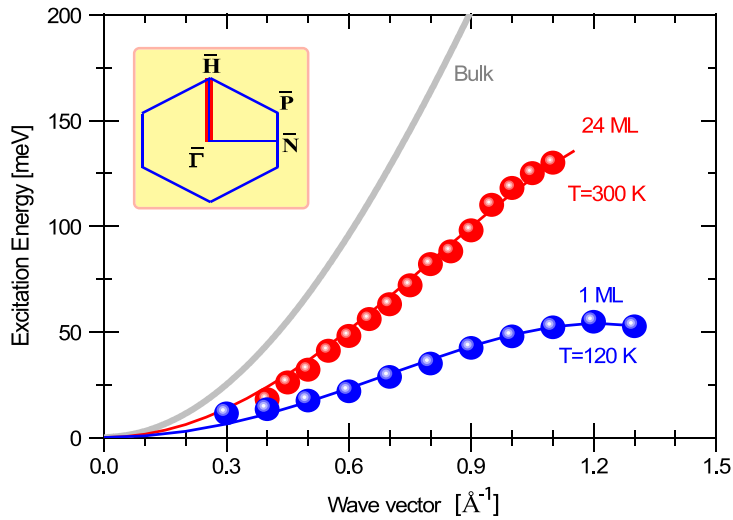


Fig. 12. The magnon dispersion relation of 1 ML Fe on W(110) measured at 120 K along the $\bar{\Gamma}$ – \bar{H} direction of the surface Brillouin zone (see the inset). The dispersion relation of the acoustic surface mode of a 24 ML thick sample is also shown. Source: Data are taken from [172]. The results are compared to the one of the bulk Fe [30]. © 2009, by the American Physical Society.

effective exchange interaction ($J_{\text{eff}} = 11$ meV) and an effective magnetic anisotropy of $K_{\text{eff}} = 2.3 \pm 1.3$ meV. These results are in reasonable agreement with the earlier theoretical [80] and experimental works obtained using static magnetic measurements [174]. Magnons in the Fe monolayer are much softer than the lowest-energy (acoustic) surface mode of Fe(110). Fitting the experimental results with the well-known parabolic dispersion (Eq. (9)) leads to a determination of the magnon stiffness constant, D . It is found that D for the monolayer system is by a factor of 2.2 smaller than the one obtained for the Fe(110) surface ($D_{\text{ML}} = 74$ meV \AA^2 and $D_{\text{surf.}} = 160$ meV \AA^2). It is only about one-fourth of the value measured for bulk Fe by INS [175,32,176].

Comparison to the theory

The magnon dispersion relation in the Fe monolayer on W(110) has been calculated by means of different theoretical approaches [54–56,80,57,148,58,149,161,140]. Fig. 13 provides a comparison among the results of calculations obtained by different groups. The calculations by Muniz et al. [54] and Costa et al. [148,149] are based on ETBT, the results obtained by Buczek et al. [161] are based on LRTDFT and the results by Udvardi and Szunyogh [81] are based on an adiabatic approach. The difference between Refs. [54,148] and Ref. [149] is that in the latter case the TB parameters are obtained directly from real-space linear muffin-tin orbital atomic sphere approximation calculations and by KKR-based electronic-structure calculations. The agreement between the theory and the experiment is much better in the second case. It seems that the results depend sensitively on the parameters used as the starting point of the calculations. In the LRTDFT based calculations the implementation of the linear response DFT has been performed within the KKR Green's function method [161,93]. Similar to the results obtained by ETBT [54,148,149], these calculations also suggest a strong magnon damping in this system [161,94]. The results have been compared to the ones of a free-standing Fe film. It has been suggested that the presence of the W substrate leads to a strong renormalization of the magnons energy, in addition to the fact that it causes the strong damping [161].

The magnon softening in the Fe monolayer may have different origins. The first one might be the temperature effect. Since the experimental results are obtained at 120 K, which is half of the Curie temperature of the system, this may cause the softening of the magnons. The second origin might be the strong hybridization of the film with the substrate and change in the electronic structure of the film caused by the W(110) substrate. The third origin might be the influence of the DM interaction, which has been shown that is very important for the Fe films grown on W(110). We will come back to this point in Section 12.

The experimental data are satisfactorily reproduced by combining the first principles calculations with the so-called atomistic spin dynamics simulations [140]. This approach enables one to investigate the effect of temperature on the magnon properties. The authors could confirm that the temperature effects and the chemical relaxations, which influence the electronic hybridization of the Fe film and W(110), lead to this magnon softening.

9. Atomic structure and magnon dispersion relation

9.1. Coordination number

In order to investigate the dimensionality effects on magnons, the magnon energy as a function of the film thickness for Fe(110) films on W(110) has been measured [177]. The results of those investigations are summarized in Fig. 14. In order

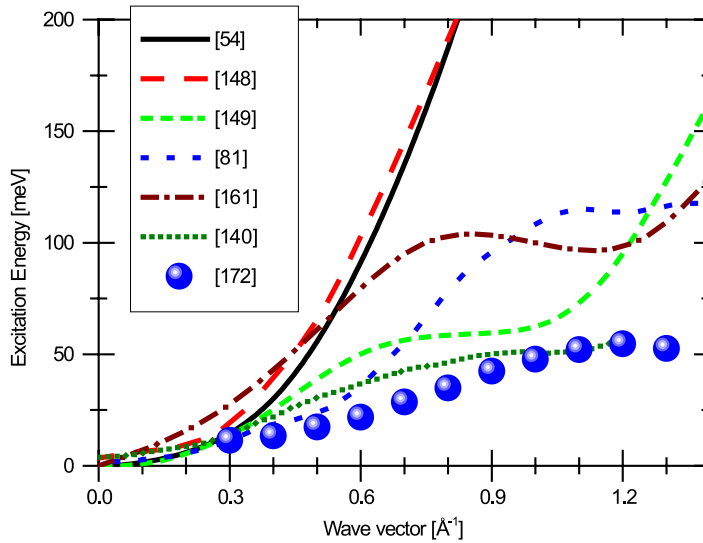


Fig. 13. The magnon dispersion relation of the Fe monolayer on W(110). A comparison among the results of calculations based on different approaches. The wave vector is along the $\bar{\Gamma}$ - H direction of the surface Brillouin zone. The calculations by Muniz et al. [54], Costa et al. [148,149] are based on ETBT, the results obtained by Buczek et al. [161] are based on LRTDFT and the results by Udvardi and Szunyogh [81] are based on an adiabatic approach. The difference between Refs. [54,148] and Ref. [149] is that in the latter case the TB parameters are obtained directly from real-space linear muffin-tin orbital atomic sphere approximation calculations and by KKR-based electronic-structure calculations. The results by Bergman et al. [140] are based on a combination of DFT calculations and spin dynamics simulations at $T = 120$ K. Except the results of Ref. [140] all the other calculations are for $T = 0$ K. The experimental results represented by solid circles are recorded at $T = 120$ K [172].
Source: The data taken from Refs. [54,81,140,148,149,161,172].

to have a better comparison of the energies, recorded for different wave vectors, the energies are normalized to the wave vector. It is apparent from Fig. 14 that the magnon energy increases by a factor of 2.2 while changing the film thickness from 1 to 2 atomic layers. To explain these results one may use simple arguments based on an adiabatic approximation. Consider one atomic layer of Fe pseudomorphically grown on W(110). In such a case the exchange coupling is confined in the plane of the film. Due to a lower coordination number one would expect lower magnon energies for the ferromagnetic monolayer with respect to a 2 ML film. The sudden increase of the magnon energy when changing the film thickness from 1 to 2 is a direct consequence of the increase of the coordination number. In the case of the 2 ML sample the Fe atoms sitting in different layers are also strongly coupled. The coupling of Fe atoms within each layer is referred to as *intralayer* coupling and the coupling of the atoms from different layers is referred to as *interlayer* coupling. The calculated effective coupling for a 2 ML sample shows that the nearest neighbor interlayer coupling is about 27 meV and the nearest neighbor intralayer coupling is about 20 meV (a detailed information is provided in Section 9.3 and Fig. 16). For these calculations, it is assumed that the in-plane lattice constant of Fe is the same as the one of the underlying W(110) surface. The out-of-plane lattice constant is taken from the surface X-ray diffraction experiments [178]. If further increasing the film thickness does not change the film structure, one would expect the same magnon energy for a 3 ML film as it is predicted by the theory (see Fig. 14). However, it is known for Fe films on W(110) that the films start to relax when the thickness is larger than 2 ML. The lattice relaxation has a direct consequence on the magnon energy and is discussed in the next section.

9.2. Lattice relaxation

Taking into account the lattice relaxation one can explain the decrease of the magnon energy for the 3 ML sample. The magnon energy reaches an asymptotic value for films thicker than 5 ML where the structure is transformed into a bulk like film.

Another result of the calculations is that the mode seen in the experiment is a surface mode, since the main contribution to this mode is coming from the surface layer. There are however cases in which the lowest-energy magnon mode (usually referred to as acoustic mode) originates mainly from the interface layer. This unusual case happens when the effective exchange coupling in the interface layer is smaller than the one in the surface layer. We will come back to this point in Section 13.

9.3. Lattice modification

The modern methods of the fabrication of low-dimensional structures allow creating materials of given chemical content with different atomic structures. For instance by introducing a thin Au buffer layer between the Fe film and the W(110)

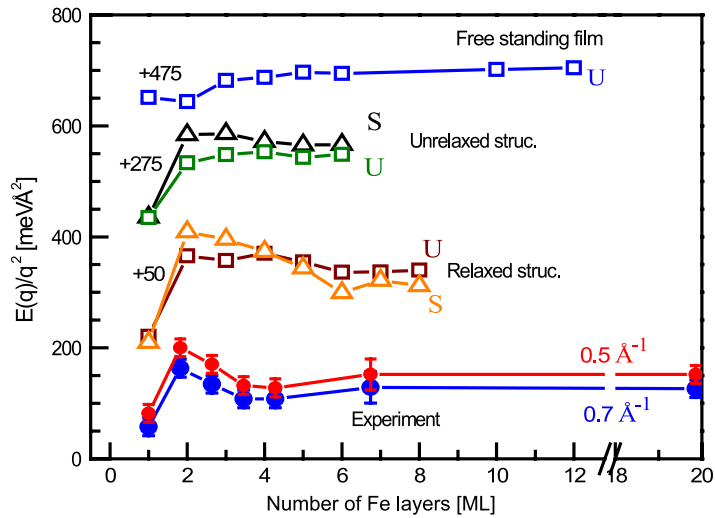


Fig. 14. Normalized magnon energy as a function of the film thickness: experiment and theory. Letters U and S denote the uniform and surface modes, respectively. In the uniform (surface) mode the amplitude of the moments is assumed to be equal in all atomic layers (maximum in the surface layer). For all theoretical curves $\Delta K_{\parallel} = 0.5 \text{ \AA}^{-1}$.

Source: Reprinted figure with permission from Zhang et al. [177].
© 2010, by the American Physical Society.

substrate one can change the Fe surface structure from bcc-like stacking with (110) surface to fcc-like stacking with (111) surface orientation [179]. In order to investigate the effect of the lattice modification on the magnon dispersion relation, the Fe film thickness has been kept unchanged (2 atomic layers) and just its structure is changed by introducing the Au buffer layer [179]. The magnon dispersion relation measured for both Fe(110)/W(110) and Fe(111)/Au/W(110) is presented in Fig. 15(a). The results indicate a large difference in the magnon dispersion relation of the two systems. These changes could be understood on the basis of the first principles calculations in the adiabatic approximation. The change in the Fe lattice has a direct consequence on the magnetic exchange interaction in the film. Although the interlayer exchange constants increase when changing the lattice structure from simple bcc stacking to the new (111)-close-packed structure, the intralayer exchange constants decrease. Since the intralayer coupling constants are counted more effectively, the dispersion relation of the Fe(111)/Au/W(110) system is lower in energy with respect to the one of the Fe(110)/W(110) system (the number of nearest neighbors in each layer is 4 while in the neighboring layer is 2). A comparison of the exchange constants for two systems, Fe/W(110) and Fe/Au/W(110), shows that the interlayer and intralayer coupling constants feature opposite trends (see Fig. 16(a)–(c)). As an example, the largest interlayer coupling constant J_{\perp} increases from 27 meV in Fe(110)/W(110) to 69 meV in Fe(111)/Au/W(110) whereas the largest intralayer coupling constant J_{\parallel} decreases from 20 to 14 meV for the interface layer, and from 13 to 9 meV for the surface layer. The analysis shows that the softening of the magnons in Fe(111)/Au/W(110) is the consequence of the decreased intralayer exchange parameters that overcomes the opposite trend of increasing the exchange parameters between the layers.

Calculations showed that increasing the interlayer distance in the Fe(110)/Au/W(110) structure leads to an expected decrease of the interlayer exchange parameters (see Fig. 16(a)). This is a consequence of the decrease of the interlayer hybridization. At the same time, an increase in the intralayer exchange parameters was observed (see Fig. 16(b) and (c)). Interestingly, this increase takes place for unchanged interatomic distances within the layers. This fact is a consequence of complex reconstruction of the electronic structure due to the increase of the interlayer distance. While changing the interlayer distance of Fe layers from 1.71 to 2.09 Å, the nearest neighbor intralayer coupling increases by a factor of 1.5 and 2.3 for the atoms in the interface and surface layer, respectively. In order to shed light onto the origin of this effect, one may carefully analyze the change in the density of states of different atomic orbitals. Fig. 16(d) and (e) show the spin- and orbital-resolved DOS of 3d electrons calculated for different interlayer distances for Fe(110)/Au/W(110). The projected DOS of different orbitals are plotted separately. The 3d states responsible for the interlayer hybridization (d_{xz} , d_{yz} , and d_{z^2}) appear substantially higher in energy than the states responsible for the intralayer hybridization ($d_{x^2-y^2}$ and d_{xy}). With increasing interlayer distance all states move to lower energies as a consequence of decreasing 3d band width. However, this shift is more important for d_{xz} , d_{yz} , and d_{z^2} states, since $d_{x^2-y^2}$ and d_{xy} are located well below the Fermi level for the smallest value of the interlayer distance. Increasing the interlayer distance increases the spin-down density of 3d states near the Fermi level. The appearance of a large number of states near the Fermi energy is an important factor in the enhancement of intralayer exchange interaction. These results clearly indicate that the magnetic properties of complex systems cannot be understood without careful microscopic study of the exchange interaction. In addition, the evolution of the electronic structure cannot be separated into features related to the interlayer and intralayer distances since the influences of both distances are strongly interconnected [179].

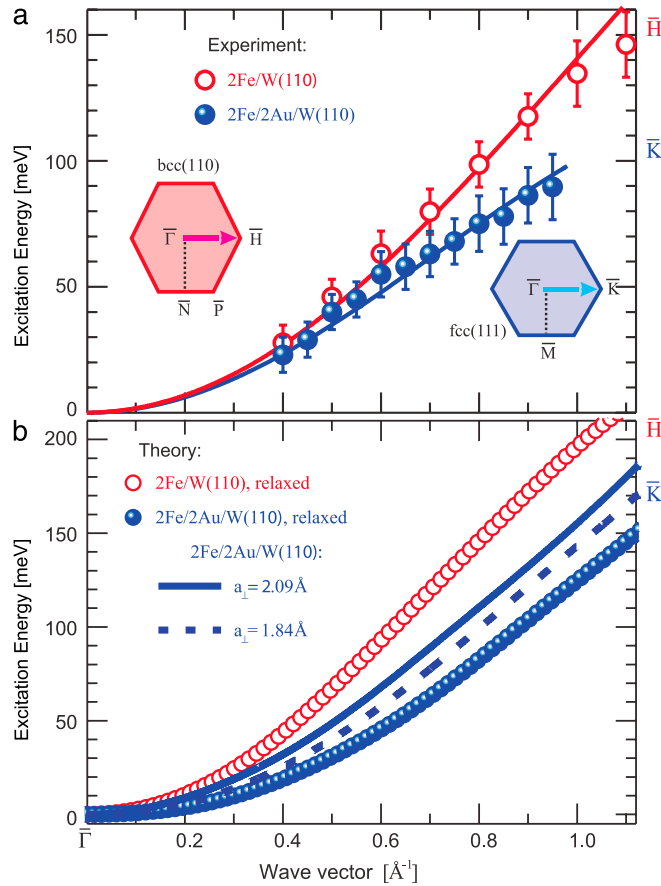


Fig. 15. (a) The magnon dispersion relation measured on a 2 ML Fe film on 2 ML Au on W(110) and a 2 ML Fe film directly grown on W(110). The symbols represent the experimental results and the solid lines are the guide to the eyes. (b) Theoretical magnon dispersion relation for the same systems. The symbols represent the results of the calculations for the relaxed structure. The lines are the results for the Fe/Au/W(110) system calculated for different values of Fe interlayer spacing, a_{\perp} . Insets show the surface Brillouin zone. Source: Reprinted figure with permission from Chuang et al. [179]. © 2012, by the American Physical Society.

10. The magnon lifetime

As discussed in Section 1 one of the key properties of quasi-particles is their lifetime. In this section we shall review the experimental findings regarding magnons lifetime. These findings may help for a better understanding of the magnetic damping mechanism of high-energy magnons in low-dimensional systems and a possible way of tuning magnetic relaxation in ferromagnets. They may also offer a way of estimating the ultimate time scale of magnetic switching in low-dimensional ferromagnets.

The broadening of the magnon excitation peak provides a way of estimating the magnon lifetime. In the SPEELS experiments one usually analyzes the difference spectra ($I_{\text{Diff}} = I_{\downarrow} - I_{\uparrow}$). To extract the intrinsic linewidth, the data are fitted by using a convolution of a Gaussian and a Lorentzian function, in which the Gaussian represents the instrumental broadening and the Lorentzian represents the intrinsic magnon signal. Doing so one realizes that the intrinsic linewidth of magnon excitations is typically from 20 up to a few hundreds of meV. Note that if the spectra are not spin-resolved one cannot obtain the difference spectra. In such a case one may analyze the total spectra. Such analysis are performed for an 8 ML Co film on Cu(001) in Ref. [180]. The linewidth broadening has been found to be very similar to the results obtained based on the analysis of the difference spectra. As an example, a fit through the data measured on 2 ML Fe(110)/W(110) at $\Delta K = 0.6 \text{\AA}^{-1}$ shows that the intrinsic linewidth of the magnon is about $42 \pm 7 \text{ meV}$, while the instrumental broadening is about 20 meV. The large broadening of the loss spectrum indicates that magnons are strongly damped in time. The magnon lifetime can be obtained from the Fourier transform of the magnon signal. The Fourier transform of the Lorentzian in energy (or frequency) domain is an exponential decay in the time domain, $\exp(-t\Gamma/2\hbar)$, where Γ represents the intrinsic linewidth of the Lorentzian peak in energy and \hbar is the reduced Planck constant. The lifetime $\tau = 2\hbar/\Gamma$ is usually defined as a time in which the amplitude drops to its e^{-1} value. The magnon lifetime obtained using this approach is plotted in Fig. 17 for two systems; 2 ML Fe(110)/W(110) and 8 ML Co(100)/Cu(100). The lifetime depends strongly on the wave vector. It is about 100 fs

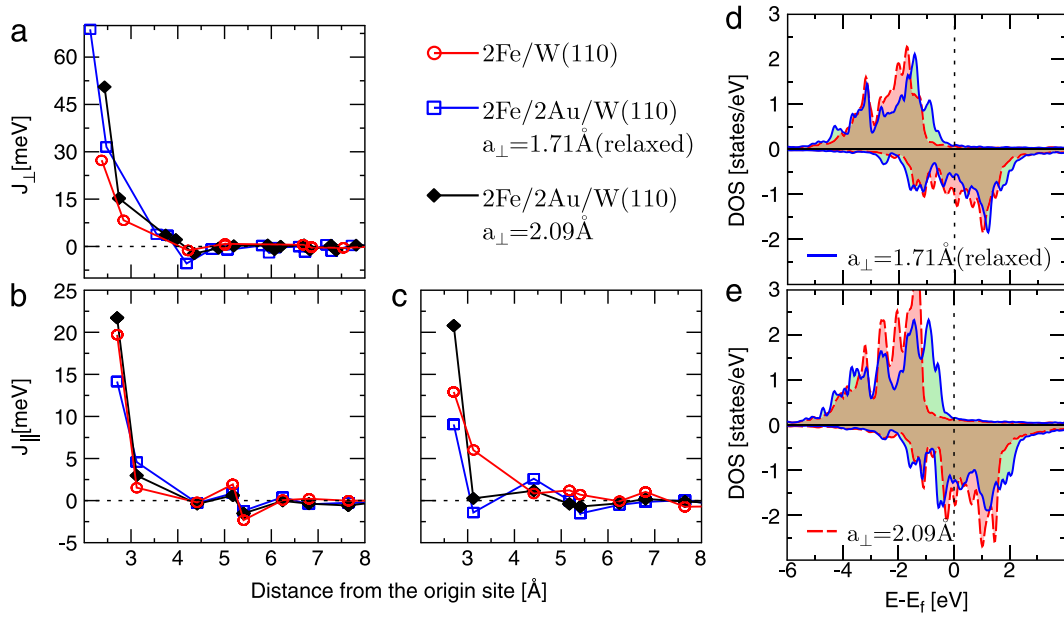


Fig. 16. Calculated site-resolved interlayer J_{\perp} (a) and intralayer J_{\parallel} exchange constants for the atoms located in the interface layer (b) and in the surface layer (c). Open and filled symbols represent the calculations for the relaxed and expanded structures, respectively. Spin-resolved DOS of $3d$ states in $2\text{Fe}/2\text{Au}/\text{W}(110)$, separated in a part with d_{xy} and $d_{x^2-y^2}$ states (d) and a part corresponding to d_{xz} , d_{yz} and d_{z^2} orbitals (e). The solid and dashed lines represent the results for relaxed and expanded structures, respectively.

Source: Reprinted figure with permission from Chuang et al. [179].

© 2012, by the American Physical Society.

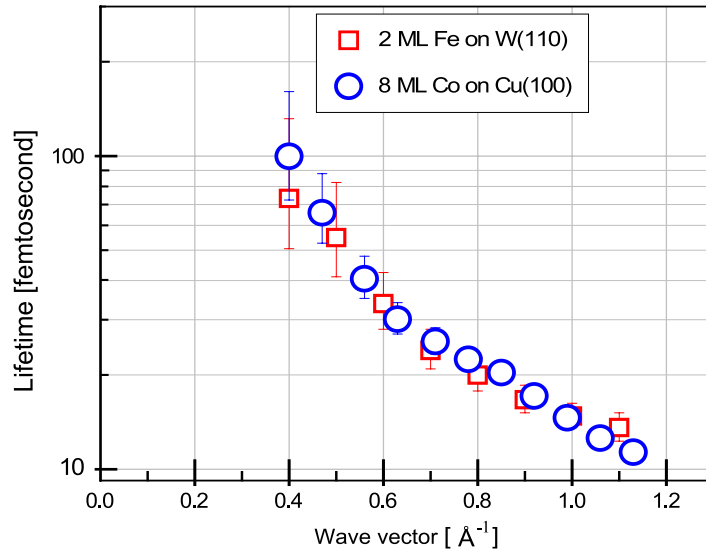


Fig. 17. The magnon lifetime as a function of the in-plane wave vector in a semi-logarithmic plot. The data are for 2 ML body-centered cubic Fe(110) film grown on W(110) (open squares) and an 8 ML face-centered cubic Co(100) film grown on Cu(100) (open circles). The Brillouin zone boundary for Fe/W(110) is at 1.5 while for Co/Cu(100) is at 1.23Å^{-1} .

Source: Reprinted figure with permission from Zhang et al. [181].

© 2012, by the American Physical Society.

at $\Delta K_{\parallel} = 0.4\text{Å}^{-1}$ and decreases to a value of about 10 fs for large wave vectors. Surprisingly, it is found that the lifetime for these two different systems is very similar in spite of the fact that the magnon energies are by a factor of two different.

Comparing to the spin relaxation of a single atom on the insulating substrate, whose relaxation time is about 10^{-7}s [182], the lifetime of magnons in thin ferromagnetic films is almost 10^7 times shorter. Such a short lifetime of high-energy magnons is attributed to the strong damping due to the presence of the conduction electrons in the metal film and the substrate [56,57,93]. Since the high-energy magnons are a coherent superposition of the correlated electron-hole pairs across the

Fermi level, their damping may be regarded as the results of the decay of these collective magnons into the available Stoner states near the Fermi level. It has been shown that the Stoner excitations in the surface states play an important role in the decay effect [119,94,122]. If the ferromagnetic film is grown on a metallic substrate, the states of the film may hybridize with the ones of the substrate. If the hybridization of the electronic states of the film with the ones of the substrate is such that a large number of Stoner states are formed near the Fermi level, the lifetime of magnons will be very short. In Refs. [93,94] it has been discussed that the key point to understand the strong damping of magnons in ultrathin magnetic films grown on a substrate is the formation of the interfacial electronic complexes at the interface. In particular, if the substrate features surface states, these states can, in principle, hybridize very efficiently with the states of the magnetic film and form the interfacial electronic complexes. Due to the formation of the electronic complexes, a large number of Stoner states can appear near the Fermi-level. In such cases the magnons excited in the magnetic film will decay rather quickly. Interestingly, both W(110) and Cu(001) possess prominent surface states. The similarity of the magnon lifetime in Fe and Co films, in spite of the fact that the magnon energy in the Co(100) film is almost twice of that in the Fe(110) film, may indicate that magnons can experience similar damping effects even though the electronic band structure of two systems are different.

Besides the intrinsic damping effects due to the Stoner excitations, it has been proposed that thermal effects may also play a role in the broadening of magnon peaks [141]. However, experiments performed on a 2 ML Fe film at different temperatures revealed that the temperature dependence of the intrinsic linewidth is negligible (see Fig. 8).

As the total magnetization of the sample is unchanged after creation and damping of a magnon, one cannot directly connect the magnon lifetime to the ultimate time scale of magnetization switching. However, this relaxation time can be directly compared to the time interval provided in the excitation scheme. For instance, if the aim is to switch the magnetization of a nano-island using a spin-polarized current within a few femtoseconds, the high-energy magnons are governing this process. Hence, the time interval between electrons injected to the sample has to be shorter than the lifetime of the magnons involved. Otherwise, the magnons do not contribute to this switching process and die out. The same analogy applies to the other methods used to switch the magnetization.

A strong spin dependence of the decay rate of the image potential state has been observed in photoemission experiments and is attributed to the magnon generation and relaxation within a few tens of femtoseconds [183]. The observed decay rate is similar to the relaxation time of the magnons measured by SPEELS.

11. Real space representation of magnons

For a real space representation of the magnons one may use a two-dimensional Fourier transformation of the magnons' distribution in the reciprocal space. If one measures the magnon intensity spectra for different wave vectors, a contour map can be constructed by plotting the difference spectra. Such data for a 2 ML Fe(110) film on W(110) are presented in Fig. 18(a). If one assumes that the scattering geometry does not drastically influence the intensity distribution in far off-specular, one may estimate the spatial distribution of the magnon wave packets from the intensity profile presented in Fig. 18(a). For simplicity one may neglect the broadening in wave vectors due to the finite instrumental energy resolution. This is a rather good assumption, since the instrumental broadening is fairly small compared to the intrinsic linewidth. The spectral distribution as a function of the wave vector is fitted directly by a single Gaussian distribution. For example, the profile in Fig. 18(c) shows a full width at half maximum (FWHM) of about 0.32 \AA^{-1} .

After a Fourier transform, one obtains again a Gaussian wave packet representing the magnon envelope function with a full width at half maximum (FWHM) of about 2 nm. Now the magnon wave packet can be constructed from the experimental data. An example is presented in Fig. 18(d), where the magnon wave packet for $\Delta K = 0.7 \text{ \AA}^{-1}$ and $\varepsilon = 82 \text{ meV}$ is plotted. The wave packet is the product of three components: a moving Gaussian, $\exp[-(x - v_g t)^2 / 2\sigma^2]$, representing the motion of the wave packet (the envelop function), an exponential decay factor $\exp(-t/\tau)$ for the evolution of the amplitude in time, and finally a wave form, $\cos(\Delta K_{\parallel} \cdot x - \omega t)$, representing its wave nature ($\omega = \varepsilon/\hbar$ is the angular frequency of the wave). The velocity of the envelope function v_g is the group velocity of the wave packet, which is obtained from the slope of the dispersion relation, $v_g = \partial\omega/\partial\Delta k_{\parallel}$. σ and τ are the natural broadening of the wave packet in space and lifetime, respectively, which are obtained from the Fourier transform of the intensity spectra in Fig. 18(a).

To visualize the strong damping effects on high-energy magnons in ultrathin itinerant ferromagnets, one may compare three states of magnons for 8 ML Co(100)/Cu(100) and 2 ML Fe(110)/W(110). State S_{Fe} represents the magnon wave packet in the Fe(110) film, and states S_{Co}^1 and S_{Co}^2 are the states in the Co(100) film. S_{Fe} and S_{Co}^1 share the same wave vector ($\Delta K = 0.8 \text{ \AA}^{-1}$), while S_{Fe} and S_{Co}^2 have the same energy ($\varepsilon = 100 \text{ meV}$). Fig. 19 represents the evolution of the magnon wave packets for all three states mentioned above. The group velocities of the wave packets are about 26, 46 and 41 km/s for the S_{Fe} , S_{Co}^1 and S_{Co}^2 states, respectively.

In a classic picture the amplitude of the waves in Fig. 19 can be regarded as the amplitude of the transverse component of moments projected along a certain direction on the surface e.g. the propagation direction of the wave. It may be also regarded as the modulus of the magnon wavefunction. Fig. 19 demonstrates that the high wave vector magnons are strongly damped within a few tens of femtoseconds and confined in a few nanometers for both Fe and Co. The wave packets only moved ahead by about 2–3 nm during their lifetime (much shorter than the spin diffusion length in 3d ferromagnets). For the states from the same system i.e. S_{Co}^1 and S_{Co}^2 , the one at higher wave vector (S_{Co}^1) has a shorter lifetime than the one at lower wave vector (S_{Co}^2). The wave packet of S_{Co}^1 propagates a shorter distance than S_{Co}^2 . These results demonstrate that

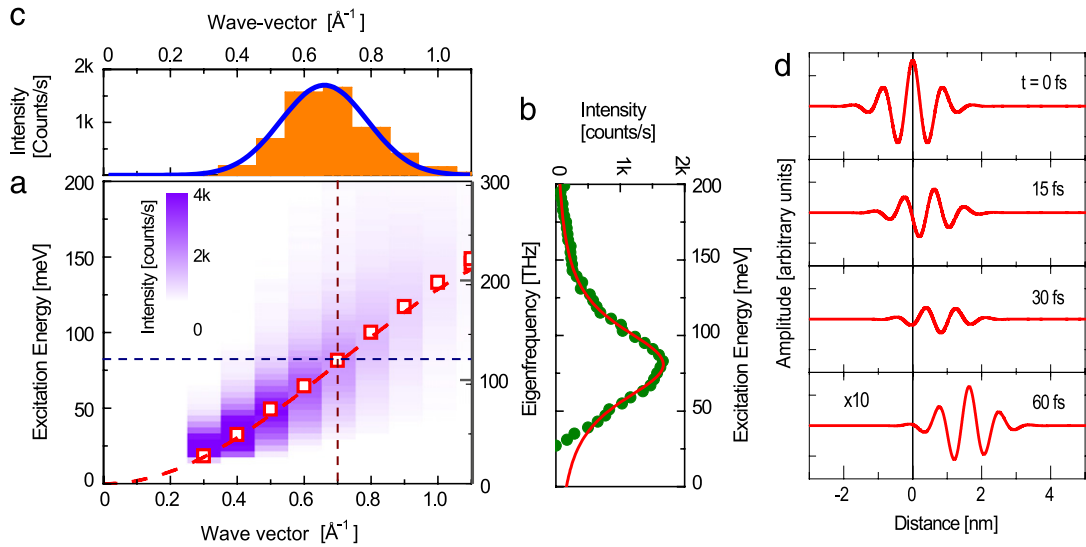


Fig. 18. (a) The difference spectra measured on a 2 ML Fe film on W(110), plotted as a contour map, for the wave vectors from 0 to 1 \AA^{-1} . The line scans at $\Delta K_{\parallel} = 0.7 \text{ \AA}^{-1}$ and $\varepsilon \simeq 82 \text{ meV}$ are shown in (b) and (c), respectively. The magnon peak in (b) is fitted by the convolution of a Gaussian and a Lorentzian function. The intrinsic linewidth of the peak is 55 meV. The intensity profile along the horizontal line at $\varepsilon \simeq 82 \text{ meV}$ in (c) is fitted by a Gaussian profile shown as the solid blue curve. (d) The magnon wave packet at $\Delta K_{\parallel} = 0.7 \text{ \AA}^{-1}$ and $\varepsilon \simeq 82 \text{ meV}$ constructed from the experimental data. The amplitude may be regarded as the transverse component of a precessing spin projected to the wave propagation direction or the modulus of the magnon wavefunction. Source: The data are taken from [181].

the decay of a magnon does strongly depend on its wave vector. Interestingly, for the states on different surfaces but with similar wave vectors i.e. S_{Fe} and S_{Co}^1 , it is noticed that although the S_{Fe} has a much lower energy, it exhibits a similar lifetime and broadening of the wave packet as S_{Co}^1 . S_{Fe} and S_{Co}^2 have the same energy. The state at higher wave vector (S_{Fe}) clearly shows shorter lifetime as compared to the low wave vector one, S_{Co}^2 . Regarding the propagation speed, both wave packets in the Co(100) film are much faster than the ones in the Fe(110) film as they experience a higher group velocity.

12. The effect of spin-orbit coupling on magnons

Spintronics is based on the spin dependent phenomena in solids [184]. In early 60s Rashba has proposed a formalism, which describes the existence of a spin-split band structure in wurtzite crystals [185]. Later on, Bychkov and Rashba showed that such a spin splitting can also occur in quantum wells [186]. The physical explanation of this spin splitting phenomenon is rather straightforward: in a semiconductor quantum well, if the potential well is asymmetric, the electrons move in an effective electric field \mathbf{E} induced by the potential gradient of the quantum well. In the reference frame of the electron this electric field acts like an effective magnetic field \mathbf{B} which causes a splitting in the energy levels of electrons with different spins. A similar effect is expected for the electrons in the absence of inversion symmetry and in the presence of a large spin-orbit coupling. The simple picture suggested above does not explain the dependence of the Rashba effect on the electronic band structure. A discussion on this topic does not fit within the space of this review. For a detailed explanation of the above phenomenology the reader is referred to Ref. [187]. A spin-split band structure has also been observed on some metallic surfaces, where the inversion symmetry is broken [188] and could be explained in analogy to the conventional Rashba effect in semiconductor heterostructures [189–191]. The idea has been further tailored to the surface alloys composed of heavy elements. The combination of strong spin-orbit interaction of the heavy elements with structural effects enhances the local potential gradients at the surface and thereby results in a large Rashba splitting [192]. The Rashba effect has been explored in detail in various systems and even some spintronic devices are proposed based on this effect [193–196].

One of the most interesting phenomena is the effect of the relativistic spin-orbit coupling on magnons as bosonic quasi-particles. Such an effect has not been explored in detail. It will be discussed in Section 12.1 that the magnon dispersion relation in the presence of a large spin-orbit coupling and absence of inversion symmetry shows a splitting for different magnetization directions, similar to the electrons. Section 12.2 is dedicated to the effect of the spin-orbit coupling on the magnon lifetime.

12.1. The magnon Rashba effect

In order to observe the effect of the spin-orbit coupling on the magnons, the magnon dispersion relation has been measured for an ultrathin Fe(110) film grown on W(110) with a thickness of 2 ML. The measurements have been performed

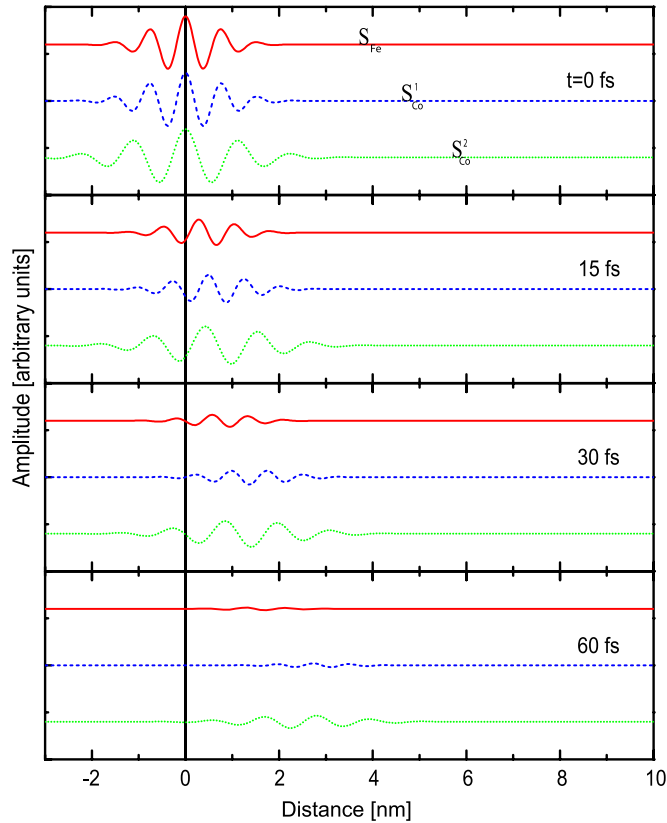


Fig. 19. Evolution of the magnons' wave packets for the states S_{Fe} (0.80 \AA^{-1} , 95 meV) at the Fe surface, S_{Co}^1 (0.81 \AA^{-1} , 174 meV) and S_{Co}^2 Co (0.55 \AA^{-1} , 101 meV) at the Co surface. The amplitude may be regarded as the transverse component of a precessing moment projected to the magnon propagation direction or the modulus of the magnon wavefunction.

Source: Reprinted figure with permission from Zhang et al. [181].

© 2012, by the American Physical Society.

for the magnetization parallel to the $[\bar{1}10]$ - and $[\bar{1}\bar{1}0]$ -direction [197,198]. The results of those measurements are summarized in Fig. 20, demonstrating that the magnon dispersion relation is split into two branches for magnetization along two opposite directions. The dispersion relation is antisymmetric, meaning that the magnon energies for positive wave vectors are equal to the ones with negative wave vectors and opposite magnetization direction and vice versa. The conclusion of these results is that the presence of the relativistic spin–orbit coupling in the absence of time reversal and space inversion symmetry breaks the degeneracy of the surface magnons and leads to the splitting of the magnon band structure.

The asymmetric dispersion relation can be understood in terms of the antisymmetric Dzyaloshinskii–Moriya interaction, which is a consequence of the spin–orbit coupling and absence of the inversion symmetry [197,81]. As discussed in Section 2.3, in such cases the Heisenberg spin Hamiltonian, including the DM term (Eq. (6)) may be used to obtain the components of the DM vector. Such an analysis has been performed in Ref. [197]. The measured dispersion relation has been fitted by the dispersion relation obtained based on a spin Hamiltonian which includes both the symmetric and antisymmetric exchange terms (the terms introduced in Eqs. (5) and (6), respectively). The analysis has resulted in the component of the DM vector along the magnetization $|2D_1^x + \hat{D}_1^x| = 0.9(3) \text{ meV}$ and $|D_2^x| = 0.5(3) \text{ meV}$. The superscript x indicates the component of the DM vector along the magnetization direction and the subscript 1(2) represents the nearest neighbor (next nearest neighbor) interaction. D_1^x (\hat{D}_1^x) is the longitudinal component of the DM vector of the nearest neighbors in the same atomic plane (in the neighboring atomic plane). A detailed discussion concerning this effect can be found in Ref. [197]. Very recently the values of the components of the DM vector and the resulting energy asymmetry have been calculated using *ab initio* DFT calculations and spin dynamics simulations, respectively [142]. The results are in good agreement with the experimental values.

The splitting of the magnon band structure shown in Fig. 20 is very similar to the well-known Rashba effect observed for electrons in two-dimensional electron gas or at metal surfaces [189–191]. Since in this experiment the ultrathin Fe film is grown on a nonmagnetic substrate with a large spin–orbit coupling, due to the interaction with the substrate the inversion symmetry is broken. The system is very similar to a two-dimensional electron gas system (or electrons at metal surfaces) in the presence of the spin–orbit coupling and absence of the space inversion symmetry. Here the lack of both the space

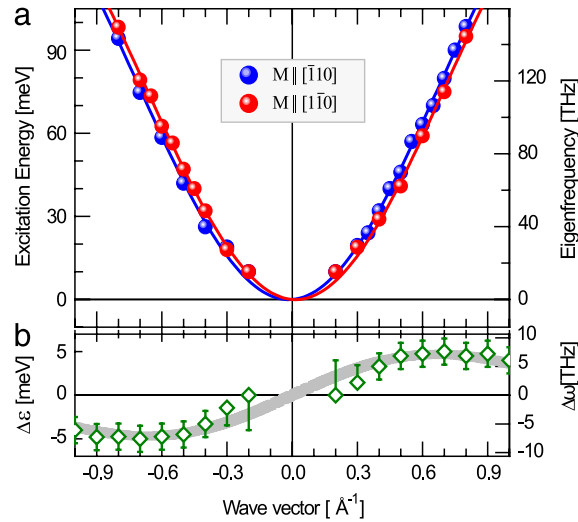


Fig. 20. (a) The magnon dispersion relation measured on 2 ML Fe/W(110) for two different magnetization directions. (b) The energy splitting, defined as $\Delta\varepsilon(q) = \varepsilon_{\mathbf{M}||[110]}(q) - \varepsilon_{\mathbf{M}||[1\bar{1}0]}(q)$, obtained from (a). The symbols represent the experimental results, while the solid lines represent the fits based on the extended Heisenberg spin Hamiltonian, including both the symmetric exchange term and the antisymmetric DM term.

Source: Reprinted figure with permission from Zakeri et al. [198].

© 2012, by the American Physical Society.

inversion and the time-reversal symmetry leads to two branches for the dispersion curves. This makes a one to one analogy to the Rashba type spin splitting of the electronic band structure. Therefore, the effect maybe called as “*magnon Rashba effect*” [149]. It is important to mention that in two-dimensional electron gas systems and at the normal metal surfaces the presence of the time-reversal symmetry requires two branches, one being the mirror image of the other. However, in ferromagnets, time-reversal symmetry is broken and there is one branch to the dispersion curve of each magnetization direction.

12.2. The effect of spin–orbit coupling on the magnon lifetime

Interestingly, it has been observed that the spin–orbit coupling influences the lifetime of magnons [198]. Measurements performed on 2 ML Fe/W(110) have shown that the lifetime for a given positive wave vector is not the same as the one for the negative wave vector. This effect has also been observed in the theoretical calculations based ETBT scheme [149]. To answer the question: How the high-energy magnons may be influenced by the spin–orbit coupling, let us start with an intuitive picture. In a very naïve picture one may imagine the spin–orbit coupling as a magnetic field that is acting on the magnons. It acts on the spins and thereby causes an additional damping. The direction of the spin–orbit field, which acts on the electrons is perpendicular to the electrons’ wave vector. A time reversal would just change the direction of the effective magnetic field, associated with the spin–orbit coupling, and thereby would invert the asymmetry in the lifetime. As it was discussed in Section 10, the damping of high-energy magnons is mainly governed by decay into the Stoner states. However, if the spin–orbit is large, it may cause an additional damping in the system. The spin–orbit induced damping is a well known damping mechanism for small wave vector magnons, in particular in the case of the uniform FMR mode ($q = 0$). As a simple model for the intrinsic FMR damping, one may imagine the precession of the spin that is coupled to its orbital motion via the spin–orbit coupling. The orbital motion is perturbed by the lattice simultaneously and hence cannot anymore follow the same phase and it results in a damping. A similar mechanism may also be expected here, which is superimposed to the Landau type of damping. In addition, when the electronic bands are perturbed by a large spin–orbit coupling, the inter- and intra-band transitions become also important. In order to correctly account for the damping of the magnons in such a system both inter- and intra-band transitions which lead to the decay of magnons need to be considered.

The calculations based the ETBT scheme [149] have shown that the additional linewidth broadening caused by the spin–orbit coupling is rather small compared to the linewidth caused by the Landau damping. The calculations have been performed for two cases: with and without spin–orbit coupling. It has been observed that for a given wave vector, the linewidth of the lower energy magnon branch in the presence of the spin–orbit coupling can be smaller than the linewidth in the absence of the spin–orbit coupling [149]. This observation is explained based on the argument that the density of Stoner states increases monotonically with the energy in this region of the spectrum. Thus, the decay into the Stoner excitations dominates the magnon linewidth, for the magnons with a finite wave vector. In the experiment it is not possible to separate the contributions caused by the spin–orbit coupling and the ones caused by the Landau damping to the measured linewidth. What can be clearly seen in the experiment is that, for a given wave vector, the linewidth of the spectra depends on the sign of the wave vector i.e. the propagation direction of the magnons. The difference in the linewidth for the two opposite propagation directions is rather small when is compared to the total broadening of the spectrum (for quantitative values see the discussion below).

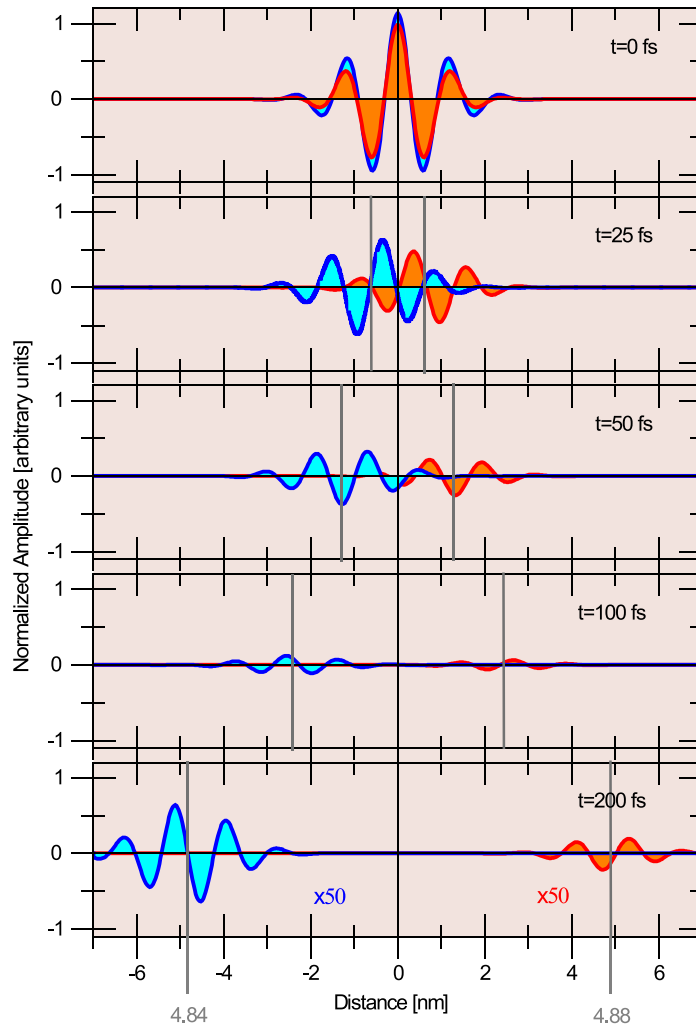


Fig. 21. A real time and space representation of the magnon wave packets with $\varepsilon = 46.5$ meV. The wave packets start to propagate at $t = 0$ with the maximum amplitude at $x = 0$. The red wave packet propagates along the [001]-direction, and the blue one propagates along the [00 $\bar{1}$]-direction. The vertical gray lines indicate the center of the wave packets. The difference in the wave packets which are propagating to the left and right is a direct consequence of the spin-orbit coupling. (For interpretation of the references to colour in this figure legend, the reader is referred to the web version of this article.)

Source: Reprinted figure with permission from Zakeri et al. [198].

© 2012, by the American Physical Society.

To see the relativistic effects on the magnon wave packets, a real space representation of the magnons may be provided using the procedure explained in Section 11. However, in order to have a very precise comparison of the intensity, the spectra have to be measured at a fixed scattering geometry and with exactly the same parameters (like incidence energy, beam current and energy resolution). Since the magnon intensity depends on the scattering's matrix elements, keeping the scattering geometry and experimental parameters unchanged, during the experiment, would avoid the effects caused by geometry on the electron scattering processes and thereby on the magnon intensity. To achieve the negative wave vectors the sample magnetization can be switched to opposite direction. This would be equivalent to a time inversion experiment. The experiment has to be designed such that the magnons propagate in the mirror symmetry plane of the magnetization. This would allow one to measure the magnons with positive and negative wave vectors without changing the scattering geometry. Such an experiment has been reported in Ref. [198].

It has been shown that for the magnons with an energy of $\varepsilon = 46.5$ meV the wave vectors are $+0.50 \text{ \AA}^{-1}$ and -0.52 \AA^{-1} . The corresponding wavelengths are about 12.6 \AA and 12.1 \AA , respectively. Note that in the absence of relativistic effects the absolute values of the wave vectors (wavelengths) for the positive and negative branches shall be exactly the same. The difference in the absolute value of the wave vectors (wavelengths) is a direct consequence of the spin-orbit coupling. The real time and space representation of the magnons with the energy of $\varepsilon = 46.5$ meV is presented in Fig. 21 indicating a very different propagation for the wave packets along different directions. This is a consequence of having different lifetime, group and phase velocity. The lifetime obtained for positive and negative wave vectors are $\tau_+ \approx 37 \pm 5$ fs and $\tau_- \approx 45 \pm 5$ fs,

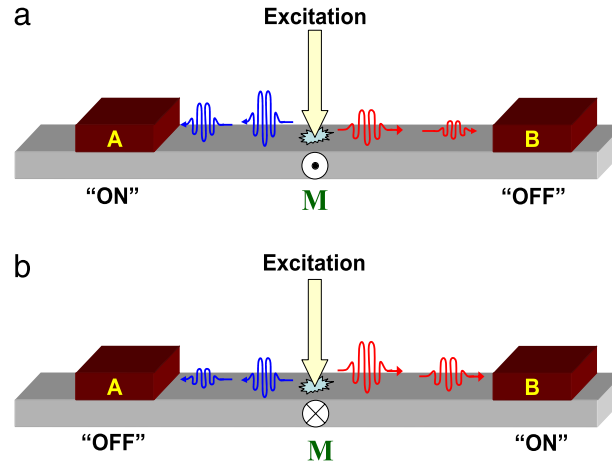


Fig. 22. A magnonic device based on the magnon Rashba effect. (a) \mathbf{M} is pointing outward. In this case a magnon signal can be detected by gate A and no magnon signal is detected by gate B (A:ON and B:OFF). (b) \mathbf{M} is pointing inward. In this case no magnon signal can be detected by gate A but a signal can be detected by gate B (A:OFF and B:ON).

Source: Reprinted figure with permission from Zakeri et al. [198].

© 2012, by the American Physical Society.

respectively. The group velocity, obtained from the slope of the dispersion curve at the given energy ($\varepsilon = 46.5$ meV) and wave vectors ($q = +0.50 \text{ \AA}^{-1}$ and -0.52 \AA^{-1}) is different. This is due to the fact that the dispersion relation is asymmetric. For the wave packet which is propagating along the $[001]$ -direction (the one with $q = +0.50 \text{ \AA}^{-1}$) $v_g = 24.4$ km/s and for the one propagating along the $[00\bar{1}]$ -direction (the one with $q = -0.52 \text{ \AA}^{-1}$) it is about $v_g = -24.2$ km/s. The differences in the group velocity, lifetime and the amplitude lead to a different propagation behavior for the magnons along two opposite directions. The phase velocity can be obtained using the simple expression $v_p = \varepsilon/q$, which results in $v_p = 14.4$ km/s for the magnons with an energy of 46.5 meV and $q = 0.50 \text{ \AA}^{-1}$. It is about -13.4 km/s for the magnons with an energy of 46.5 meV and $q = -0.52 \text{ \AA}^{-1}$.

It has been suggested that this effect may inspire ideas for device applications. The simplest device which may work based on these effects may be imagined as follows: one excites the transversal surface magnons (the ones that are propagating perpendicular to the magnetization) on a magnetic surface. Simultaneously two wave packets will be generated and then will propagate to opposite directions (see Fig. 22). Let us assume that the magnetization is pointing outward as it is shown in Fig. 22(a). This implies that the wave packet which is propagating towards gate A possesses a larger amplitude and lifetime, while the one that is propagating towards gate B will die out quickly. When the magnon wave packet arrives at gate A, it can be detected. At the same time, no magnon signal can be detected by gate B. This state may be called as A:ON and B:OFF. The switching to the state A:OFF and B:ON can be realized just by reversing the magnetization of the ferromagnet (see Fig. 22(b)). Such a device may be regarded as a magnonic switch. Just by switching the magnetization of the sample one can switch between the two different states. The advantage of such a device is that no electrical transport is involved and hence the operation of the device does not lead to any electrical losses.

Further applications are also possible. However, the field of magnonics is still in its infancy and a detailed knowledge of the effects associated with this phenomenon is required for realization of any device.

At this point let us comment on the effect of the film thickness on the observed spin-orbit effects. As it is pointed out earlier the large spin-orbit coupling in Fe films on W(110) originates mainly from the W substrate. It is expected that the spin-orbit induced effects on the magnons should be largest in the case of the Fe monolayer and shall be smaller for thicker films. In the theoretical study by Costa et al. [149] it has been shown that the effects of the spin-orbit coupling on the magnons in the case of Fe monolayer are larger than the Fe double layer. For thicker films there is no theoretical result available. This is also very difficult to investigate experimentally. The main problem is that Fe films on W(110) undergo a structural transformation as a function of the film thickness. This structural transformation which takes place between 2 and 3 ML has a direct consequence on the magnons properties as discussed in Section 9.2. However, measurements performed on a 20 ML Fe film has shown also a small energy asymmetry for the magnons with the same wave vector but opposite propagation directions. The values of the energy asymmetry in this case were much smaller than the ones measured for the Fe double layer [197].

13. Probing exchange interaction at the interface

Generally, there are a few important differences between magnons excited in layered structures grown on a substrate compared to the ones in an infinitely long crystal. In single-element bulk crystals all atoms are equivalent and contribute

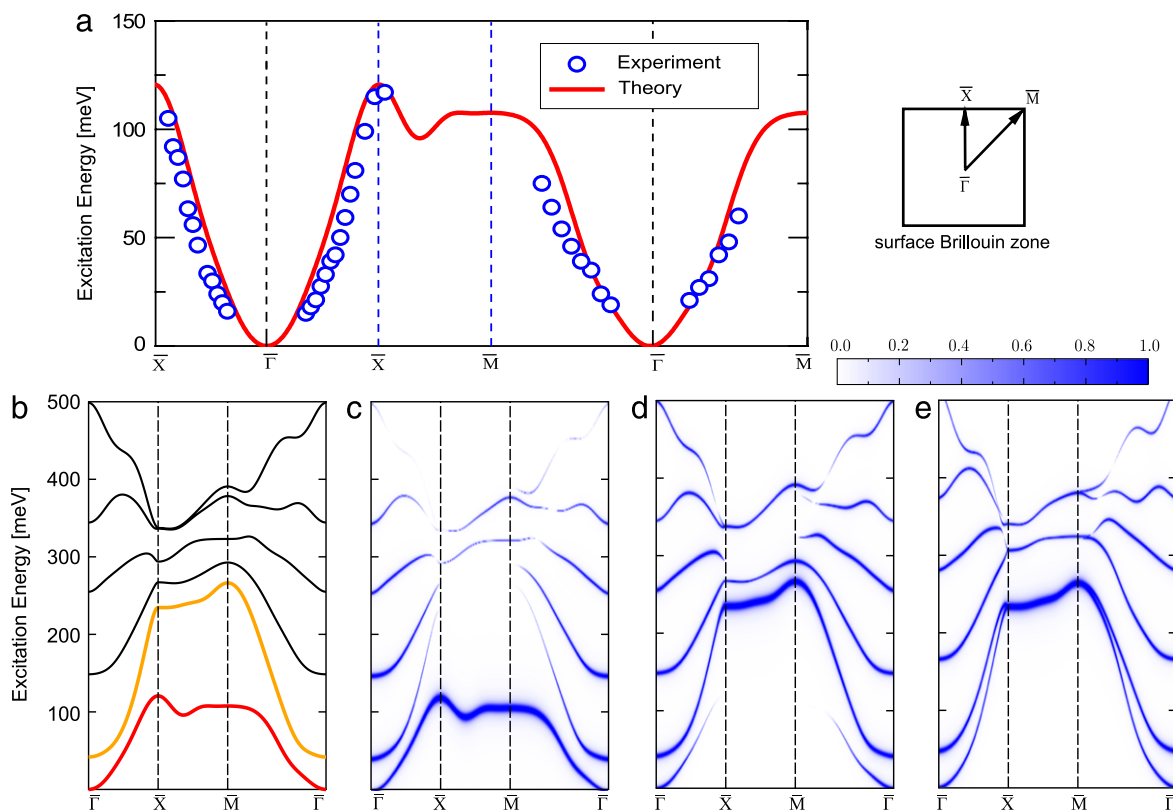


Fig. 23. The magnon dispersion relation of a 6 ML Fe film on Ir(001) measured along the main symmetry directions. (a) Experimental data plotted together with the lowest-energy mode of the theoretical calculations. (b) All the predicted magnon modes calculated by the adiabatic approach. (c) The susceptibility Bloch's spectral function projected onto the Fe layer next to Ir substrate (interface layer). (d) The susceptibility Bloch's spectral function projected onto the surface layer. (e) The susceptibility Bloch's spectral function projected onto the surface layer for a free standing Fe film consists of 6 layers. Source: Reprinted figure with permission from Zakeri et al. [200].

© 2013, by Macmillan Publishers Ltd. Nature Nanotechnology.

equally to different magnon modes (all the magnon modes degenerate in energy). However, in layered structures the atoms become inequivalent due to the absence of translational invariance in the direction perpendicular to the film plane. Moreover, the atomic environment of the surface and interface atoms is substantially different from the one of the atoms located in the inner part of the film. A direct consequence of this fact is that different atomic layers possess different electronic and magnetic properties. In particular, the exchange parameters become layer-dependent. At the surface of the film the important factor influencing the properties of the film is the reduced atomic coordination. At the interface an additional large influence comes from the hybridization of the electronic states of the atoms of the film with the ones of the substrate atoms. A natural consequence of the inequivalence of the atomic layers is a low-energy magnon mode which is formed due to the presence of the interface [199,57]. Probing this mode would shed light on the magnetic exchange interaction at the interface.

This idea has recently been realized by measuring an epitaxial thin Fe(001) films with a thickness of 6 ML grown on Ir(001). The dispersion relation of the lowest-energy magnon mode is presented in Fig. 23(a). The low excitation energy and decreasing intensity of this mode with increasing the thickness from 6 to 9 ML without any substantial change in the energies is an indication that the main contribution to this mode is coming from the interface. This fact has been supported by first-principles adiabatic calculations. It is found that the main contribution to the lowest-energy mode (shown in Fig. 23(a) by the solid red line) is coming from the Fe layer next to the substrate. The calculated atomic- or layer-resolved transverse magnetic susceptibility, which results in the spatial distribution of each magnon mode over the Brillouin zone and allows one to compare the contribution of each atomic layer to each magnon mode. Fig. 23(b) shows all magnon modes calculated using the adiabatic approach (magnetic force theorem). The susceptibility Bloch's spectral functions projected onto the interface and surface layers are presented in Fig. 23(c) and (d), respectively. In this representation the broadening of the lines indicates the contribution of the given layer to all magnon modes. For example in Fig. 23(c) the broadening of the lowest-energy mode is much stronger than of the other modes meaning that a large contribution into this mode, comes from the Fe atoms located in the atomic layer next to the Ir(001) substrate. For all magnon modes the pattern depends on the wave vector. Fig. 23(d) shows the contribution of the surface layer to all magnon modes, indicating that the contribution of the surface layer to the lowest-energy mode is small for magnon wave vectors larger than 0.5 \AA^{-1} and is zero near the zone boundaries (near

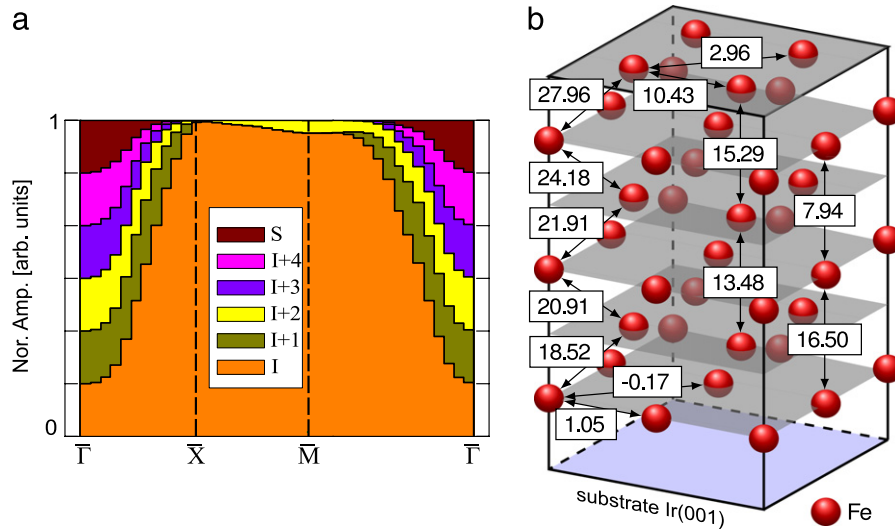


Fig. 24. (a) The contributions of each atomic layer to the lowest-energy magnon mode. (b) The calculated interatomic exchange parameters. The values are given in meV.

Source: Reprinted figure with permission from Zakeri et al. [200].

© 2013, by Macmillan Publishers Ltd. Nature Nanotechnology.

\bar{X} - and \bar{M} -points). This quantity is the amplitude of the magnon wavefunction in different layers. Since increasing magnon wave vector means larger angle ϕ between neighboring atomic moments, the difference in the exchange coupling constants for different layers becomes more important. This leads to the fact that the region of the smallest exchange parameters contribute largely to the lowest-energy magnon mode. At $q = 0$ all layers contribute equally to the lowest-energy mode. The contribution of the interface layer to this mode becomes larger as the wave vector increases whereas the contributions from the other layers become smaller such that at the \bar{X} point only the contribution of the interface layer remains (see Fig. 23(c)). The results of the calculation for a free-standing film (Fig. 23(e)) have indicated that the dispersion relation of the lowest-energy mode changes strongly whereas the other modes are unaffected. For a free-standing film the surface and interface layers are equivalent and hence the spectral weights of the two low-energy modes projected onto the surface and interface layers are identical. A comparison between Fig. 23(c)–(e) demonstrates the effect of hybridization of the electronic states of the film with ones of the substrate on the magnon dispersion relation. It is also apparent that the presence of the substrate breaks the degeneracy of the two low-energy magnon modes and leads to the formation of a mode with a lower energy. This lowest-energy mode originates from the atomic layer next to the substrate, where the exchange coupling is weaker.

It is important to mention that in the calculations presented in Fig. 23 the relativistic spin–orbit coupling is not taken into account. The lowest-energy magnon mode goes therefore to zero at the zone center ($\bar{\Gamma}$ -point). In the experiment, the data points close to the zone center ($\bar{\Gamma}$ -point) are missing and hence one cannot comment on the limit of $q \rightarrow 0$. As it is apparent from Fig. 23(a) the agreement of the experimental data and the theory in the intermediate wave vectors is not excellent (this is the region in which the spin–orbit effects may be observed, see the discussion in Section 12.1). Interestingly, a very small left–right asymmetry exists in the experimental dispersion relation, which might be the consequence of the spin–orbit coupling. However, as it is mentioned in Section 12 the spin–orbit induced effects on the magnon dispersion relation are rather small. In order to ensure that the observed effects are purely related to the spin–orbit coupling one would have to perform additional experiments with two opposite magnetization directions. Another interesting observation is that, unlike the Fe/W(110) system, which shows a giant magnetic anisotropy, the Fe/Ir(001) system shows a very small (almost negligible) magnetic anisotropy. The magnetic hysteresis loops measured along different in-plane directions are almost identical [200, 201] (the film behaves like an easy-plane anisotropy system). Generally, the energy gap in the magnon dispersion relation at $q = 0$ is proportional to the magnetic anisotropy. As this term is negligible, one would expect that the gap shall also be negligible in this system.

The contribution of each layer to the lowest-energy magnon mode as calculated by adiabatic calculations is presented in Fig. 24(a). The localization of magnons at the Fe/Ir(001) interface can be understood on the basis of the analysis of the exchange parameters. In principle, the reduction of the coordination number at surfaces/interfaces can lead to a magnon softening [79]. However, in many systems the interface electronic properties are different from the surface ones. This fact leads to a significant difference in the exchange parameters at the surface and at the interface. Remarkably, at the Fe/Ir(001) interface the magnon softening induced by the interface hybridization is much more significant than that from the surface, which indicates a strong reduction of the intralayer exchange constants at the Fe/Ir(001) interface. Fig. 24(b) shows the exchange parameters in the Fe/Ir(001) system. For simplicity, only the relevant parameters are presented. While the interlayer coupling for both surface and interface layers is strongly ferromagnetic, the intralayer exchange coupling is relatively weak.

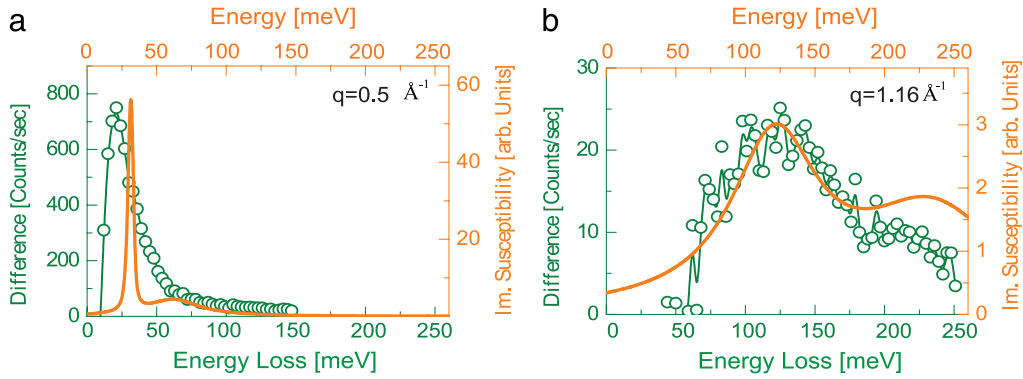


Fig. 25. A comparison between SPEELS difference spectra, recorded at (a) the middle ($\Delta K_{\parallel} = q = 0.5 \text{ \AA}^{-1}$), and (b) the edge of the Brillouin zone ($\Delta K_{\parallel} = q = 1.16 \text{ \AA}^{-1}$, \bar{X} -point), and the corresponding calculated imaginary part of the dynamical spin susceptibility using LRTDFT. Source: Reprinted figure with permission from Zakeri et al. [200]. © 2013, by Macmillan Publishers Ltd. Nature Nanotechnology.

As discussed in Section 10, another aspect which is of prime importance is the damping mechanism of the high wave vector magnons which is governed by the decay of the collective magnons into single-particle Stoner excitations. As a result for each wave vector q the lowest in energy magnon mode has a long lifetime and can be unambiguously detected in the experiment. The contribution of all other magnon modes is drastically reduced because of their strong damping (short lifetime). In the final SPEELS response function the spatial localization of different magnon modes competes with their Landau damping. As discussed above the amplitude of the interface magnons in the upper layers is small (but still significant) whereas the damping of higher-energy magnons is very strong. Although the spectral weight of interface mode is not as large as the surface mode, it has a much longer lifetime and hence dominates the spectra. Calculation of the dynamic transversal spin susceptibility considers on an equal footing both collective magnons and single-electron Stoner excitations and provides full account for the Landau damping of the magnons. These calculations are presented in Fig. 25 revealing a drastic Landau damping already of the second in energy magnon mode. This mode has appeared as a weak peak in the experimental spectra confirming the prediction of the theory based on LRTDFT. The higher energy modes have also been seen recently for Co films on Cu(001) at small wave vectors. Similar to this case, it has been observed the higher energy modes are strongly damped [180].

The method discussed above has also been employed to multilayers of Fe and Co films grown on the same substrate and also Fe layers grown on Rh(001) [200].

14. Magnons in thin films with perpendicular easy axis

Ultrathin films with large perpendicular magnetic anisotropy (PMA), have attracted much attention due to their interesting fundamental properties and also their promising technological applications in ultra-high density magnetic recording [202], magnetic tunneling junctions and also spin-transfer torque devices [203,204]. Many observed phenomena in the above mentioned devices are attributed to the emission or absorption of interface magnons while performing transport experiments. In this respect, the knowledge on high-energy magnons would have a large impact on the understanding of many observed phenomena in the transport experiments as well as the ultrafast spin dynamics in these materials. However, since the films with PMA possess an out-of-plane magnetic stray field, there has been a long-standing question concerning the possibility of probing magnons in these materials using SPEELS.

It has been recently shown that magnons in PMA systems can be excited and probed by a transversally spin-polarized beam [205]. The experiments have been performed on tetragonally distorted multilayers and alloys of Fe and Co [206,207]. In both cases the films can be grown epitaxially with the epitaxial relationship $[100]_{\text{film}} \parallel [110]_{\text{substrate}}$ on Ir(001). Both systems exhibit an out-of-plane easy axis due to the large PMA, originating from the tetragonal distortion of the epitaxial layers [206,207]. The spectra have been recorded for the spin polarization vector \mathbf{P} of the incident beam parallel to the surface, *perpendicular* to the easy magnetization direction, see Fig. 26(a).

Fig. 26(b) and (c) show the I_{+} and I_{-} SPEELS spectra measured at a wave vector of 1.1 \AA^{-1} on a 4 ML $\text{Fe}_{0.5}\text{Co}_{0.5}$ alloy film and a 4 ML Fe/Co multilayer film, respectively. I_{+} (I_{-}) denotes the intensity of the scattered beam when \mathbf{P} is parallel (antiparallel) to the $[1\bar{1}0]$ direction. In both cases, a pronounced peak appears in both I_{+} and I_{-} spectra with the same intensity and peak position. The peak intensity shows no dependence on the direction of \mathbf{P} , different from those recorded on the ultrathin films with in-plane magnetization (see Fig. 8). This is due to the fact that unlike the previous experiments, where the beam polarization vector \mathbf{P} was parallel or antiparallel to the magnetization direction (quantization axis), in this case it is perpendicular to that.

The answer to the question “How a transversally spin-polarized beam can excite the magnons?” is given in Section 4.2.3. Let us assume a spin polarized beam with an arbitrary polarization vector $\mathbf{P} = P\hat{\mathbf{e}} = \sin \vartheta \cos \varphi \hat{\mathbf{i}} + \sin \vartheta \sin \varphi \hat{\mathbf{j}} + \cos \vartheta \hat{\mathbf{k}}$ is the unit vector in space indicating the direction of the spin polarization vector (ϑ and φ are the polar and azimuthal angles,

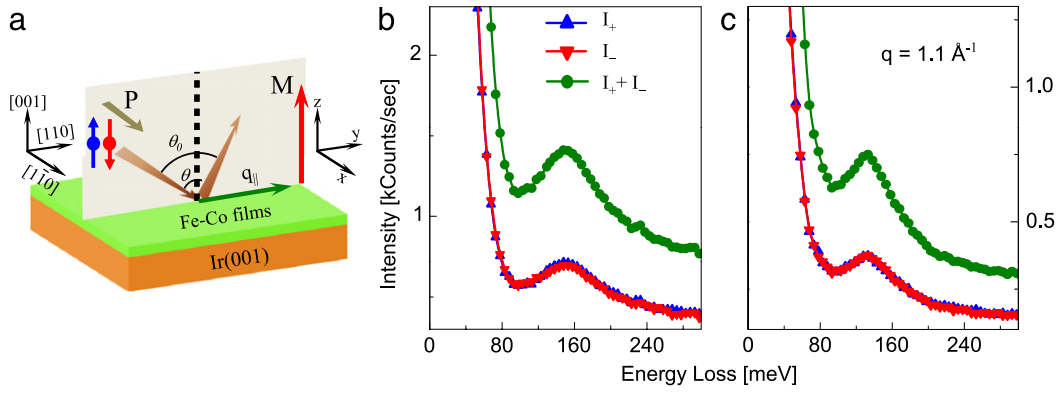


Fig. 26. (a) A schematic representation of the scattering geometry. All the crystallographic directions depicted here are the ones of Ir(001). The SPEELS spectra recorded on a 4 ML $\text{Fe}_{0.5}\text{Co}_{0.5}$ alloy film (b) and a 4 ML Fe/Co multilayer film (c) at a wave vector of $q = 1.1 \text{ \AA}^{-1}$. I_+ and I_- represent the intensity spectra when the polarization vector \mathbf{P} is parallel and antiparallel to the x direction, respectively. The total spectrum is shown by $I_+ + I_-$. Source: Reprinted figure with permission from Qin et al. [205]. © 2013, by the American Physical Society.

respectively and are defined with respect to the quantization axis, see Fig. 26(a) and P is the norm of the polarization vector. The polarization vector of a given spin-polarized beam can be expressed in terms of Dirac (Pauli) spinors defining the spin-up and spin-down states [208]. This can be simply done by finding the eigenstates of:

$$(\boldsymbol{\sigma} \cdot \hat{\mathbf{e}})\chi = \lambda\chi, \quad (31)$$

where $\boldsymbol{\sigma}$ represents the Pauli spin matrices and $\boldsymbol{\sigma} \cdot \mathbf{e}$ is the projection of spin operator in a polarization direction. λ and χ represent the eigenvalue and the eigenstate of $\boldsymbol{\sigma} \cdot \mathbf{e}$, respectively.

The solution of Eq. (31) is:

$$\chi = \begin{pmatrix} \cos \frac{\vartheta}{2} \\ \sin \frac{\vartheta}{2} e^{i\varphi} \end{pmatrix} \text{ for } \lambda = +1 \quad \text{and} \quad \chi = \begin{pmatrix} \sin \frac{\vartheta}{2} \\ -\cos \frac{\vartheta}{2} e^{i\varphi} \end{pmatrix} \text{ for } \lambda = -1. \quad (32)$$

For the case where \mathbf{P} is parallel or antiparallel to the magnetization (the quantization axis) one has $\vartheta = 0$, $\varphi = 0$ (see Fig. 26(a)) and hence Eq. (31) yields the expected eigenstate of σ_z , $\begin{pmatrix} 1 \\ 0 \end{pmatrix}$ or $\begin{pmatrix} 0 \\ 1 \end{pmatrix}$.

For the case where \mathbf{P} is parallel or antiparallel to the x direction and the magnetization (the quantization axis) is along the z direction one has $\vartheta = \pi/2$, $\varphi = 0$ and hence Eq. (31) yields the eigenstate $\chi = \frac{1}{\sqrt{2}} \begin{pmatrix} 1 \\ 0 \end{pmatrix} + \frac{1}{\sqrt{2}} \begin{pmatrix} 0 \\ 1 \end{pmatrix}$, where, $\begin{pmatrix} 1 \\ 0 \end{pmatrix}$ and $\begin{pmatrix} 0 \\ 1 \end{pmatrix}$ are the Dirac (Pauli) spinors and can be regarded as majority and minority spin states of the sample, respectively. Note that in both scenarios the quantization axis is defined as the direction of the easy axis.

In the experiments, where \mathbf{P} is parallel or antiparallel to the quantization axis, the beam is composed of either majority or minority spins (assuming a polarization of 100%, $P = 1$). Since the magnons carry a total angular momentum of $1\hbar$, they can only be excited by incident electrons of minority character via an exchange process (see Section 6). The magnon excitation is forbidden for incident electrons of majority character. Hence, one sees only the magnon excitation peak in the minority spin spectra. In the case where \mathbf{P} is perpendicular to the quantization axis, the beam can be regarded as a totally spin unpolarized beam equally composed of both majority and minority spins. Since for both polarization directions (+ and -) the beam carries the same amount of majority and minority spins, one would expect the same magnon peak intensity in I_+ and I_- spectra.

The fact that the observed loss features are magnons can be verified by different experimental proofs as it has been verified in Ref. [205]. (i) One of the advantages of magnetic thin films is that one can manipulate the direction of the easy magnetization axis by a slight modification of the film. The experiments performed on very similar samples but with in-plane easy axis have shown similar magnon energies, confirming that the observed excitations are magnons. Note that for in-plane magnetized samples one can take the advantage of spin-resolved measurements and make sure that the excitations are magnons. (ii) The observed dispersion relation does not match to any other possible excitations in FeCo films. The energies of surface phonons in Fe and Co films are less than 40 meV (see Section 7). The excitation energies of the surface plasmons are by one order of magnitude larger than the ones of the magnons. (iii) The observed (short) lifetime of the excitations matches very well to what is expected for magnons (see Section 10). (iv) If one varies the alloy concentration the observed dispersion relation changes in one side to the dispersion relation of Co films and in the other side to the dispersion relation of Fe films on the same substrate.

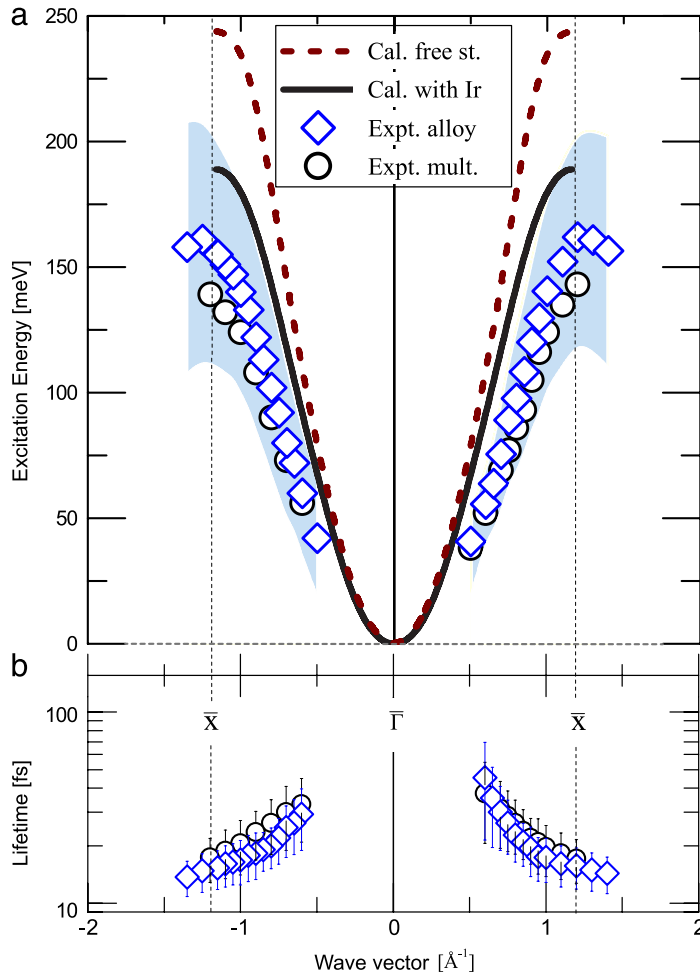


Fig. 27. (a) The magnon dispersion relation probed on a 4 ML $\text{Fe}_{0.5}\text{Co}_{0.5}$ alloy film (open diamonds) and a 4 ML Fe/Co multilayer film (open circles). The intrinsic linewidth of the spectra is depicted as the background color. The solid line represents the theoretical calculation for a 4 ML body-centered tetragonal film on Ir(001) composed of alternating layers of Co and Fe. The dashed line represents the results of the calculations for a free standing film. (b) The magnon lifetime as a function of the wave vector. Source: Reprinted figure with permission from Qin et al. [205]. © 2013, by the American Physical Society.

If the aim is to investigate a more complex surface in which the energies of phonons and magnons coincide, one would require a longitudinally spin-polarized beam. Only then it is possible to distinguish between the magnetic and non-magnetic excitations observed in the loss spectra. The physics will be very similar to what is already discussed in Section 7. The main disadvantage of a longitudinally spin-polarized beam is that the angle of the polarization vector and the sample magnetization is given by the scattering geometry, meaning that the effective spin polarization changes while changing the scattering angle.

The magnon dispersion relation measured on both $\text{Fe}_{0.5}\text{Co}_{0.5}$ alloy and Fe/Co multilayer films is presented in Fig. 27(a). At low wave vectors both systems show almost identical magnon energies. Small differences in the magnon energies appear at high wave vectors. For the $\text{Fe}_{0.5}\text{Co}_{0.5}$ alloy film, the energy reaches a value of 160 meV at the \bar{X} -point whereas for the Fe/Co multilayer film, the energy is about 140 meV. In both cases the magnon energies are much smaller than those in bulk Fe and Co. They are even smaller than those of 2 ML Fe(110)/W(110) and 8 ML Co(001)/Cu(001).

The results of first principles adiabatic calculations, are presented in Fig. 27(a) showing a rather good agreement with the experimental data. The low energy of the magnons is attributed to the presence of the Ir(001) substrate, which reduces the magnon energies by 55 meV at the \bar{X} point with respect to a free-standing film. This fact is the consequence of the weakening of the interatomic exchange interaction and beautifully manifests the importance of electronic hybridizations between the ultrathin film and the substrate. Detailed information may be found in Ref. [205].

The background color in Fig. 27(a) denotes the intrinsic linewidth of the magnon peaks as observed in the experiment. Both systems show a very similar linewidth. The intrinsic linewidth increases from 40 to 100 meV when the wave vector increases from 0.5 to 1.2 \AA^{-1} , similar to that of an 8 ML Co/Cu(100) and a 2 ML Fe/W(110). In this case the magnon lifetime is obtained using the procedure explained in Section 10 and is presented in Fig. 27(b).

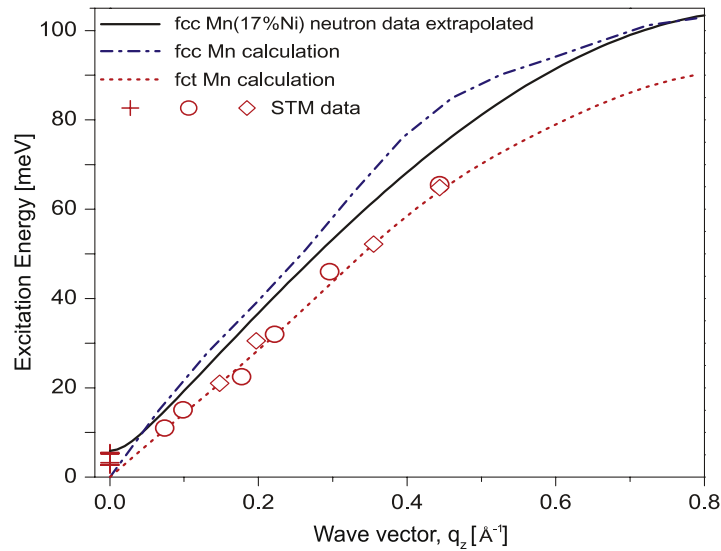


Fig. 28. The magnon dispersion relation measured on γ -Mn films grown on $\text{Cu}_3\text{Au}(001)$. Source: Reprinted figure with permission from Gao et al. [118]. © 2008, by the American Physical Society.

These results could clearly demonstrate that the high-energy magnons in ultrathin ferromagnetic films with an out-of-plane easy axis can be probed by a transversally spin-polarized beam. The excitation cross section is rather large so that a pronounced peak in the spectra can be observed. Hence, the experiments may even be performed with an unpolarized beam [209,210,180,211,212]. Since ultrathin films with PMA are of fundamental and technological interest, these pioneering experiments would open a way towards investigation of magnon excitations in this class of materials by SPEELS and also by inelastic tunneling spectroscopy.

15. Magnetic excitations in antiferromagnetic films

Antiferromagnets with reduced dimensionality are of great fundamental and technological interest. They are excellent systems for the investigation of dimensionality effects on the symmetry and magnetic interactions. Antiferromagnetic thin films have been widely used in spintronics as the so-called “pinning layers”, in order to fix the magnetization direction of an adjacent ferromagnetic layer. Although inelastic neutron scattering experiments have been widely employed to investigate the magnetic excitations in bulk antiferromagnets, these excitations in metallic antiferromagnets with reduced dimensionality have not been yet explored in detail.

15.1. The magnon dispersion relation

The antiferromagnetic magnon dispersion relation has been measured by spin-polarized inelastic tunneling spectroscopy on fct Mn films grown on $\text{Cu}_3\text{Au}(001)$ [118] over a small fraction of the Brillouin zone near the zone center. A linear dispersion relation with a slope of $160 \pm 10 \text{ meV \AA}$ and an energy gap of 2.7–5.5 meV, depending on the film thickness, have been observed. Fig. 28 shows the observed magnon dispersion relation by Gao et al. on ultrathin γ -Mn films on $\text{Cu}_3\text{Au}(001)$. As it is pointed out in Section 4.2.4 only the magnons with the wave vector perpendicular to the film can be measured by inelastic tunneling spectroscopy. The antiferromagnetic magnon dispersion relation is linear in the limit of small wave vectors and hence the group velocity does not depend on the wave vector (it is $v_g = 160 \pm 10 \text{ meV \AA}$ in the case of γ -Mn films on $\text{Cu}_3\text{Au}(001)$). The experimental results could be explained based on the first-principles adiabatic calculations. It has been found that the tetragonal distortion of the films leads to a smaller magnon stiffness constant. The calculations have suggested a larger magnon stiffness constant for the fcc film (see Fig. 28), similar to what has already been measured by inelastic neutron scattering experiments on bulk Ni-doped Mn [213].

One interesting aspect of the results is the measurement at $q = 0$. The amount of the energy needed to excite the uniform magnon mode ($q = 0$) is proportional to the magnetic anisotropy of the film. It has been observed that the energy of this magnon mode is 5.5 meV for a 4 ML sample and 2.7 meV for a 24 ML one. As the film thickness decreases, the surface anisotropy becomes more important. The larger excitation energy of this mode for the thinner film is the consequence of the surface anisotropy. One can show that the energy of the uniform magnon mode (or the energy gap) can be expressed as: $E_g = (E_{An}^2 + 2E_{An}E_{Ex})^{1/2}$, where E_g , E_{An} and E_{Ex} denote the energy gap, total magnetic anisotropy energy of the film and the exchange energy, respectively. The analysis has resulted in a surface anisotropy of $1.4 \pm 0.2 \text{ meV per Mn atom}$. The magnetic anisotropy

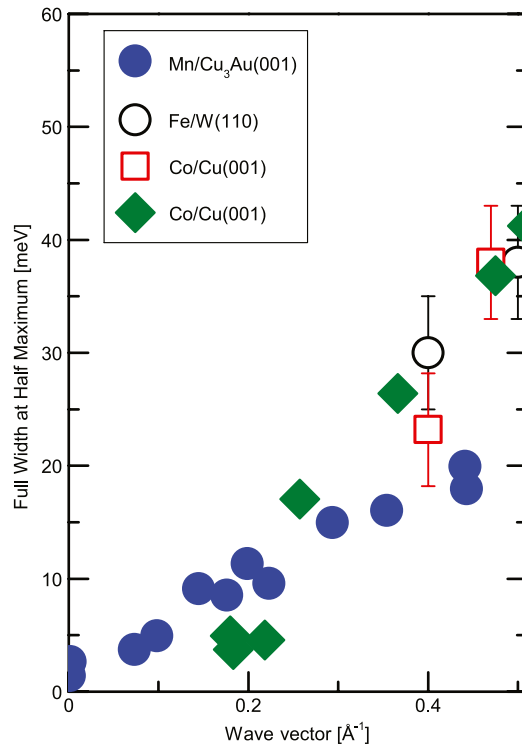


Fig. 29. The full width at half maximum of the excitation peak versus wave vector. The data of Mn films on Cu₃Au(001) are taken from Ref. [118] (solid circles). The data of Fe(110) films on W(110) are taken from Ref. [181,198] (open circles). The data of Co/Cu(001) are taken from Ref. [181] (open squares) and Ref. [180] (solid diamonds).

of antiferromagnetic films cannot be simply measured by conventional magnetometry methods. The measurement of the energy gap serves as one of the few methods for quantifying the magnetic anisotropy of an antiferromagnetic film.

15.2. The magnon lifetime

Another interesting result is the measurement of the lifetime of the magnons in these films. The measured linewidth of the magnetic excitations in γ -Mn films is plotted in Fig. 29 and is compared to the linewidth of excitations in ultrathin Fe(110) films on W(110) [181,198] and ultrathin Co(001) films on Cu(001) [181,180]. It seems that the linewidth versus wave vector shows a smaller slope in the case of Mn films, compared to the ferromagnetic Fe and Co films. For the wave vectors larger than 0.3 \AA^{-1} the linewidth of the excitations in Mn films is smaller than the one in ultrathin metallic ferromagnets. This means that the lifetime of antiferromagnetic magnons in Mn films are larger than the one of the ferromagnetic magnons in Fe and Co films. This may have its origin in a smaller Landau damping of these excitations in this material. However, more experimental and theoretical studies are required to verify this hypothesis and reveal the origin of the observed phenomenon.

Similar to what is reported for low-dimensional ferromagnets, one would expect that the dimensionality aspects affect the magnetic excitations in antiferromagnetic structures. Unfortunately, our nowadays knowledge on the magnetic excitations in metallic antiferromagnets with reduced dimensionality (in the form of thin films, and nanostructures) is very limited. In this respect more experimental and theoretical works are needed in order to gain insight into the physics of magnetic excitations in these structures. We note that the magnetic excitations in bulk quantum antiferromagnets with reduced spin dimensionality have recently been investigated by resonant inelastic X-ray scattering experiments. The reader is referred to Ref. [106] for a review.

16. Magnetic excitations in atoms and clusters

In the present section we shall briefly make a connection between the excitations in ultrathin films and adatoms (or cluster) adsorbed on surfaces. We, however, do not aim to go into the details of those systems.

The best way of investigating magnetic excitations in very small objects like adatoms (or clusters composed of a few atoms) adsorbed on a surface is to perform spin excitation tunneling spectroscopy by using a STM tip. In this way one would be able to combine the lateral resolution with the spectroscopy to get more insight into the local excitations of very small objects down to an atom. The basic concept of such an experiment is discussed in Section 4.2.4.

When electrons tunnel from the tip to the sample or vice versa, they may exchange spin angular momentum with the magnetic adatom (or cluster). Consequently this creates an excitation in the system. The spin-flip of the tunneling electron changes the total angular momentum of the adatom (or cluster) from the ground state S_g to the excited state $S_{ex} = \pm(S_g - 1)$. The energy of this inelastic process that is the difference between the excited- and ground-state energy, appears as a step in the tunneling conductance spectrum (dI/dU) of the inelastic tunneling spectroscopy.

Experiments performed on adatoms and chains on semi-insulating substrates have revealed that the states in the systems can be treated as discrete quantum states [120,214,215,121,182]. The excited states of such systems are rather long living and hence are well-defined. Hence, sharp peaks are observed in the d^2I/dU^2 spectra of the tunneling spectroscopy. Since the polarization of the tunneling conductance is given by the matrix element of the spin operators, by measuring the spin-dependent tunneling conductance, one would be able to provide a quantitative measure of the spin-dependent transition intensities [121].

When adatoms and clusters are grown on metallic substrates, they are strongly coupled to the bath of substrate's conduction electrons and hence the states are not anymore well-defined. Consequently, the created excitations have a large possibility to decay into the Stoner continuum and a larger damping is expected. Hence, the peaks observed in the d^2I/dU^2 spectra of tunneling spectroscopy, are broad [119,60,123,122]. This is another evidence that the main source of the damping in high-energy spin excitations is the presence of the Stoner continuum. Recently, the spin excitations in rare-earth adatoms on metallic surfaces have been investigated. Interestingly, it has been found that the states are rather long living (lifetime is found to be in the order of 100–150 fs). This observation is attributed to the strongly localized character of $4f$ electrons [216].

17. Conclusions and outlook

We discussed the experimental results of the high-energy spin excitations in low-dimensional magnets, mainly in ultrathin ferromagnetic films grown on metallic substrates. The main mechanisms leading to the creation of magnons by spin-polarized electrons are outlined and explained based on the current understanding. The magnon excitation process is based on the exchange scattering mechanism. When a spin-polarized beam with a well-defined energy is scattered from the sample surface, magnons can only be excited (annihilated) if the incoming beam is of minority (majority) spin character. Since magnons possess a total angular momentum of $1\hbar$, the outgoing electron is of majority (minority) spin character. This fact leads to a peak in the energy loss (gain) region of the intensity spectra when minority (majority) electrons are incident. The scattering process itself is elastic and the observed energy loss (or gain) is due to the fact that the ejected electron stems from a lower (or higher) energy level of the excited solid. Such a process is purely mediated by exchange interaction that is of the Coulomb nature and no explicit spin–spin interaction is involved.

The spin-polarized electron spectroscopy provides also a way of measuring magnons and phonons simultaneously, without the need of any spin-resolved detection. Magnons can only be excited by incidence of minority electrons and annihilated by incidence of majority ones whereas, phonons can be excited and annihilated by incidence of electrons with any spin orientation. This fact leads to a sign change in the asymmetry curve in the gain and loss regions where the magnons are excited. For the case of phonons, no change in the sign of the asymmetry curve is expected. This means that the magnons and phonons can be distinguished by comparing the sign of the asymmetry curves in loss and gain regions and there is no need of further spin resolved detection of the scattered electrons. These pioneering results would open a way towards probing the quasi-particles involved in lattice- and spin dynamics and their possible coupling, in particular, in the multifunctional complex hybrid and oxide materials as well as strongly correlated electron systems. This knowledge would be of substantial importance to investigate the possible coupling scenarios between different quasi-particles.

The response of the magnon energies to the changes in the geometrical structure, number of atomic layers and rearrangement of atoms within the structure is explained in term of the complexity of the electronic structure of the ferromagnetic films and the substrate. It is demonstrated how the complexity of the electronic structure and the different contribution of orbitals to the hybridization and exchange interaction may lead to unusual behavior of the fundamental magnetic interactions in low-dimensional magnets. These results suggest a way of tailoring magnetic coupling in low-dimensional magnetic structures.

The experimental results have had a very large impact on the development of the quantum theory of low-dimensional magnetism, in particular on the theory of spin excitations in low-dimensional itinerant magnets.

Magnons in ultrathin Fe and Co films possess lifetimes ranging from tens to hundreds of femtoseconds depending on the wave vector. The analysis has revealed that the magnons at the Fe(110) and Co(100) surfaces are strongly confined in time and space due to the large damping effects. Interestingly, the lifetime of both systems are very similar at a given wave vector in spite of the fact that the excitation energies in the Co(100) film are almost twice of that in the Fe(110) film. High-energy magnons propagate only a few nanometers within their lifetime. These experiments may inspire further theoretical investigations for a better understanding of magnetic damping mechanism of high-energy magnons in low-dimensional magnets. This understanding would help us to find a possible way of tuning the magnetic relaxation in nanoscale ferromagnets. It may also offer a way of estimating the ultimate time scale of magnetic switching in nanostructures. The magnon lifetime needs to be investigated in more detail. It is believed that the main damping mechanism of high-energy magnons is their dissipation into single particle electron–hole pairs. In the case of low-dimensional ferromagnets in contact to metallic hosts, the angular momentum of magnons is transferred to the host via conduction electrons. It would be of fundamental interest

to prove this scenario. To this end one would need to grow the ferromagnetic films on a(n) (semi-)insulating substrate and investigate the magnon lifetime for different thicknesses of the ferromagnetic film.

The first direct experimental evidence of the magnon Rashba effect is discussed. It is demonstrated that the dispersion relation of the surface magnons in the presence of relativistic spin–orbit coupling and in the absence of time-reversal and inversion symmetry shows a splitting for different magnetization directions, similar to the electron dispersion relation at metal surfaces and in the presence of spin–orbit coupling.

In a pioneering experiment, it is demonstrated that the lifetime, amplitude, group and phase velocity of the surface magnons propagating along two opposite (but equivalent) directions perpendicular to the magnetization are different meaning that magnons with the same energy propagate differently along two opposite directions. A new type of spintronic devices based on surface magnons may be proposed. This finding may open new routes towards possibilities of using surface magnons for information processing. Specially, in the devices made of ferromagnetic insulators, where the information cannot be carried by means of electrons and the role of magnons for carrying the information is essential. It would be interesting to investigate in more detail the effect of spin–orbit coupling on the low-energy magnons. Such experiments may be performed using BLS spectroscopy.

It has been recently shown that a spontaneous skyrmion lattice is formed in an Fe monolayer on Ir(111) due to the interplay between symmetric Heisenberg exchange, the four-spin and the antisymmetric DM interaction [217]. Measuring the magnon dispersion relation in such an exotic magnetic state would be very interesting in order to gain information regarding the dynamics of skyrmions. Such an investigation may be done by means of SPEELS. However, one should not expect to observe a spin-resolved spectrum since the net magnetic moment of a skyrmion is zero. The calculations have revealed that the Heisenberg exchange parameters are smaller than the ones in the Fe monolayer on W(110) [217], meaning that the excitation energies shall be low.

It is illustrated that SPEELS may be used to probe the interface exchange parameters. If the magnetic coupling at the interface is weaker than at the surface, the lowest-energy magnon mode originates mainly from the interface layer. Probing of this magnon mode would lead to an unambiguous determination of the exchange coupling constants at the interface. Since the SPEELS technique provides unique results on spin excitations, it has a large capability to be used for the investigation of the magnetic exchange interaction in many systems.

Magnons in ultrathin films with out-of-plane easy axis are of particular fundamental interest. As a matter of fact, the pioneering SPEELS experiments on FeCo films with an out-of-plane easy axis have illustrated the capability of the method for investigation of such structures. The idea can be tailored to a large variety of ultrathin film systems, in which the magnetization is oriented perpendicular to the film. If the substrate used for growing the film possesses a large spin–orbit coupling one may observe interesting phenomena associated with the broken inversion symmetry and the large spin–orbit coupling.

Magnons in multilayer structures of alternating layers of ferromagnetic metals are also of fundamental interest. In this case one shall observe different magnon modes associated with different layers in the structure.

Magnons in an ultrathin antiferromagnetic film are also of great fundamental interest. In principle, one can investigate all the effects presented here in an antiferromagnetic film. One candidate for such investigation is an ultrathin film of FeRh. It is expected that this material should show a ferromagnetic to antiferromagnetic phase transitions as a function of temperature and film thickness. It would be interesting to investigate the magnons in both ferromagnetic and antiferromagnetic phases and also observe the changes in the magnon spectrum across the transition temperature. Theoretical predictions of the magnons' behavior in each of these phases have recently been reported [218].

Acknowledgments

The author would like to gratefully thank J. Kirschner for many discussions, strong support and continuous encouragement. Thanks to all the former and present members of the SPEELS team who contributed to the experiments discussed here. Fruitful collaborations and discussions with V.S. Stepanyuk, P.A. Ignatiev, A. Ernst, L.M. Sandratskii and P. Buczek are gratefully acknowledged.

References

- [1] I.I. Mazin, D.J. Singh, M.D. Johannes, M.H. Du, Unconventional superconductivity with a sign reversal in the order parameter of $\text{LaFeAsO}_{1-x}\text{F}_x$, Phys. Rev. Lett. 101 (2008) 057003. URL <http://link.aps.org/doi/10.1103/physrevlett.101.057003>.
- [2] I.I. Mazin, M.D. Johannes, A key role for unusual spin dynamics in ferropnictides, Nat. Phys. 5 (2) (2009) 141–145. URL <http://dx.doi.org/10.1038/nphys1160>.
- [3] M. Le Tacon, G. Ghiringhelli, J. Chaloupka, M.M. Sala, V. Hinkov, M.W. Haverkort, M. Minola, M. Bakr, K.J. Zhou, S. Blanco-Canosa, C. Monney, Y.T. Song, G.L. Sun, C.T. Lin, G.M. De Luca, M. Salluzzo, G. Khaliullin, T. Schmitt, L. Braicovich, B. Keimer, Intense paramagnon excitations in a large family of high-temperature superconductors, Nat. Phys. 7 (9) (2011) 725–730. URL <http://dx.doi.org/10.1038/nphys2041>.
- [4] S. Zhang, P.M. Levy, A.C. Marley, S.S.P. Parkin, Quenching of magnetoresistance by hot electrons in magnetic tunnel junctions, Phys. Rev. Lett. 79 (1997) 3744–3747. URL <http://link.aps.org/doi/10.1103/PhysRevLett.79.3744>.
- [5] X.-F. Han, A.C.C. Yu, M. Oogane, J. Murai, T. Daibou, T. Miyazaki, Analyses of intrinsic magnetoelectric properties in spin-valve-type tunnel junctions with high magnetoresistance and low resistance, Phys. Rev. B 63 (2001) 224404. URL <http://link.aps.org/doi/10.1103/PhysRevB.63.224404>.
- [6] P.M. Levy, A. Fert, Spin transfer in magnetic tunnel junctions with hot electrons, Phys. Rev. Lett. 97 (2006) 097205. URL <http://link.aps.org/doi/10.1103/PhysRevLett.97.097205>.
- [7] V. DREWELLO, J. Schmalhorst, A. Thomas, G. Reiss, Evidence for strong magnon contribution to the t_{mr} temperature dependence in mgo based tunnel junctions, Phys. Rev. B 77 (2008) 014440. URL <http://link.aps.org/doi/10.1103/PhysRevB.77.014440>.

- [8] F. Bloch, Zur theorie des ferromagnetismus, *Z. Phys.* A 61 (1930) 206–219. URL <http://dx.doi.org/10.1007/BF01339661>.
- [9] T. Holstein, H. Primakoff, Field dependence of the intrinsic domain magnetization of a ferromagnet, *Phys. Rev.* 58 (1940) 1098–1113. URL <http://link.aps.org/doi/10.1103/PhysRev.58.1098>.
- [10] W. Heisenberg, Zur theorie des ferromagnetismus, *Z. Phys.* A 49 (1928) 619–636. URL <http://dx.doi.org/10.1007/BF01328601>.
- [11] C. Herring, Exchange Interactions among Itinerant Electrons, 2nd Edn., vol. IV, Academic Press, New York and London, 1966.
- [12] E.C. Stoner, Collective electron specific heat and spin paramagnetism in metals, *P. R. Soc. Lond. A. Mat.* 154 (883) (1936) 656–678. URL <http://www.jstor.org/stable/96686>.
- [13] E.C. Stoner, Collective electron ferromagnetism, *P. R. Soc. Lond. A. Mat.* 165 (922) (1938) 372–414. URL <http://www.jstor.org/stable/97057>.
- [14] E.P. Wohlfarth, The theoretical and experimental status of the collective electron theory of ferromagnetism, *Rev. Mod. Phys.* 25 (1953) 211–219. URL <http://link.aps.org/doi/10.1103/RevModPhys.25.211>.
- [15] J.H.E. Griffiths, *Nature* 158 (1946) 670. URL <http://www.nature.com/nature/journal/v158/n4019/abs/158670a0.html>.
- [16] C. Kittel, Interpretation of anomalous larmor frequencies in ferromagnetic resonance experiment, *Phys. Rev.* 71 (1947) 270–271. URL <http://link.aps.org/doi/10.1103/PhysRev.71.270.2>.
- [17] C. Kittel, On the theory of ferromagnetic resonance absorption, *Phys. Rev.* 73 (1948) 155–161. URL <http://link.aps.org/doi/10.1103/PhysRev.73.155>.
- [18] J.H. Van Vleck, Concerning the theory of ferromagnetic resonance absorption, *Phys. Rev.* 78 (1950) 266–274. URL <http://link.aps.org/doi/10.1103/PhysRev.78.266>.
- [19] J. Van Kranendonk, J.H. Van Vleck, Spin waves, *Rev. Mod. Phys.* 30 (1958) 1–23. URL <http://link.aps.org/doi/10.1103/RevModPhys.30.1>.
- [20] C. Herring, C. Kittel, On the theory of spin waves in ferromagnetic media, *Phys. Rev.* 81 (1951) 869–880. URL <http://link.aps.org/doi/10.1103/PhysRev.81.869>.
- [21] F. Keffer, H. Kaplan, Y. Yafet, Spin waves in ferromagnetic and antiferromagnetic materials, *Amer. J. Phys.* 21 (4) (1953) 250–257. URL <http://dx.doi.org/10.1119/1.1933416>.
- [22] F.J. Dyson, General theory of spin-wave interactions, *Phys. Rev.* 102 (1956) 1217–1230. URL <http://link.aps.org/doi/10.1103/PhysRev.102.1217>.
- [23] R.N. Sinclair, B.N. Brockhouse, Dispersion relation for spin waves in a fcc cobalt alloy, *Phys. Rev.* 120 (1960) 1638–1640. URL <http://link.aps.org/doi/10.1103/PhysRev.120.1638>.
- [24] R.A. Waldron, What is ferromagnetic resonance?, *Br. J. Appl. Phys.* 11 (2) (1960) 69. URL <http://stacks.iop.org/0508-3443/11/69>.
- [25] G. Shirane, R. Nathans, O. Steinsvoll, H.A. Alperin, S.J. Pickart, Measurement of the magnon dispersion relation of iron, *Phys. Rev. Lett.* 15 (1965) 146–148. URL <http://link.aps.org/doi/10.1103/PhysRevLett.15.146>.
- [26] G. Shirane, V.J. Minkiewicz, R. Nathans, Spin waves in 3d metals, *J. Appl. Phys.* 39 (2) (1968) 383–390. URL <http://link.aip.org/link/?JAP/39/383/1>.
- [27] H.A. Mook, R.M. Nicklow, E.D. Thompson, M.K. Wilkinson, Spin-wave spectrum of nickel metal, *J. Appl. Phys.* 40 (3) (1969) 1450–1451. URL <http://link.aip.org/link/?JAP/40/1450/1>.
- [28] E.D. Thompson, H.A. Mook, Energy bands, stoner modes, and spin waves in iron, *J. Appl. Phys.* 41 (3) (1970) 1227–1228. URL <http://link.aip.org/link/?JAP/41/1227/1>.
- [29] R. Lowde, C. Windsor, On the magnetic excitations in nickel, *Adv. Phys.* 19 (82) (1970) 813–909. URL <http://www.tandfonline.com/doi/abs/10.1080/00018737000101201>.
- [30] H.A. Mook, R.M. Nicklow, Neutron scattering investigation of the magnetic excitations in iron, *Phys. Rev. B* 7 (1973) 336–342. URL <http://link.aps.org/doi/10.1103/PhysRevB.7.336>.
- [31] H.A. Mook, D. Tocchetti, Neutron-scattering measurements of the generalized susceptibility $\chi(q, e)$ for Ni, *Phys. Rev. Lett.* 43 (1979) 2029–2032. URL <http://link.aps.org/doi/10.1103/PhysRevLett.43.2029>.
- [32] J.W. Lynn, H.A. Mook, Temperature dependence of the dynamic susceptibility of nickel, *Phys. Rev. B* 23 (1981) 198–206. URL <http://link.aps.org/doi/10.1103/PhysRevB.23.198>.
- [33] R.W. Damon, J.R. Eshbach, Magnetostatic modes of a ferromagnet slab, *J. Phys. Chem.* 19 (3–4) (1961) 308–320. URL [http://dx.doi.org/10.1016/0022-3697\(61\)90041-5](http://dx.doi.org/10.1016/0022-3697(61)90041-5).
- [34] M. Sparks, Ferromagnetic resonance in thin films. i. Theory of normal-mode frequencies, *Phys. Rev. B* 1 (1970) 3831–3856. URL <http://link.aps.org/doi/10.1103/PhysRevB.1.3831>.
- [35] M. Sparks, Ferromagnetic resonance in thin films. ii. Theory of linewidths, *Phys. Rev. B* 1 (1970) 3856–3869. URL <http://link.aps.org/doi/10.1103/PhysRevB.1.3856>.
- [36] M. Sparks, Ferromagnetic resonance in thin films. iii. Theory of mode intensities, *Phys. Rev. B* 1 (1970) 3869–3880. URL <http://link.aps.org/doi/10.1103/PhysRevB.1.3869>.
- [37] D.M. Edwards, Spin waves in ferromagnetic metals, *P. R. Soc. Lond. A. Mat.* 269 (1338) (1962) 338–351. URL <http://rspa.royalsocietypublishing.org/content/269/1338/338.abstract>.
- [38] D.M. Edwards, Spin wave energies in the band theory of ferromagnetism, *P. R. Soc. Lond. A. Mat.* 300 (1462) (1967) 373–390. URL <http://www.jstor.org/stable/2415949>.
- [39] J. Callaway, Spin waves in ferromagnetic metals, *Phys. Lett. A* 27 (4) (1968) 215–216. URL <http://www.sciencedirect.com/science/article/pii/0375960168910992>.
- [40] J. Callaway, Spin waves in metals, *Int. J. Journal of Quantum Chem.f* 2 (S2) (1968) 277–283. URL <http://dx.doi.org/10.1002/qua.560020728>.
- [41] J.B. Sokoloff, Polar spin waves in ferromagnetic metals, *Phys. Rev.* 173 (1968) 617–630. URL <http://link.aps.org/doi/10.1103/PhysRev.173.617>.
- [42] J.B. Sokoloff, Theory of inelastic neutron scattering in the itinerant model antiferromagnetic metals. i, *Phys. Rev.* 185 (1969) 770–782. URL <http://link.aps.org/doi/10.1103/PhysRev.185.770>.
- [43] J.B. Sokoloff, Theory of neutron scattering in the itinerant model of antiferromagnetic metals. ii, *Phys. Rev.* 185 (1969) 783–791. URL <http://link.aps.org/doi/10.1103/PhysRev.185.783>.
- [44] D.M. Edwards, J.A. Hertz, Electron–magnon interactions in itinerant ferromagnetism. ii. Strong ferromagnetism, *J. Phys. F: Met. Phys.* 3 (12) (1973) 2191–2205.
- [45] D.M. Edwards, M.A. Rahman, The transverse dynamical susceptibility of ferromagnets and antiferromagnets within the local exchange approximation, *J. Phys. F: Met. Phys.* 8 (7) (1978) 1501. URL <http://stacks.iop.org/0305-4608/8/1501>.
- [46] J.F. Cooke, J.W. Lynn, H.L. Davis, Calculations of the dynamic susceptibility of nickel and iron, *Phys. Rev. B* 21 (1980) 4118–4131. URL <http://link.aps.org/doi/10.1103/PhysRevB.21.4118>.
- [47] D.M. Edwards, R.B. Muniz, Spin waves in ferromagnetic transition metals. i. General formalism and application to nickel and its alloys, *J. Phys. F: Met. Phys.* 15 (11) (1985) 2339. URL <http://stacks.iop.org/0305-4608/15/i=11/a=016>.
- [48] R.B. Muniz, J.F. Cooke, D.M. Edwards, Spin waves in ferromagnetic transition metals. ii. Iron and its alloys, *J. Phys. F: Met. Phys.* 15 (11) (1985) 2357. URL <http://stacks.iop.org/0305-4608/15/i=11/a=017>.
- [49] H. Tang, M. Plihal, D. Mills, Theory of the spin dynamics of bulk fe and ultrathin fe films, *J. Magn. Magn. Mater.* 187 (1) (1998) 23–46. URL <http://www.sciencedirect.com/science/article/pii/S0304885398000882>.
- [50] S.Y. Savrasov, Linear response calculations of spin fluctuations, *Phys. Rev. Lett.* 81 (1998) 2570–2573. URL <http://link.aps.org/doi/10.1103/PhysRevLett.81.2570>.
- [51] J. Hong, D.L. Mills, Spin excitations in ferromagnetic ni: Electrons and neutrons as a probe, *Phys. Rev. B* 61 (2000) R858–R861. URL <http://link.aps.org/doi/10.1103/PhysRevB.61.R858>.
- [52] N. Karchev, Magnon–paramagnon effective theory of itinerant ferromagnets, *J. Phys.: Condens. Matter.* 15 (17) (2003) 2797. URL <http://stacks.iop.org/0953-8984/15/i=17/a=329>.
- [53] E. Şaşıoğlu, A. Schindlmayr, C. Friedrich, F. Freimuth, S. Blügel, Wannier-function approach to spin excitations in solids, *Phys. Rev. B* 81 (2010) 054434. URL <http://link.aps.org/doi/10.1103/PhysRevB.81.054434>.

- [54] R.B. Muniz, D.L. Mills, Theory of spin excitations in Fe(110) monolayers, *Phys. Rev. B* 66 (2002) 174417. URL <http://link.aps.org/doi/10.1103/PhysRevB.66.174417>.
- [55] R.B. Muniz, A.T. Costa, D.L. Mills, Microscopic theory of spin waves in ultrathin ferromagnetic films: Fe on W(110), *J. Phys.: Condens. Matter* 15 (5) (2003) S495. URL <http://stacks.iop.org/0953-8984/15/i=5/a=305>.
- [56] A.T. Costa, R.B. Muniz, D.L. Mills, Theory of spin excitations in Fe(110) multilayers, *Phys. Rev. B* 68 (22) (2003) 224435. URL <http://link.aps.org/abstract/PRB/v68/e224435>.
- [57] A.T. Costa, R.B. Muniz, D.L. Mills, Spin waves and their damping in itinerant ultrathin ferromagnets: intermediate wave vectors, *Phys. Rev. B* 74 (2006) 214403. URL <http://link.aps.org/doi/10.1103/PhysRevB.74.214403>.
- [58] R. Muniz, A. Costa, D. Mills, dynamics of itinerant electron ferromagnetic nanostructures, *IEEE Trans. Magn.* 44 (7) (2008) 1974–1977. URL <http://ieeexplore.ieee.org/xpl/articleDetails.jsp?arnumber=4544922>.
- [59] P. Buczek, A. Ernst, P. Bruno, L.M. Sandratskii, Energies and lifetimes of magnons in complex ferromagnets: A first-principle study of Heusler alloys, *Phys. Rev. Lett.* 102 (2009) 247206. URL <http://link.aps.org/doi/10.1103/PhysRevLett.102.247206>.
- [60] S. Lounis, A.T. Costa, R.B. Muniz, D.L. Mills, Dynamical magnetic excitations of nanostructures from first principles, *Phys. Rev. Lett.* 105 (2010) 187205. URL <http://link.aps.org/doi/10.1103/PhysRevLett.105.187205>.
- [61] S. Lounis, A.T. Costa, R.B. Muniz, D.L. Mills, Theory of local dynamical magnetic susceptibilities from the Korringa–Kohn–Rostoker green function method, *Phys. Rev. B* 83 (2011) 035109. URL <http://link.aps.org/doi/10.1103/PhysRevB.83.035109>.
- [62] N.D. Mermin, H. Wagner, Absence of ferromagnetism or antiferromagnetism in one- or two-dimensional isotropic Heisenberg models, *Phys. Rev. Lett.* 17 (22) (1966) 1133. URL <http://link.aps.org/abstract/PRL/v17/p1133>.
- [63] D. Loss, F.L. Pedrocchi, A.J. Leggett, Absence of spontaneous magnetic order of lattice spins coupled to itinerant interacting electrons in one and two dimensions, *Phys. Rev. Lett.* 107 (2011) 107201. URL <http://link.aps.org/doi/10.1103/PhysRevLett.107.107201>.
- [64] Y. Yafet, J. Kwo, E.M. Gyorgy, Dipole–dipole interactions and two-dimensional magnetism, *Phys. Rev. B* 33 (1986) 6519–6522. URL <http://link.aps.org/doi/10.1103/PhysRevB.33.6519>.
- [65] M. Bander, D.L. Mills, Ferromagnetism of ultrathin films, *Phys. Rev. B* 38 (16) (1988) 12015–12018. URL <http://link.aps.org/abstract/PRB/v38/p12015>.
- [66] P. Bruno, Spin-wave theory of two-dimensional ferromagnets in the presence of dipolar interactions and magnetocrystalline anisotropy, *Phys. Rev. B* 43 (1991) 6015–6021. URL <http://link.aps.org/doi/10.1103/PhysRevB.43.6015>.
- [67] M. Farle, Ferromagnetic resonance of ultrathin metallic layers, *Rep. Prog. Phys.* 61 (7) (1998) 755. URL <http://stacks.iop.org/0034-4885/61/i=7/a=001>.
- [68] L.D. Landau, E.M. Lifshitz, Theory of the dispersion of magnetic permeability in ferromagnetic bodies, *Phys. Z. Sowjetunion* 8 (1935) 153.
- [69] E. Ising, Beitrag zur theorie des ferromagnetismus, *Z. Phys.* A 31 (1925) 253–258. URL <http://dx.doi.org/10.1007/BF02980577>.
- [70] I.E. Dzyaloshinskii, Thermodynamic theory of “weak” ferromagnetism in antiferromagnetic substances, *SOV. PHYS. JETP* 5 (6) (1957) 1259–1272.
- [71] T. Moriya, Anisotropic superexchange interaction and weak ferromagnetism, *Phys. Rev.* 120 (1960) 91–98. URL <http://link.aps.org/doi/10.1103/PhysRev.120.91>.
- [72] M. Bode, M. Heide, K. von Bergmann, P. Ferriani, S. Heinze, G. Bihlmayer, A. Kubetzka, O. Pietzsch, S. Blügel, R. Wiesendanger, Chiral magnetic order at surfaces driven by inversion asymmetry, *Nature* 447 (7141) (2007) 190–193. URL <http://dx.doi.org/10.1038/nature05802>.
- [73] M. Heide, G. Bihlmayer, S. Blügel, Dzyaloshinskii–Moriya interaction accounting for the orientation of magnetic domains in ultrathin films: Fe/W(110), *Phys. Rev. B* 78 (2008) 140403. URL <http://link.aps.org/doi/10.1103/PhysRevB.78.140403>.
- [74] P. Ferriani, K. von Bergmann, E.Y. Vedmedenko, S. Heinze, M. Bode, M. Heide, G. Bihlmayer, S. Blügel, R. Wiesendanger, Atomic-scale spin spiral with a unique rotational sense: Mn monolayer on W(001), *Phys. Rev. Lett.* 101 (2008) 027201. URL <http://link.aps.org/doi/10.1103/PhysRevLett.101.027201>.
- [75] M. Heide, G. Bihlmayer, S. Blügel, Describing Dzyaloshinskii–Moriya spirals from first principles, *Physica B*: 404 (18) (2009) 2678–2683. URL <http://www.sciencedirect.com/science/article/pii/S0921452609004177>.
- [76] C.D. Hu, Relationship between ferroelectricity and dzyaloshinskii–moriya interaction in multiferroics and the effect of bond-bending, *Phys. Rev. B* 77 (2008) 174418. URL <http://link.aps.org/doi/10.1103/PhysRevB.77.174418>.
- [77] M.I. Katsnelson, Y.O. Kvashnin, V.V. Mazurenko, A.I. Lichtenstein, Correlated band theory of spin and orbital contributions to dzyaloshinskii–moriya interactions, *Phys. Rev. B* 82 (2010) 100403. URL <http://link.aps.org/doi/10.1103/PhysRevB.82.100403>.
- [78] K. Zakeri, J. Kirschner, Probing Magnons by Spin-Polarized Electrons, in: *Topics in Applied Physics Magnetism from Fundamentals to Applications*, vol. 125, Springer, Berlin, Heidelberg, 2013, pp. 84–99. http://dx.doi.org/10.1007/978-3-642-30247-3_7. Ch. 7.
- [79] K. Zakeri, Y. Zhang, J. Kirschner, Surface magnons probed by spin-polarized electron energy loss spectroscopy, *J. Electron Spectrosc. Relat. Phenom.* 189 (2013) 157–163. URL <http://www.sciencedirect.com/science/article/pii/S0368204812000643>.
- [80] L. Udvardi, L. Szunyogh, K. Palotas, P. Weinberger, First-principles relativistic study of spin waves in thin magnetic films, *Phys. Rev. B* 68 (10) (2003) 104436. URL <http://link.aps.org/abstract/PRB/v68/e104436>.
- [81] L. Udvardi, L. Szunyogh, Chiral asymmetry of the spin-wave spectra in ultrathin magnetic films, *Phys. Rev. Lett.* 102 (2009) 207204. URL <http://link.aps.org/doi/10.1103/PhysRevLett.102.207204>.
- [82] T. Moriya, Y. Takahashi, Itinerant electron magnetism, *Annu. Rev. Mater. Sci.* 14 (1) (1984) 1–25. <http://dx.doi.org/10.1146/annurev.ms.14.080184.000245>.
- [83] J.K. Kübler, *Theory of Itinerant Electron Magnetism*, in: *International Series of Monographs on Physics*, 106, Clarendon Press, Oxford, 2000.
- [84] J.C. Slater, The theory of ferromagnetism: Lowest energy levels, *Phys. Rev.* 52 (1937) 198–214. URL <http://link.aps.org/doi/10.1103/PhysRev.52.198>.
- [85] J. Kirschner, D. Rebenstorff, H. Ibach, High-resolution spin-polarized electron-energy-loss spectroscopy and the stoner excitation spectrum in nickel, *Phys. Rev. Lett.* 53 (1984) 698–701. URL <http://link.aps.org/doi/10.1103/PhysRevLett.53.698>.
- [86] H. Hopster, R. Raue, R. Clauber, Spin-flip stoner excitations in a ferromagnet observed by inelastic spin-polarized electron scattering, *Phys. Rev. Lett.* 53 (1984) 695–697. URL <http://link.aps.org/doi/10.1103/PhysRevLett.53.695>.
- [87] H. Hopster, Direct observation of stoner excitations in itinerant ferromagnets by spin-polarized inelastic electron scattering (invited; abstract), *J. App. Phys.* 57 (8) (1985) 3017. URL <http://link.aip.org/link/?JAP/57/3017/1>.
- [88] J. Kirschner, Direct and exchange contributions in inelastic scattering of spin-polarized electrons from iron, *Phys. Rev. Lett.* 55 (1985) 973–976. URL <http://link.aps.org/doi/10.1103/PhysRevLett.55.973>.
- [89] G. Vignale, K.S. Singwi, Spin-flip electron-energy-loss spectroscopy in itinerant-electron ferromagnets: Collective modes versus stoner excitations, *Phys. Rev. B* 32 (1985) 2824–2834. URL <http://link.aps.org/doi/10.1103/PhysRevB.32.2824>.
- [90] R. Saniz, S.P. Apell, Model calculation of stoner-excitation cross sections in spin-polarized crystals, *Phys. Rev. B* 48 (1993) 3206–3211. URL <http://link.aps.org/doi/10.1103/PhysRevB.48.3206>.
- [91] M.P. Gokhale, D.L. Mills, Spin excitations of a model itinerant ferromagnetic film: Spin waves, stoner excitations, and spin-polarized electron-energy-loss spectroscopy, *Phys. Rev. B* 49 (1994) 3880–3893. URL <http://link.aps.org/doi/10.1103/PhysRevB.49.3880>.
- [92] J. Kirschner, Polarized electrons at surfaces, in: *Springer Tracts in Modern Physics*, Springer-Verlag, 1985, URL <http://books.google.de/books?id=KBIHjlkH-VsC>.
- [93] P. Buczek, A. Ernst, L.M. Sandratskii, Different dimensionality trends in the Landau damping of magnons in iron, cobalt, and nickel: Time-dependent density functional study, *Phys. Rev. B* 84 (2011) 174418. URL <http://link.aps.org/doi/10.1103/PhysRevB.84.174418>.
- [94] P. Buczek, A. Ernst, L.M. Sandratskii, Interface electronic complexes and Landau damping of magnons in ultrathin magnets, *Phys. Rev. Lett.* 106 (2011) 157204. URL <http://link.aps.org/doi/10.1103/PhysRevLett.106.157204>.
- [95] J. S.-Y. Wang, Energy width of ferromagnetic-exchange magnons in a magnetic field, *Phys. Rev. B* 6 (1972) 1908–1912. URL <http://link.aps.org/doi/10.1103/PhysRevB.6.1908>.
- [96] V.V. Zolotarev, Magnon damping in the Heisenberg ferromagnet, *Phys. Status Solidi (b)* 64 (2) (1974) K139–K141. URL <http://dx.doi.org/10.1002/pssb.2220640258>.

- [97] K. Zakeri, J. Lindner, I. Barsukov, R. Meckenstock, M. Farle, U. von Hörsten, H. Wende, W. Keune, J. Rucker, S.S. Kalarickal, K. Lenz, W. Kuch, K. Baberschke, Z. Frait, Spin dynamics in ferromagnets: Gilbert damping and two-magnon scattering, *Phys. Rev. B* 76 (2007) 104416. URL <http://link.aps.org/doi/10.1103/PhysRevB.76.104416>.
- [98] C. Kittel, Excitation of spin waves in a ferromagnet by a uniform rf field, *Phys. Rev.* 110 (1958) 1295–1297. URL <http://link.aps.org/doi/10.1103/PhysRev.110.1295>.
- [99] M.H. Seavey, P.E. Tannenwald, Direct observation of spin-wave resonance, *Phys. Rev. Lett.* 1 (1958) 168–169. URL <http://link.aps.org/doi/10.1103/PhysRevLett.1.168>.
- [100] K. Zakeri, T. Kebe, J. Lindner, M. Farle, Magnetic anisotropy of fe/gaas(001) ultrathin films investigated by in situ ferromagnetic resonance, *J. Magn. Magn. Mater.* 299 (1) (2006) L1–L10. URL <http://www.sciencedirect.com/science/article/pii/S0304885305004129>.
- [101] A. Banholzer, R. Narkowicz, C. Hassel, R. Meckenstock, S. Stienen, O. Posth, D. Suter, M. Farle, J. Lindner, Visualization of spin dynamics in single nanosized magnetic elements, *Nanotechnology* 22 (29) (2011) 295713. URL <http://stacks.iop.org/0957-4484/22/i=29/a=295713>.
- [102] P.A. Fleury, S.P.S. Porto, L.E. Cheesman, H.J. Guggenheim, Light scattering by spin waves in FeF_2 , *Phys. Rev. Lett.* 17 (1966) 84–87. URL <http://link.aps.org/doi/10.1103/PhysRevLett.17.84>.
- [103] B. Hillebrands, P. Baumgart, G. Güntherodt, Brillouin light scattering from spin waves in magnetic layers and multilayers, *Appl. Phys. A* 49 (6) (1989) 589–598. URL <http://dx.doi.org/10.1007/BF00616984>.
- [104] S. Demokritov, B. Hillebrands, A. Slavin, Brillouin light scattering studies of confined spin waves: linear and nonlinear confinement, *Phys. Rep.* 348 (6) (2001) 441–489. URL <http://www.sciencedirect.com/science/article/pii/S0370157300001162>.
- [105] B. Hillebrands, K. Ounadjela, Spin dynamics in confined magnetic structures II, in: *Topics in Applied Physics*, Springer, 2003, URL <http://books.google.de/books?id=naCmgmfqnAsc>.
- [106] L. Ament, M. van Veenendaal, T. Devereaux, J. Hill, J. vanden Brink, Resonant inelastic X-ray scattering studies of elementary excitations, *Rev. Mod. Phys.* 83 (2) (2011) 705.
- [107] M.P.M. Dean, R.S. Springell, C. Monney, K.J. Zhou, J. Pereiro, I. Božović, B. Dalla Piazza, H.M. Rønnow, E. Morenzoni, J. Van Den Brink, T. Schmitt, J.P. Hill, Spin excitations in a single La_2CuO_4 layer, *Nature Mater.* 11 (10) (2012) 850–854.
- [108] J. Kirschner, Sources and detectors for polarized electrons, in: *Polarized Electrons in Surface Physics*, World Scientific, 1985.
- [109] H. Ibach, D. Mills, *Electron Energy Loss Spectroscopy and Surface Vibrations*, Academic Press, New York, London, Paris, 1982, URL <http://www.amazon.com/Electron-Energy-Spectroscopy-Surface-Vibrations/dp/0123693500>.
- [110] H. Ibach, Electron energy loss spectroscopy with resolution below 1 meV, *J. Electron Spectrosc. Relat. Phenom.* 64–65 (0) (1993) 819–823. URL <http://www.sciencedirect.com/science/article/pii/S036820489380155F>.
- [111] H. Hopster, Spin-polarized electron energy loss spectroscopy, *Surf. Rev. Lett.* 01 (01) (1994) 89–96. URL <http://www.worldscientific.com/doi/abs/10.1142/S0218625X94000114>.
- [112] H. Ibach, M. Balden, S. Lehwald, Recent advances in electron energy loss spectroscopy of surface vibrations, *J. Chem. Soc., Faraday Trans.* 92 (1996) 4771–4774. URL <http://dx.doi.org/10.1039/FT9969204771>.
- [113] H. Ibach, D. Bruchmann, R. Vollmer, M. Etzkorn, P.S.A. Kumar, J. Kirschner, A novel spectrometer for spin-polarized electron energy-loss spectroscopy, *Rev. Sci. Instrum.* 74 (9) (2003) 4089–4095. URL <http://link.aip.org/link/?RSI/74/4089/1>.
- [114] H. Ibach, M. Etzkorn, J. Kirschner, Electron spectrometers for inelastic scattering from magnetic surface excitations, *Surf. Interface Anal.* 38 (12–13) (2006) 1615–1617. URL <http://dx.doi.org/10.1002/sia.2425>.
- [115] P. Drescher, H. Andresen, K. Aulenbacher, J. Bermuth, T. Dombo, H. Fischer, H. Euteneuer, N. Faleev, M. Galaktionov, D. von Harrach, et al., Rapid communication photoemission of spinpolarized electrons from strained GaAs , *Appl. Phys. A* 63 (2) (1996) 203–206.
- [116] T. Balashov, A.F. Takács, W. Wulfhchel, J. Kirschner, Magnon excitation with spin-polarized scanning tunneling microscopy, *Phys. Rev. Lett.* 97 (2006) 187201. URL <http://link.aps.org/doi/10.1103/PhysRevLett.97.187201>.
- [117] T. Balashov, A.F. Takács, M. Däne, A. Ernst, P. Bruno, W. Wulfhchel, Inelastic electron–magnon interaction and spin transfer torque, *Phys. Rev. B* 78 (2008) 174404. URL <http://link.aps.org/doi/10.1103/PhysRevB.78.174404>.
- [118] C.L. Gao, A. Ernst, G. Fischer, W. Hergert, P. Bruno, W. Wulfhchel, J. Kirschner, Spin wave dispersion on the nanometer scale, *Phys. Rev. Lett.* 101 (2008) 167201. URL <http://link.aps.org/doi/10.1103/PhysRevLett.101.167201>.
- [119] T. Balashov, T. Schuh, A.F. Takács, A. Ernst, S. Ostanin, J. Henk, I. Mertig, P. Bruno, T. Miyamachi, S. Suga, W. Wulfhchel, Magnetic anisotropy and magnetization dynamics of individual atoms and clusters of Fe and Co on Pt(111), *Phys. Rev. Lett.* 102 (2009) 257203. URL <http://link.aps.org/doi/10.1103/PhysRevLett.102.257203>.
- [120] A.J. Heinrich, J.A. Gupta, C.P. Lutz, D.M. Eigler, Single-atom spin-flip spectroscopy, *Science* 306 (5695) (2004) 466–469. URL <http://www.sciencemag.org/content/306/5695/466.abstract>.
- [121] S. Loth, C.P. Lutz, A.J. Heinrich, Spin-polarized spin excitation spectroscopy, *New J. Phys.* 12 (12) (2010) 125021. URL <http://stacks.iop.org/1367-2630/12/i=12/a=125021>.
- [122] A.A. Khajetoorians, S. Lounis, B. Chilian, A.T. Costa, L. Zhou, D.L. Mills, J. Wiebe, R. Wiesendanger, Itinerant nature of atom-magnetization excitation by tunneling electrons, *Phys. Rev. Lett.* 106 (2011) 037205. URL <http://link.aps.org/doi/10.1103/PhysRevLett.106.037205>.
- [123] T. Schuh, T. Balashov, T. Miyamachi, S.-Y. Wu, C.-C. Kuo, A. Ernst, J. Henk, W. Wulfhchel, Magnetic anisotropy and magnetic excitations in supported atoms, *Phys. Rev. B* 84 (2011) 104401. URL <http://link.aps.org/doi/10.1103/PhysRevB.84.104401>.
- [124] A. Liechtenstein, M. Katsnelson, V. Antropov, V. Gubanov, Local spin density functional approach to the theory of exchange interactions in ferromagnetic metals and alloys, *J. Magn. Magn. Mater.* 67 (1) (1987) 65–74. URL <http://www.sciencedirect.com/science/article/pii/0304885387907219>.
- [125] V.P. Antropov, M.I. Katsnelson, M.van Schilfgaarde, B.N. Harmon, *Ab Initio* spin dynamics in magnets, *Phys. Rev. Lett.* 75 (1995) 729–732. URL <http://link.aps.org/doi/10.1103/PhysRevLett.75.729>.
- [126] S.Y. Savrasov, Linear-response theory and lattice dynamics: A muffin-tin-orbital approach, *Phys. Rev. B* 54 (1996) 16470–16486. URL <http://link.aps.org/doi/10.1103/PhysRevB.54.16470>.
- [127] V.P. Antropov, M.I. Katsnelson, B.N. Harmon, M.van Schilfgaarde, D. Kusnezov, Spin dynamics in magnets: Equation of motion and finite temperature effects, *Phys. Rev. B* 54 (1996) 1019–1035. URL <http://link.aps.org/doi/10.1103/PhysRevB.54.1019>.
- [128] S.V. Halilov, A.Y. Perlov, P.M. Oppeneer, H. Eschrig, Magnon spectrum and related finite-temperature magnetic properties: A first-principle approach, *Europhys. Lett.* 39 (1) (1997) 91. URL <http://stacks.iop.org/0295-5075/39/i=1/a=091>.
- [129] S.V. Halilov, H. Eschrig, A.Y. Perlov, P.M. Oppeneer, Adiabatic spin dynamics from spin-density-functional theory: Application to Fe, Co, and Ni, *Phys. Rev. B* 58 (1998) 293–302. URL <http://link.aps.org/doi/10.1103/PhysRevB.58.293>.
- [130] Q. Niu, L. Kleinman, Spin-wave dynamics in real crystals, *Phys. Rev. Lett.* 80 (1998) 2205–2208. URL <http://link.aps.org/doi/10.1103/PhysRevLett.80.2205>.
- [131] V.P. Antropov, B.N. Harmon, A.N. Smirnov, Aspects of spin dynamics and magnetic interactions, *J. Magn. Magn. Mater.* 200 (1–3) (1999) 148–166. URL <http://www.sciencedirect.com/science/article/B6TJJ-3Y2NV45-R/2/fb00e680a9a2f00946af94a6fca5c716>.
- [132] Q. Niu, X. Wang, L. Kleinman, W.-M. Liu, D.M.C. Nicholson, G.M. Stocks, Adiabatic dynamics of local spin moments in itinerant magnets, *Phys. Rev. Lett.* 83 (1999) 207–210. URL <http://link.aps.org/doi/10.1103/PhysRevLett.83.207>.
- [133] R.H. Brown, D.M.C. Nicholson, X. Wang, T.C. Schulthess, First principles theory of spin waves in Fe, Co, and Ni, *J. Appl. Phys.* 85 (8) (1999) 4830–4832. URL <http://dx.doi.org/10.1063/1.370035>.
- [134] R. Gebauer, S. Baroni, Magnons in real materials from density-functional theory, *Phys. Rev. B* 61 (2000) R6459–R6462. URL <http://link.aps.org/doi/10.1103/PhysRevB.61.R6459>.
- [135] M. Pajda, J. Kudrnovský, I. Turek, V. Drchal, P. Bruno, *Ab initio* calculations of exchange interactions, spin-wave stiffness constants, and Curie temperatures of Fe, Co, and Ni, *Phys. Rev. B* 64 (2001) 174402. URL <http://link.aps.org/doi/10.1103/PhysRevB.64.174402>.

- [136] O. Grotheer, C. Ederer, M. Fähnle, Fast *ab initio* methods for the calculation of adiabatic spin wave spectra in complex systems, Phys. Rev. B 63 (2001) 100401. URL <http://link.aps.org/doi/10.1103/PhysRevB.63.100401>.
- [137] P. Bruno, Exchange interaction parameters and adiabatic spin-wave spectra of ferromagnets: A “Renormalized” magnetic force theorem, Phys. Rev. Lett. 90 (2003) 087205. URL <http://link.aps.org/doi/10.1103/PhysRevLett.90.087205>.
- [138] I. Turek, J. Kudrnovsky, V. Drchal, P. Bruno, Exchange interactions, spin waves, and transition temperatures in itinerant magnets, Phil. Mag. 86 (12) (2006) 1713–1752. URL <http://dx.doi.org/10.1080/14786430500504048>.
- [139] R. Singer, F. Dietermann, D. Steiauf, M. Fähnle, *Ab initio* calculations of adiabatic magnon spectra using the atomic-sphere approximation for the spin direction, Phys. Rev. B 76 (2007) 052403. URL <http://link.aps.org/doi/10.1103/PhysRevB.76.052403>.
- [140] A. Bergman, A. Taroni, L. Bergqvist, J. Hellsvik, B. Hjörvarsson, O. Eriksson, Magnon softening in a ferromagnetic monolayer: A first-principles spin dynamics study, Phys. Rev. B 81 (2010) 144416. URL <http://link.aps.org/doi/10.1103/PhysRevB.81.144416>.
- [141] A. Taroni, A. Bergman, L. Bergqvist, J. Hellsvik, O. Eriksson, Suppression of standing spin waves in low-dimensional ferromagnets, Phys. Rev. Lett. 107 (2011) 037202. URL <http://link.aps.org/doi/10.1103/PhysRevLett.107.037202>.
- [142] L. Bergqvist, A. Taroni, A. Bergman, C. Etz, O. Eriksson, Atomistic spin dynamics of low-dimensional magnets, Phys. Rev. B 87 (2013) 144401. URL <http://link.aps.org/doi/10.1103/PhysRevB.87.144401>.
- [143] L. Sandratskii, Noncollinear magnetism in itinerant-electron systems: theory and applications, Adv. Phys. 47 (1) (1998) 91–160.
- [144] J.A. Blackman, T. Morgan, J.F. Cooke, Prediction of high-energy spin-wave excitation in iron, Phys. Rev. Lett. 55 (1985) 2814–2817. URL <http://link.aps.org/doi/10.1103/PhysRevLett.55.2814>.
- [145] A.T. Costa, R.B. Muniz, D.L. Mills, Theory of spin waves in ultrathin ferromagnetic films: The case of co on cu(100), Phys. Rev. B 69 (2004) 064413. URL <http://link.aps.org/doi/10.1103/PhysRevB.69.064413>.
- [146] D. Mills, Quantum theory of spin waves in finite samples, J. Magn. Magn. Mater. 306 (1) (2006) 16–23. URL <http://www.sciencedirect.com/science/article/pii/S0304885306003994>.
- [147] D.L. Mills, Spin Waves: History and a Summary of Recent Developments, in: Handbook of Magnetism and Advanced Magnetic Materials, 1, Wiley & Sons, Ltd., 2007, pp. 247–282. Ch. Fundamentals and Theory.
- [148] A.T. Costa, R.B. Muniz, J.X. Cao, R.Q. Wu, D.L. Mills, Magnetism of an fe monolayer on w(110), Phys. Rev. B 78 (2008) 054439. URL <http://link.aps.org/doi/10.1103/PhysRevB.78.054439>.
- [149] A.T. Costa, R.B. Muniz, S. Lounis, A.B. Klautau, D.L. Mills, Spin-orbit coupling and spin waves in ultrathin ferromagnets: The spin-wave rashba effect, Phys. Rev. B 82 (2010) 014428. URL <http://link.aps.org/doi/10.1103/PhysRevB.82.014428>.
- [150] G. Barnea, G. Horwitz, Complex spin waves in metallic ferromagnets, J. Phys. C: Solid State Phys. 6 (4) (1973) 738–749. URL <http://stacks.iop.org/0022-3719/6/738>.
- [151] F. Aryasetiawan, K. Karlsson, Green’s function formalism for calculating spin-wave spectra, Phys. Rev. B 60 (1999) 7419–7428. URL <http://link.aps.org/doi/10.1103/PhysRevB.60.7419>.
- [152] E. Şaşıoğlu, C. Friedrich, S. Blügel, softening in tetragonal fcco compounds, Phys. Rev. B 87 (2013) 020410. URL <http://link.aps.org/doi/10.1103/PhysRevB.87.020410>.
- [153] J. Callaway, C.S. Wang, Transverse magnetic susceptibility in the local exchange approximation, J. Phys. F: Met. Phys. 5 (11) (1975) 2119–2128. URL <http://stacks.iop.org/0305-4608/5/2119>.
- [154] J. Callaway, A.K. Chatterjee, Dynamic longitudinal spin susceptibility of bloch electrons, J. Phys. F: Met. Phys. 8 (12) (1978) 2569–2577. URL <http://stacks.iop.org/0305-4608/8/2569>.
- [155] J. Callaway, D.G. Laurent, C.S. Wang, Magnetic susceptibility and spin waves in ferromagnetic metals, Phys. Rev. B 24 (11) (1981) 6491–6496. URL <http://dx.doi.org/10.1103/PhysRevB.24.6491>.
- [156] S.Y. Savrasov, A linearized direct approach for calculating the static response in solids, Solid State Commun. 74 (2) (1990) 69–72. URL <http://www.sciencedirect.com/science/article/B6TVW-46SP4P-1B/2/e486637f6f834b7ead11104d423db890>.
- [157] S.Y. Savrasov, Linear response calculations of lattice dynamics using muffin-tin basis sets, Phys. Rev. Lett. 69 (1992) 2819–2822. URL <http://link.aps.org/doi/10.1103/PhysRevLett.69.2819>.
- [158] J.B. Staunton, J. Poulter, B. Ginatempo, E. Bruno, D.D. Johnson, Incommensurate and commensurate antiferromagnetic spin fluctuations in cr and cr alloys from *Ab Initio* dynamical spin susceptibility calculations, Phys. Rev. Lett. 82 (1999) 3340–3343. URL <http://link.aps.org/doi/10.1103/PhysRevLett.82.3340>.
- [159] Z. Qian, G. Vignale, Spin dynamics from time-dependent spin-density-functional theory, Phys. Rev. Lett. 88 (2002) 056404. URL <http://link.aps.org/doi/10.1103/PhysRevLett.88.056404>.
- [160] P.A. Buczek, Spin dynamics of complex itinerant magnets (Ph.D. thesis), Martin Luther Universität Halle-Wittenberg, 2009, <http://digital.bibliothek.uni-halle.de/hs/content/titleinfo/234732>.
- [161] P. Buczek, A. Ernst, L. Sandratskii, P. Bruno, The energies and life times of magnons in bulk iron and one-monolayer fe film, J. Magn. Magn. Mater. 322 (2010) 1396–1398. Proceedings of the Joint European Magnetic Symposia. URL <http://www.sciencedirect.com/science/article/pii/S0304885309002479>.
- [162] P. Buczek, A. Ernst, L.M. Sandratskii, Standing spin waves as a basis for the control of terahertz spin dynamics: Time dependent density functional theory study, Phys. Rev. Lett. 105 (2010) 097205. URL <http://link.aps.org/doi/10.1103/PhysRevLett.105.097205>.
- [163] R. Vollmer, M. Etzkorn, P.S.A. Kumar, H. Ibach, J. Kirschner, Spin-polarized electron energy loss spectroscopy of high energy, large wave vector spin waves in ultrathin fcco films on cu(001), Phys. Rev. Lett. 91 (2003) 147201. URL <http://link.aps.org/doi/10.1103/PhysRevLett.91.147201>.
- [164] R. Vollmer, M. Etzkorn, P.S.A. Kumar, H. Ibach, J. Kirschner, Spin-wave excitation in ultrathin co and fe films on cu(001) by spin-polarized electron energy loss spectroscopy (invited), J. Appl. Phys. 95 (11) (2004) 7435–7440. URL <http://link.aip.org/link/?JAP/95/7435/1>.
- [165] R. Vollmer, M. Etzkorn, P. Kumar, H. Ibach, J. Kirschner, Spin-wave excitation observed by spin-polarized electron energy loss spectroscopy: a new method for the investigation of surface- and thin-film spin waves on the atomic scale, Thin Solid Films 464–465 (2004) 42–47. URL <http://www.sciencedirect.com/science/article/pii/S0040609004007679>.
- [166] R. Vollmer, M. Etzkorn, P.A. Kumar, H. Ibach, J. Kirschner, Spin-polarized electron energy loss spectroscopy: a method to measure magnon energies, J. Magn. Magn. Mater. 272–276 (2004) 2126–2130. URL <http://www.sciencedirect.com/science/article/pii/S0304885303022017>.
- [167] W.X. Tang, Y. Zhang, I. Tudosa, J. Prokop, M. Etzkorn, J. Kirschner, Large wave vector spin waves and dispersion in two monolayer fe on w(110), Phys. Rev. Lett. 99 (2007) 087202. URL <http://link.aps.org/doi/10.1103/PhysRevLett.99.087202>.
- [168] K. Zakeri, Y. Zhang, J. Prokop, T.H. Chuang, W.X. Tang, J. Kirschner, Magnon excitations in ultrathin fe layers: the influence of the dzyaloshinskii-moriya interaction, J. Phys.: Conf. Ser. 303 (1) (2011) 012004. URL <http://stacks.iop.org/1742-6596/303/i=1/a=012004>.
- [169] Y. Zhang, P.A. Ignatiev, J. Prokop, I. Tudosa, T.R.F. Peixoto, W.X. Tang, K. Zakeri, V.S. Stepanyuk, J. Kirschner, Elementary excitations at magnetic surfaces and their spin dependence, Phys. Rev. Lett. 106 (2011) 127201. URL <http://link.aps.org/doi/10.1103/PhysRevLett.106.127201>.
- [170] K. Parlinski, Z.Q. Li, Y. Kawazoe, First-principles determination of the soft mode in cubic zro₂, Phys. Rev. Lett. 78 (1997) 4063–4066. URL <http://link.aps.org/doi/10.1103/PhysRevLett.78.4063>.
- [171] G. Fahsold, G. Knig, W. Theis, A. Lehmann, K.-H. Rieder, Epitaxial feo films from ultrathin fe on mgo(001) studied by he-atom scattering, Appl. Surf. Sci. 137 (1–4) (1999) 224–235. URL <http://www.sciencedirect.com/science/article/pii/S0169433298005339>.
- [172] J. Prokop, W.X. Tang, Y. Zhang, I. Tudosa, T.R.F. Peixoto, K. Zakeri, J. Kirschner, Magnons in a ferromagnetic monolayer, Phys. Rev. Lett. 102 (2009) 177206. URL <http://link.aps.org/doi/10.1103/PhysRevLett.102.177206>.
- [173] H.J. Elmers, Ferromagnetic monolayers, Internat. J. Modern Phys. B 09 (24) (1995) 3115–3180. URL <http://www.worldscientific.com/doi/abs/10.1142/S0217979295001191>.
- [174] M. Pratzler, H.J. Elmers, M. Bode, O. Pietzsch, A. Kubetzka, R. Wiesendanger, Atomic-scale magnetic domain walls in quasi-one-dimensional fe nanostripes, Phys. Rev. Lett. 87 (2001) 127201. URL <http://link.aps.org/doi/10.1103/PhysRevLett.87.127201>.

- [175] J.W. Lynn, Temperature dependence of the magnetic excitations in iron, *Phys. Rev. B* 11 (1975) 2624–2637. URL <http://link.aps.org/doi/10.1103/PhysRevB.11.2624>.
- [176] J. Lynn, H. Mook, Nature of the magnetic excitations above t_c in ni and fe, *J. Magn. Magn. Mater.* 54–57, Part 3 (0) (1986) 1169–1170. URL <http://www.sciencedirect.com/science/article/pii/0304885386907675>.
- [177] Y. Zhang, P. Buczek, L. Sandratskii, W.X. Tang, J. Prokop, I. Tudosa, T.R.F. Peixoto, K. Zakeri, J. Kirschner, Nonmonotonic thickness dependence of spin wave energy in ultrathin fe films: Experiment and theory, *Phys. Rev. B* 81 (2010) 094438. URL <http://link.aps.org/doi/10.1103/PhysRevB.81.094438>.
- [178] H.L. Meyerheim, D. Sander, R. Popescu, J. Kirschner, P. Steadman, S. Ferrer, Surface structure and stress in fe monolayers on w(110), *Phys. Rev. B* 64 (2001) 045414. URL <http://link.aps.org/doi/10.1103/PhysRevB.64.045414>.
- [179] T.-H. Chuang, K. Zakeri, A. Ernst, L. Sandratskii, P. Buczek, Y. Zhang, H. Qin, W. Adeagbo, W. Hergert, J. Kirschner, Impact of atomic structure on the magnon dispersion relation: A comparison between fe(111)/au/w(110), *Phys. Rev. Lett.* 109 (2012) 207201.
- [180] J. Rajeswari, H. Ibach, C.M. Schneider, A.T. Costa, D.L.R. Santos, D.L. Mills, Surface spin waves of fcc cobalt films on cu(100): high-resolution spectra and comparison to theory, *Phys. Rev. B* 86 (2012) 165436. URL <http://link.aps.org/doi/10.1103/PhysRevB.86.165436>.
- [181] Y. Zhang, T.-H. Chuang, K. Zakeri, J. Kirschner, Relaxation time of terahertz magnons excited at ferromagnetic surfaces, *Phys. Rev. Lett.* 109 (2012) 087203. URL <http://link.aps.org/doi/10.1103/PhysRevLett.109.087203>.
- [182] S. Loth, M. Etzkorn, C.P. Lutz, D.M. Eigler, A.J. Heinrich, Measurement of fast electron spin relaxation times with atomic resolution, *Science* 329 (5999) (2010) 1628–1630. URL <http://www.sciencemag.org/content/329/5999/1628.abstract>.
- [183] A.B. Schmidt, M. Pickel, M. Donath, P. Buczek, A. Ernst, V.P. Zhukov, P.M. Echenique, L.M. Sandratskii, E.V. Chulkov, M. Weinelt, Ultrafast magnon generation in an fe film on cu(100), *Phys. Rev. Lett.* 105 (2010) 197401. URL <http://link.aps.org/doi/10.1103/PhysRevLett.105.197401>.
- [184] S.A. Wolf, D.D. Awschalom, R.A. Buhrman, J.M. Daughton, S. von Molnr, M.L. Roukes, A.Y. Chtchelkanova, D.M. Treger, Spintronics: a spin-based electronics vision for the future, *Science* 294 (5546) (2001) 1488–1495. URL <http://www.sciencemag.org/content/294/5546/1488.abstract>.
- [185] E. Rashba, Properties of semiconductors with an extremum loop. 1. cyclootron and combinational resonance in a magnetic field perpendicular to the plane of the loop, *Sov. Phys. Solid State* 2 (1960) 1109–1122.
- [186] Y.A. Bychkov, E.I. Rashba, Properties of a 2d electron gas with lifted spectral degeneracy, *JETP Lett.* 39 (1984) 78. URL http://www.jetpletters.ac.ru/ps/1264/article_19121.shtml.
- [187] R. Winkler, *Spin-Orbit Coupling Effects in 2D Electron and Hole Systems*, Springer, Berlin, 2003.
- [188] S. LaShell, B.A. McDougall, E. Jensen, Spin splitting of an au(111) surface state band observed with angle resolved photoelectron spectroscopy, *Phys. Rev. Lett.* 77 (1996) 3419–3422. URL <http://link.aps.org/doi/10.1103/PhysRevLett.77.3419>.
- [189] J. Henk, A. Ernst, P. Bruno, Spin polarization of the *L*-gap surface states on au(111), *Phys. Rev. B* 68 (2003) 165416. URL <http://link.aps.org/doi/10.1103/PhysRevB.68.165416>.
- [190] O. Krupin, G. Bihlmayer, K. Starke, S. Gorovikov, J.E. Prieto, K. Döbrich, S. Blügel, G. Kaindl, Rashba effect at magnetic metal surfaces, *Phys. Rev. B* 71 (2005) 201403. URL <http://link.aps.org/doi/10.1103/PhysRevB.71.201403>.
- [191] G. Bihlmayer, Y. Koroteev, P. Echenique, E. Chulkov, S. Blgel, The rashba-effect at metallic surfaces, *Surf. Sci.* 600 (18) (2006) 3888–3891. URL <http://www.sciencedirect.com/science/article/pii/S0039602806004195>.
- [192] C. Ast, J. Henk, A. Ernst, L. Moreschini, M. Falub, D. Pacilé, P. Bruno, K. Kern, M. Grioni, Giant spin splitting through surface alloying, *Phys. Rev. Lett.* 98 (18) (2007) 186807.
- [193] S. Datta, B. Das, Electronic analog of the electro-optic modulator, *Appl. Phys. Lett.* 56 (7) (1990) 665–667. URL <http://link.aip.org/link/APL56/665/1>.
- [194] T. Koga, J. Nitta, H. Takayanagi, S. Datta, Spin-filter device based on the rashba effect using a nonmagnetic resonant tunneling diode, *Phys. Rev. Lett.* 88 (12) (2002) 126601.
- [195] H.C. Koo, J.H. Kwon, J. Eom, J. Chang, S.H. Han, M. Johnson, Control of spin precession in a spin-injected field effect transistor, *Science* 325 (5947) (2005) 1515–1518. URL <http://www.sciencemag.org/content/325/5947/1515.abstract>.
- [196] M.I. Miron, G. Gaudin, S. Auffret, B. Rodmacq, A. Schuhl, S. Pizzini, P. Vogel, J. amd Gambardella1, Current-driven spin torque induced by the rashba effect in a ferromagnetic metal layer, *Nature Mater.* 9 (2010) 230–234. URL <http://dx.doi.org/10.1038/nmat2613>.
- [197] K. Zakeri, Y. Zhang, J. Prokop, T.-H. Chuang, N. Sakr, W.X. Tang, J. Kirschner, Asymmetric spin-wave dispersion on fe(110): direct evidence of the dzyaloshinskii-moriya interaction, *Phys. Rev. Lett.* 104 (2010) 137203. URL <http://link.aps.org/doi/10.1103/PhysRevLett.104.137203>.
- [198] K. Zakeri, Y. Zhang, T.-H. Chuang, J. Kirschner, Magnon lifetimes on the fe(110) surface: the role of spin-orbit coupling, *Phys. Rev. Lett.* 108 (2012) 197205. URL <http://link.aps.org/doi/10.1103/PhysRevLett.108.197205>.
- [199] D.L. Mills, Surface corrections to the specific heat of ferromagnetic films, *Phys. Rev. B* 1 (1970) 264–274. URL <http://link.aps.org/doi/10.1103/PhysRevB.1.264>.
- [200] K. Zakeri, T.-H. Chuang, A. Ernst, L. Sandratskii, P. Buczek, H. Qin, Y. Zhang, J. Kirschner, Direct probing of the exchange interaction at buried interfaces, *Nature Nanotechnol.* 8 (11) (2013) 853–858. URL <http://dx.doi.org/10.1038/nnano.2013.188>.
- [201] T.-H. Chuang, K. Zakeri, A. Ernst, Y. Zhang, H.J. Qin, Y. Meng, Y.-J. Chen, J. Kirschner, Magnetic properties and magnon excitations in Fe(001) films grown on ir(001), *Phys. Rev. B* 89 (2014) 174404. URL <http://link.aps.org/doi/10.1103/PhysRevB.89.174404>.
- [202] D. Weller, A. Moser, L. Folks, M.E. Best, W. Lee, M.F. Toney, M. Schwickert, J.-U. Thiele, M.F. Doerner, High ku materials approach to 100 gbits in2, *IEEE Trans. Magn.* 36 (2000) 10.
- [203] L. Liu, C.-F. Pai, Y. Li, H.W. Tseng, D.C. Ralph, R.A. Buhrman, Spin-torque switching with the giant spin hall effect of tantalum, *Science* 336 (6081) (2012) 555–558. URL <http://dx.doi.org/10.1126/science.1218197>.
- [204] L. Liu, O.J. Lee, T.J. Gudmundsen, D.C. Ralph, R.A. Buhrman, Current-induced switching of perpendicularly magnetized magnetic layers using spin torque from the spin hall effect, *Phys. Rev. Lett.* 109 (2012) 096602. URL <http://link.aps.org/doi/10.1103/PhysRevLett.109.096602>.
- [205] H.J. Qin, K. Zakeri, A. Ernst, T.-H. Chuang, Y.-J. Chen, Y. Meng, J. Kirschner, Magnons in ultrathin ferromagnetic films with a large perpendicular magnetic anisotropy, *Phys. Rev. B* 88 (2013) 020404. URL <http://link.aps.org/doi/10.1103/PhysRevB.88.020404>.
- [206] T. Burkert, L. Nordström, O. Eriksson, O. Heinonen, Giant magnetic anisotropy in tetragonal fcco alloys, *Phys. Rev. Lett.* 93 (2004) 027203. URL <http://link.aps.org/doi/10.1103/PhysRevLett.93.027203>.
- [207] F. Yildiz, M. Przybylski, X.-D. Ma, J. Kirschner, Strong perpendicular anisotropy in Fe_{1-x}Co_x alloy films epitaxially grown on mismatching Pd(001), Ir(001), and Rh(001) substrates, *Phys. Rev. B* 80 (2009) 064415. URL <http://link.aps.org/doi/10.1103/PhysRevB.80.064415>.
- [208] J. Kesseler, *Polarized Electrons*, Springer, Berlin, 1985.
- [209] H. Ibach, J. Rajeswari, C.M. Schneider, An electron energy loss spectrometer designed for studies of electronic energy losses and spin waves in the large momentum regime, *Rev. Sci. Instrum.* 82 (12) (2011) 123904. URL <http://link.aip.org/link/RSI82/123904/1>.
- [210] H. Ibach, J. Rajeswari, Electron energy loss spectrometers: An advanced operation mode for the lens system and the quantitative calculation of solid angle and transmission, *J. Electron Spectrosc. Relat. Phenom.* 185 (3–4) (2012) 61–70. URL <http://www.sciencedirect.com/science/article/pii/S0368204812000059>.
- [211] J. Rajeswari, H. Ibach, C.M. Schneider, Large wave vector surface spin waves of the nanomartensitic phase in ultrathin iron films on cu(100), *Europhys. Lett.* 101 (1) (2013) 17003. URL <http://stacks.iop.org/0295-5075/101/i=1/a=17003>.
- [212] J. Rajeswari, H. Ibach, C.M. Schneider, Observation of large wave vector interface spin waves: Ni(100)/fcc co(100) and cu(100)/co(100), *Phys. Rev. B* 87 (2013) 235415. URL <http://link.aps.org/doi/10.1103/PhysRevB.87.235415>.
- [213] J. Jankowska-Kisielinska, K. Mikke, J. Milczarek, Spin waves in antiferromagnetic fct mn(17%ni) alloy, *J. Magn. Magn. Mater.* 140–144, Part 3 (0) (1995) 1973–1974. URL <http://www.sciencedirect.com/science/article/pii/0304885394008434>.
- [214] C.F. Hirjibehedin, C.P. Lutz, A.J. Heinrich, Spin coupling in engineered atomic structures, *Science* 312 (5776) (2006) 1021–1024. URL <http://www.sciencemag.org/cgi/content/abstract/312/5776/1021>.
- [215] C.F. Hirjibehedin, C.-Y. Lin, A.F. Otte, M. Ternes, C.P. Lutz, B.A. Jones, A.J. Heinrich, Large magnetic anisotropy of a single atomic spin embedded in a surface molecular network, *Science* 317 (5842) (2007) 1199–1203. URL <http://www.sciencemag.org/content/317/5842/1199.abstract>.

- [216] T. Schuh, T. Miyamachi, S. Gerstl, M. Geilhufe, M. Hoffmann, S. Ostanin, W. Hergert, A. Ernst, W. Wulfhekel, Magnetic excitations of rare earth atoms and clusters on metallic surfaces, *Nano Lett.* 12 (9) (2012) 4805–4809. URL <http://pubs.acs.org/doi/abs/10.1021/nl302250n>.
- [217] S. Heinze, K.von Bergmann, M. Menzel, J. Brede, A. Kubetzka, R. Wiesendanger, G. Bihlmayer, S. Blügel, Spontaneous atomic-scale magnetic skyrmion lattice in two dimensions, *Nature Phys.* 7 (9) (2011) 713–718. URL <http://dx.doi.org/10.1038/nphys2045>.
- [218] L.M. Sandratskii, P. Buczek, Lifetimes and chirality of spin waves in antiferromagnetic and ferromagnetic ferh from the perspective of time-dependent density functional theory, *Phys. Rev. B* 85 (2012) 020406. URL <http://link.aps.org/doi/10.1103/PhysRevB.85.020406>.